A Novel Self-Healing Shape Memory Polymer-Cementitious System

Simon Craig Dunn

dunnsc@cardiff.ac.uk

Cardiff School of Engineering

CARDIFF, WALES, UK

PhD, 2010

ProQuest LLC
789 East Eisenhower Parkway
P.O. Box 1346
Ann Arbor, MI 48106-1346

Declaration

This work has not previously been accepted in substance for any degree and is not concurrently submitted in candidature for any degree.

Signed: Simon Dunn (candidate) Date: 25th November 2010

STATEMENT 1

This thesis is being submitted in partial fulfilment of the requirements for the degree of PhD.

Signed: Simon Dunn (candidate) Date: 25th November 2010

STATEMENT 2

This thesis is the result of my own independent work/investigation, except where otherwise stated. Other sources are acknowledged by explicit references.

Signed: Simon Dunn (candidate) Date: 25th November 2010

STATEMENT 3

I hereby give consent for my thesis, if accepted, to be available for photocopying and for inter-library loan, and for the title and summary to be made available to outside organisations.

Signed: Simon Dunn (candidate) Date: 25th November 2010

Acknowledgements

The help and support I have received through my PhD has come from so many people.

I would like to thank my family, most notably Peter and Brenda, without your willingness to help me both in my education and life in general I would not be the person I am today. I also have to thank my girlfriend, Nikki, your love and support especially in the last few months have been a massive help; knowing I have you to make things fun when I am stressed has been great.

I would like to thank the many friends that I have made throughout my University life, most of all those made through *Cardiff University Football Club*. You gave me the opportunity to "let my hair down" and relax away from my academic studies.

I would like to thank everyone from the School of Engineering who have helped me throughout the PhD and for the financial support they have given. In particular I would like to thank my fellow PhD student Ben Isaacs with whom it has been a pleasure to work with and the other research group members; Bob, Tony, Diane, Barry, Chris, Andrea, Simon C and Iulia, you have all helped me in so many ways. I do though owe sincere thanks to Tony Jefferson for his support and guidance, I could not have asked for a better and more dedicated supervisor.

I would like to thank the Institution of Civil Engineers (ICE) and the various people who have supported me from industry, most notably Alun Griffiths Contractors and Halcrow.

Finally and most importantly I would like to thank my parents, I would like to thank my Mum for all the support she has given me through the hard times and praise she has given me during the good times. Your support, both moral and financial, has been very much appreciated. However, the biggest thanks must go to my late Dad, this thesis is for you, your bravery and courage during your illness has inspired me, and encouraged me to live life to the full and enjoy every moment, no matter how difficult, I would never of been able to complete this PhD without you. This thesis is therefore dedicated to my Dad.

Abstract

This thesis describes the development of a new and innovative polymer-cementitious self-healing material system, called LatConX.

The LatConX system was developed by a group of researchers at Cardiff University, of which the author was a member. The work of the author focussed on the behaviour of shrinkable polymers and the numerical simulation of the LatConX system and therefore this thesis concentrates on these aspects of the work. The thesis provides a detailed description of the LatConX system and of the experiments used to prove that the system provides a viable solution to the healing of cracks in cementitious materials.

A series of experiments are described which explore the shrinkage behaviour of polyethylene terephthalate (PET). The aim of this work was to investigate how and when stress develops with temperature, under restrained conditions; and also to examine the effect of varying factors such as geometry and soak time (i.e. the time a material is subjected to a certain temperature). The experiments yielded a clear relationship between Young's modulus and temperature and showed that there was a clearly defined glass transition region.

A numerical model is then presented which simulates the transient thermo-mechanical behaviour of drawn PET specimens. It is shown that the model is able to accurately represent the behaviour measured in the experimental studies.

The polymer model is incorporated into a simulation for the entire material system which is based on a beam idealisation and in which a strong discontinuity approach is used to simulate cracking. It is shown that this model is able to accurately simulate the experiments carried out on the LatConX system.

Publications

The following are publications on which the author is named:

1. Jefferson, A.D., Joseph, C., Lark, R.J., Dunn, S.C., Isaacs, B. & Weager, B., 2010. A new system for crack closure and post-tensioning of cementitious materials using shrinkable polymers. Cement and Concrete Research, 40(5), pp.795-801.
2. Dunn, S.C., Jefferson, A.D., Lark, R.L. & Isaacs, B., 2011. Investigation into the shrinkage behaviour of Polyethylene Terephthalate (PET) for a new cementitious–shrinkable polymer material system. Applied Polymer Science, Vol. 120, issue 5, pages 2516-2526
3. Isaacs, B., Lark, R.L., Jefferson, A.D., Dunn, S.C. & Joseph, C., 2010. Autogenous Healing in an SMP Cementitious Material System. Cement and Concrete Composites.

The author is also named on the following conference proceedings and presented at the conferences as first author on two of the papers:

1. Dunn, S.C., Jefferson, A.D., Lark, R.J., Isaacs, B. & Joseph, C., 2009. A numerical model for the shrinkage of polymer elements in active self-healing. Chicago, 2009. 2nd International Conference for Self-healing Materials.
2. Dunn, S.C., Jefferson, A.D. & Lark, R.J., 2009. The numerical simulation of highly shrinkable polymers. In 17th UK National Conference on Computational Mechanics in Engineering. Nottingham, 2009. ACME2009.
3. Lark, R.J., Jefferson, A.D., Joseph, C., Dunn, S.C. & Isaacs, B., 2009. Active confinement of cementitious composites with shape memory plastics. In 2nd International Conference of Self-Healing Materials. Chicago, 2009. ICSHM2009.
4. Isaacs, B., Joseph, C., Jefferson, A.D., Lark, R.J. & Dunn, S.C., 2009. Enhancement of self-healing in cementitious materials, post-tensioned with shrinkable polymers. In 2nd International Conference of Self-Healing Materials. Chicago, 2009. ICSHM2009.

The author is also a member of the RILEM Technical Committee 221-SHC: Self-Healing phenomena in Cement-based materials and has contributed to the production of a State of the Art Report (STAR) into self-healing cementitious materials.

Table of Contents

List of Tables

List of Figures

List of Symbols, Abbreviations and Nomenclature

The following symbols and abbreviations are used in this thesis:

AH	Activation Healing
BHET	Bis-Hydroxyethyl-Terephthalate
BSI	British Standards Institute
CG	Clip Gauge
CMOD	Crack Mouth Opening Displacement
CoV	Coefficient of Variance
CPET	Crystalline Polyethylene Terephthalate
CSH	Calcium-Silicate-Hydrate
CTRL1/CTRL2	Control Specimen
CUPD	Cardiff University Procedure Development
CUST	Cardiff University Screening Tests
DIC	Digital Image Correlation
DSC	Digital Scanning Calorimetry
ECC	Engineering Cementitious Composite
FE	Finite Element
Fe-Mn-Si	Iron-Maganese-Silicon
FPZ	Fracture Process Zone
FRP	Fibre Reinforced Polymer
GFRPP	Glass Fibre Reinforced Polypropylene
HDPE	High Density Polyethylene
LDPE	Low Density Polyethylene
LR	Load Recovery
MDR	Molecular Draw Ratio
NCST	NetComposite Screening Tests
Ni-Ti	Nickel-Titanium
OPC	Ordinary Portland Cement
PC	Polymer Concrete
PET	Polyethylene Terephthalate
PETr	PET Removed Specimen

PIC	Polymer-impregnated Cement
PP	Polypropylene
PPCC	Polymer Portland-cement Concrete
PVC	Polyvinylchloride
RC	Reinforced Concrete
RILEM	Réunion Internationale des Laboratories d'Essais et de Recherches sur les Matériaux et les Constructions.
SDA	Strong Discontinuity Approach
SLS	Standard Linear Solid
SLV	Standard Linear Viscoelastic
SM	Shape Memory
SMA	Shape Memory Alloy
SMP	Shape Memory Polymer
TMA	Thermo-mechanical Analyser
TPA	Terephthalic Acid
W/C	Water/Cement
WLF	Williams-Landel-Ferry
WPP	Woven Polypropylene
XFEM	Extended Finite Element Method
$\dot{e}_0$	Pre-exponential Factor
E_{TH}, E_1	Young's Modulus at High Temperatures
E_{TL}	Young's Modulus at Low Temperatures
E_{TOT}	Instantaneous Young's Modulus
T_0	Ambient Temperature
T_H	Lower Plateau Temperature
T_L	Upper Plateau Temperature
T_g	Glass Transition Temperature
T_m	Melting Temperature
k_B	Boltzmann Constant
α_T	Coefficient of Thermal Expansion
α_t	Shift Factor

$\bar{\varepsilon}$	Strain at Neutral Axis
ε_0	Pre-Strain
ε_c	Creep Strain
ε_c	Compressive Strain Capacity
ε_{loss}	Pre-Strain Loss
ε_s	Irrecoverable Strain
ε_s	Stored Strain
ε_{sh}	Free Shrinkage Strain
ε_t	Tensile Strain Capacity
ε_{ve}	Viscous Strain
ε_{ve0}	Initial Viscous Strain
ε_θ	Mid-interval Strain
η_H	Viscosity at High Temperatures
η_L	Viscosity at Low Temperatures
η_R	Long Term Viscosity
θ_η	Time Interval Parameter
σ_c	Creep Limit Stress
σ_{res}	Frozen in Stress
σ_y	Yield Stress
ϕ_f	Frozen Fraction
$\Delta G_1, \Delta G_2$	Barrier Heights
$\Delta H^\ddagger$	Enthalpy of Activation
$\Delta S^\ddagger$	Entropy of Activation
a,b,c,d	Material Parameters
b	Width
c	Specific Heat Capacity
dn	Simple Crack Depth
E	Young's Modulus
f_c	Compressive Strength
F_{red}	Reduced Load Vector
f_t	Tensile Strength
G_f	Fracture Energy

H	Planck's Constant
h	Depth
h_c	Convection Heat Transfer Coefficient
k	Thermal Conductivity
K_{cra}	"Beam-Hinge" Stiffness Matrix
K_e	Elastic Stiffness Matrix
K_H	Hinge Stiffness Matrix
k_{shr}	Crack Parameter (Shear)
L	Span
L_e	Elastic Element Length
M	Percentage Loss of Moisture
N	Number of Chains per Unit Volume in Network
P_p	Applied Polymer Pre-load
Q	Body Generated Energy
R	Gas Constant
t	Time
T	Absolute Temperature
w_c	FPZ Width
z	Layer Depth
α	Crack Depth Ratio
ζ	Maximum Strain Parameter
θ_H	Rotation at Hinge
ρ	Density
ω	Damage Parameter
Ω_c	Crack Parameter (Moment)
γ	Total Strain
ε	Strain
η	Viscosity
λ	Retardation Time
σ	Stress
τ	Relaxation Time
υ	Activation Volume

Chapter One: **Introduction**

1.1 Cementitious Materials

Cementitious materials are one of the oldest construction materials, with early examples including pozzolanic materials used in ancient Rome and in the Egyptian pyramids (Marusin, 1996) (although this is still disputed by some authors (Campbell & Folk, 1991)). The modern form of cement we know today was not discovered until the middle of the 19th century and is known as Ordinary Portland Cement (OPC). The versatility and strength of cementitious materials, such as mortar and concrete, have made it the most used man made material on earth, with some 2.5 metric tonnes of concrete used per person alive each year (van Oss, 2005).

Although concrete has a relatively high strength in compression (of between 20MPa and 60MPa for normal strength concrete and up to 200MPa for high strength concrete), it behaves poorly when under tension. The tensile strength is approximately 10 times smaller than the compressive strength, which causes great problems when flexural loading is applied. To overcome this weakness, steel reinforcement is commonly placed in the tensile region in order to carry the tensile forces, while the compressive forces are carried by the concrete.

Despite the fact that the design of reinforced concrete addresses cracking, and restricts cracks to defined limits, durability problems still arise in reinforced concrete structures (Richardson, 2002).

1.2 Major Problems with Cementitious Materials

1.2.1 Durability in Cementitious Materials

The issue of durability in concrete is one that has plagued material scientists and engineers alike since the first use of modern OPC concrete in structures. Concrete nearly always contains cracks, initially in the form of micro-cracks which can both coalesce to form a macro-crack and allow the ingress of harmful chemicals.

Present code based design methods assume that the development of macro-cracks does not become an issue until a specified crack width is exceeded. The crack width varies depending on the structure's use (BSI, 2004) and once exceeded, loss of durability becomes a problem. This may reduce the capacity of the structure and, in extreme cases, can lead to complete failure. It is often the ingress of harmful chemicals and the action of freeze-thaw in the crack that causes most damage. Chemicals can corrode the steel reinforcement, especially in applications where salt water or de-icing salts are present. Further issues include concrete spalling caused by the expansion of the steel as corrosion develops. Along with macro-cracks; spalling can be unsightly and discouraging for users. The effect of cracking is of particular importance in certain situations, for example the integrity of structures for nuclear applications and fluid retaining structures.

1.2.2 Sustainability of Cementitious Materials

Sustainability is another major issue with cementitious materials, which has only recently come to the forefront with concerns over climate change and the need to reduce carbon dioxide emissions. The production of a tonne of cement generates up to a tonne of CO_2, placing the cement industry as the third largest contributor of CO_2 in the world, generating 8% of all worldwide emissions (Energy Efficiency News, 2008). In addition to this environmental sustainability issue; is the economic sustainability of concrete structures. Such structures require periodic inspection and maintenance which can come at great cost both financially and with time. Such inspection is often dangerous and in some cases virtually impossible; as access to certain areas of modern innovative structures can be difficult. It also leads to an issue of social sustainability with structures and highways being closed for inspection and maintenance causing congestion and nuisance for the general public. Furthermore, "damaged concrete infrastructure accounts for 30% of all road fatalities in the USA" (Li et al., 2004), highlighting another major social sustainability issue.

1.3 Existing Solutions – Overcoming the Durability Issue

Currently design engineers overcome durability issues by either preventing cracks with the use of pre-stressing techniques or by limiting crack widths to acceptable levels by the provision of appropriate reinforcement with the necessary cover. Such pre-stressed solutions include both pre- and post-tensioning techniques, which put structural members into a state of compression and thereby reduce the potential for tensile cracking to occur. The other, more common, approach involves designing the size, spacing and distribution of reinforcement such that cracks are not wider than a specified limit, which is typically 0.3mm for standard concrete structures (BSI, 2004).

In addition, despite being a conceptually valid solution, pre- and post-stressing has been seen to contain cracks. Thus highlighting that the issue of durability is still one that plagues engineers who have to resort to a policy of regular inspection and maintenance to ensure cracking does not become a serious problem. Inspection itself is not always possible and is often dangerous and disruptive, and cannot be 100% guaranteed as it relies on human perception and experience. Furthermore, inspection only occurs in specified programmes and defects can go unnoticed between inspection periods in addition to being very costly. A variety of repair methods have been developed and are now in regular use; these include techniques in which resin and/or grout are injected into macro cracks, bolting or gluing fibre reinforced strips to the tension face of flexural elements and other forms of commercial patch repair such as Tarmac CEMROK/AM (Tarmac, 2007).

In the last 20 years, material scientists and engineers have turned their attention towards smarter materials such as shape memory and self-healing materials. The development of self-healing materials is a very interesting concept and its popularity among researchers was seen at the 2nd International Conference on Self-Healing Materials, which saw over 150 papers presented. The inaugural conference 2 years prior had approximately 100 papers submitted showing the rapid increase in interest in the research area. Self-healing cementitious materials have also gained public attention on the Radio 4 "Materials World" show (BBC Radio 4, 2010). Self-healing materials have the ability to respond to damage and, as seen in nature, repair themselves. It is the concept of self-healing materials that will form the basis of this thesis.

1.4 Motivation for the Research

The motivation for this research is the development of a more sustainable cementitious material which reduces the requirement for regular inspection and maintenance. As mentioned previously, self-healing materials offer such a solution. This thesis will investigate the development of a new material system called LatConX, which has been developed at Cardiff University.

1.4.1 Proposed Novel Solution – The LatConX Concept

The new and innovative system that is proposed is subject to a patent pending (University College Cardiff Consultants Limited, 2007) and is the result of collaborative work of a group of researchers at Cardiff University. The system makes use of shape memory polymers (SMPs), which, when activated (e.g. under heat), shrink and induce a compressive force in the concrete.

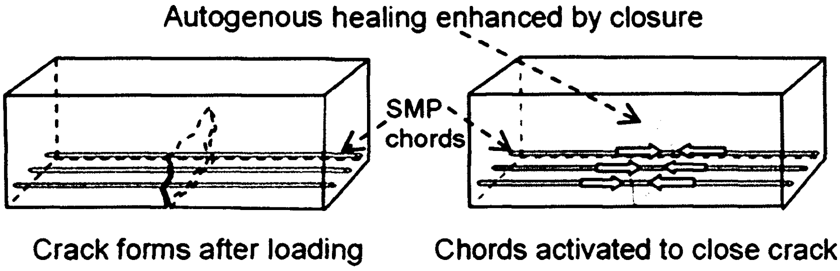

Figure 1.1 - LatConX System

Currently these SMPs are capable of applying a shrinkage-stress of between 20-80MPa (Liu et al., 2006), although stresses in excess of 80MPa have been recorded in polyethylene terephthalate (PET) filaments (Long & Ward, 1991). The system seen in Figure 1.1 is summarized as follows (Jefferson et al., 2010):

1. Cracking occurs in the cementitious material due to early age shrinkage and/or mechanical loading.
2. The shrinkage mechanism in the anchored embedded polymer tendon is activated by heating, which results in closure of the crack and compressive stresses being developed across the crack faces
3. Autogenous healing, which is enhanced by crack closure, serves to enhance the durability of the structural component and in effect cause self-healing.

The SMP tendons, that are either debonded or placed in a cavity in the cementitious matrix, are anchored at either end of the structural component. A suitable "off the shelf" polymer is polyethylene terephthalate called "Shrinktite" produced by Aerovac Industries, which produces a shrinkage-stress of approximately 32.5MPa (Weager, 2008).

The proposed LatConX system, enhances the natural autogenous healing abilities of concrete by using an autonomic system. The author has combined the two terms, autonomic and autogenous to create the new term *"autogenomic"*, to describe the LatConX system.

1.4.2 Numerical Simulation – The LatConX Concept

One of the primary aims of the present work was to develop a numerical model for the LatConX system. The model needed to be capable of:

- Simulating the development of shrinkage-stress with temperature in the polymer.
- Simulating the cracking behaviour of cementitious materials.
- Accurately simulating the coupling between the cementitious and polymeric components of the system.

A new model with the above capability was developed, as described in Chapter 6 of this thesis.

1.5 Scope and Objectives of the Research

The objectives of the research presented in this thesis are to:

- Develop a viable approach using SMPs for closing and/or preventing cracks in cementitious materials
- Characterise the behaviour of the polymer component
- Develop a numerical model to simulate the SMP behaviour
- Evaluate the response of the combined polymer-cementitious composite system
- Develop a numerical model for the combined system

1.6 Outline of the Thesis

This thesis is divided into seven chapters with two appendices. Chapter 2 reviews the current literature on self-healing materials and the various methods adopted for cementitious materials. It also explores solutions for producing more sustainable concrete. A review of work on the thermal shrinkage behaviour of shrinkable polymers is presented, which covers both experimental and numerical aspects.

Chapter 3 reviews the experimental work to date that has been carried out by the author and co-workers at Cardiff University on the development of the LatConX concept. This includes the proof of concept work (Jefferson et al., 2010) and a study which aimed to enhance natural autogenous healing in the material system (Isaacs et al., 2010).

A detailed overview of the experimental work carried out by the author on shrinkable polyethylene terephthalate (PET) material is given in Chapter 4. The work details preliminary studies carried out to identify a suitable polymer for LatConX and then describes a series of tests which explored stress development and the variation of Young's modulus with temperature and the effect of heating rate on both of these parameters. Geometric effects were also studied. This work, along with the associated numerical work described in Chapter 5, has recently been published in "*Applied Polymer Science*" (Dunn et al., 2011).

A new transient thermo-mechanical model for the shrinkage behaviour of PET is presented in Chapter 5, which was developed using the experimental data presented in Chapter 4. Results from other authors are also considered and finally the model is validated using experimental data not used for the calibration of the model functions.

Finally, a numerical model for the complete LatConX system is developed and presented in Chapter 6. This uses beam elements with embedded discontinuities to model the behaviour of the cementitious beams, to which are added an axial prestressing element, the behaviour of which is governed by the new polymer model. The model is successfully validated against the data presented in Chapter 3. A thermal analysis is also presented for the LatConX system. The work contained within Chapter 6 has also been prepared for submission for publication. Conclusions and recommendations for future work are given in Chapter 7.

Chapter Two: **Literature Review**

This literature review considers the development and use of self-healing materials for use in the construction industry. Particular focus is given to the background to the new LatConX system.

Sustainability issues of cementitious materials are considered and solutions discussed. A brief introduction to concrete and the important processes of creep and shrinkage is given. A review of the use of polymers in concrete is also presented.

Some basic polymer science relevant to the LatConX concept, such as shrinkage and temperature behaviour is discussed. Experimental and numerical techniques for polymers are considered here but a detailed review of numerical modelling of these materials is left until Chapter 5.

Other work relevant to the LatConX system, such as the use of shape memory alloy bars in concrete, is also reviewed.

2.1 Advanced Composite Materials – An Introduction

The area of advanced material science is wide and varied; a brief overview of the basic terminology will be given to highlight the position of self-healing materials in the wider context of developments in advanced materials. The definitions are based upon those proposed by Joseph (Joseph, 2008) and a "State of the Art Report (STAR)" produced by a RILEM committee on self-healing in cementitious materials, of which the author is a member (RILEM, 2009).

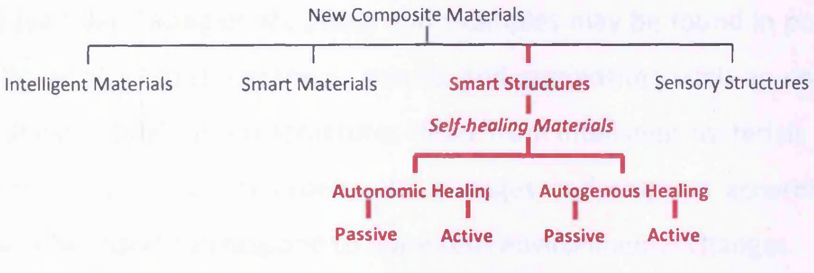

Figure 2.1 - Tree Diagram Highlighting New Advanced Composite Materials

Figure 2.1 shows the breadth of new advanced composite materials and identifies 4 key strands; intelligent materials, smart materials, smart structures and sensory structures, which will now each be considered.

2.1.1 Intelligent Materials

Many natural materials such as living human tissue can be classed as intelligent materials. They not only have the ability to sense and respond to various external stimuli but also repeat this over and over without a loss of function (Takagi, 1996). Schmets (Schmets, 2003) discusses how scientists can learn from nature and develop man made intelligent materials that can adapt to their environment. Mihashi et al (Mihashi et al., 2000) states that this is a consequence of their highly organised structure. Such attempts have been made by the group of Professor Aksay at Princeton who have simulated the clotting process of the human body (Trau et al., 1997). However, due to the complexity of such materials they are currently not used in practice and only exist at the concept stage, mainly in the areas of medicine, bionics and aeronautics (Joseph, 2008).

2.1.2 Smart Materials

Smart materials are engineered materials which, under the effect of a particular change in their environment, have the ability to respond in a unique and beneficial manner. Examples of such materials include interactive film layers, shape memory materials, piezoelectric materials and magnetostrictive materials (Sharp & Clemena, 2004). The difference between a smart and an intelligent material can be defined by the degree to which the material gathers, processes and responds to information (Joseph, 2008).

2.1.3 Smart Structures

Smart structures are those which exhibit the sensing and actuation properties of smart materials, but are engineered composites of conventional materials. Self-healing materials are in this category (van der Zwaag et al., 2009) and examples may be found in polymers (Chen et al., 2002) (White et al., 2001), ceramics, metals and composites such as concrete (van der Zwaag, 2007) (Ghosh, 2009). Smart structures differ from intelligent materials in that they are designed to sense only certain environmental changes and respond accordingly. Intelligent materials on the other hand can respond to numerous environmental changes.

The first manufactured self-healing material was a passive autonomic system employed in polymers by Prof. White at University of Illinois (White et al., 2001). The system utilises microcapsules containing liquid monomers and catalyst particles randomly dispersed throughout the system. The system can be seen in Figure 2.2 in which; (a) a crack develops, (b) the microcapsule ruptures releasing the healing agent (liquid monomer) and filling the crack, (c) the liquid monomer then reacts with a catalyst particle and polymerises the monomer, therefore healing the crack.

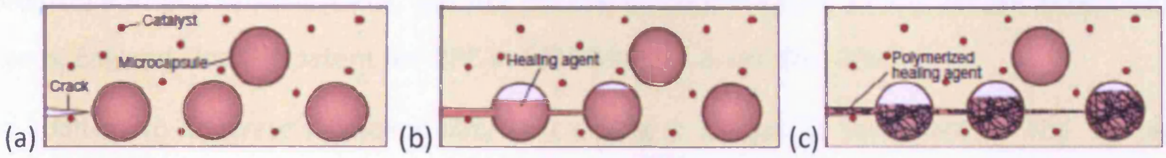

Figure 2.2 - Self Healing Polymer System (White et al., 2001)

2.1.4 Sensory Structures

This final category of advanced materials includes those materials that have the ability to sense a change in their environment but lack the ability to act upon it. Examples include smart paints which contain silicon-microsphere sensors that enable monitoring of their condition. Another example is the "smart brick" that monitors temperature, vibration and movements within buildings (Joseph, 2008). However, in order for a response to be made to such a change, a separate non-related process will have to be implemented if the change requires an action.

2.2 Towards a More Sustainable Cement Industry

Concrete is a quasi-brittle material and as such often contains cracks. In compression, traditional concrete has strengths which range between 20MPa and 60MPa and rises to between 150MPa and 200MPa in high strength concretes. Very high performance cement-based composites have been produced with compressive strengths of 800MPa (RILEM, 2009). However, in tension, concrete behaves very poorly, with tensile strengths rarely exceeding 10% of the compressive strength (Neville, 1995). It is for this reason that concrete structures are reinforced in the tension zone. Generally, the reinforcement controls, rather than prevents, cracking and thus many reinforced concrete elements are cracked under working loads. All reinforced concrete (RC) structures are designed according to local design codes such as Eurocodes (BSI, 2004). Such codes specify that cover to reinforcement and partial load and material factors are applied to address cracking and can, in some instances, render structures overdesigned. Conversely, there remain inadequacies in the design process since failure of the concrete cover still accounts for 90% of durability problems (van Breugel, 2009).

Despite its clear drawback in resisting tensile loads, concrete is the most widely used construction material on earth and its use dates back to ancient times. McLeod (McLeod, 2005) reports that twice as much concrete is used worldwide than the total of all other building materials. Despite its ancient origin, the modern concrete used in our structures, made using ordinary Portland cement (OPC), was not discovered until the early 1800's. Joseph Aspdin from Leeds, England filed the patent for OPC in 1824 (Hendrik & van Oss, 2005).

In addition to concrete's susceptibility to cracking is its lack of sustainability. The two are interrelated as cracking can reduce the life of a structure. Furthermore poor manufacture, aggressive environments and poor maintenance can severely weaken concrete and ultimately cause failure.

2.2.1 Current Sustainability Issues

2.2.1.1 Environmental Sustainability

Cement acts as the binder in concrete and provides the strength, however it has the greatest environmental impact (RILEM, 2009). Calcination (0.55 tonnes of CO_2 per tonne cement) and the fuel consumption required to power the kiln (0.4 tonnes of CO_2 per tonne cement) combine to produce approximately a tonne of CO_2 for every tonne of cement produced (McLeod, 2005). In light of the fact that $2.3x10^9$ tonnes of cement is produced each year (Taylor et al., 2005), this makes the cement industry the 3rd largest global contributor of CO_2 in the world. Not far behind the transportation and energy generation sectors (McLeod, 2005) and ahead of the aviation industry (2%) (Pearce, 1997). The annual contribution of the cement industry is around 8% of all worldwide emissions (2008 Figures) (RILEM, 2009) up from 5% in 2001 (Worrell et al., 2001).

2.2.1.2 Economic Sustainability

Concrete has a major economic impact. In the UK 45% (£40billion) of the annual spend on construction is on maintenance, as seen in Figure 2.3 (Department of Trade and Industry, 2006). This is reflected around the world, with a very large proportion of the maintenance spend being on concrete structures (RILEM, 2009). However this only considers the direct costs, when indirect costs are considered, such as traffic jams and related loss of productivity, the figure can be expected to increase 10 fold over the life of a structure (Freyermuth, 2001).

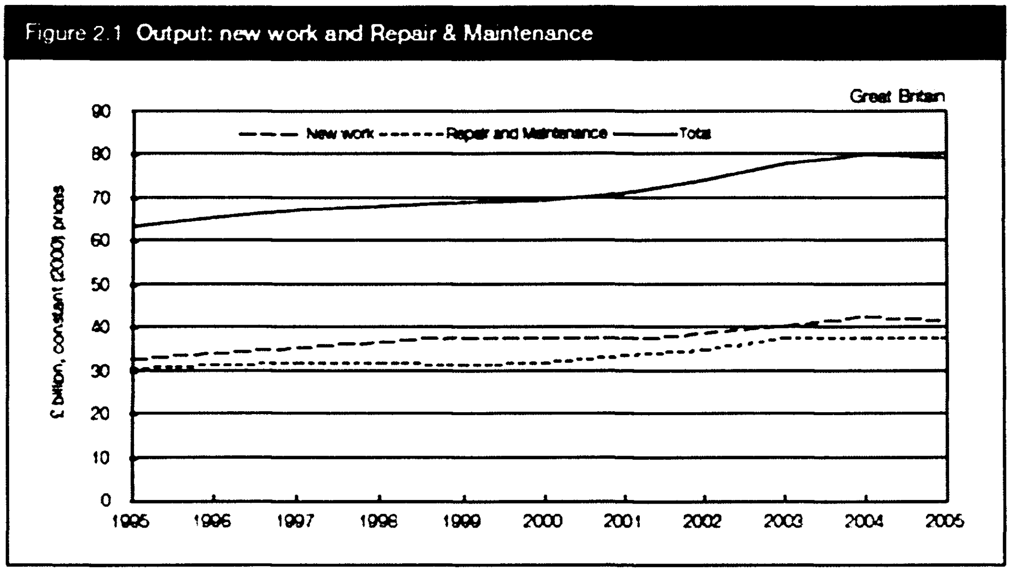

Figure 2.3 - Construction Spend in UK 2006 (Department of Trade and Industry, 2006)

2.2.1.3 Social Sustainability

Social sustainability issues include public nuisance caused by maintenance and inspection and reduced safety for the general public due to a poorly maintained highway infrastructure. For example in 2000, 30% of all traffic fatalities in the USA were due to inadequate road conditions (Li et al., 2004).

2.2.1.4 Future Issues

The demand for cement is increasing year on year and with the emergence of an increased demand from developing countries, the demand is set to increase further as can be seen in Figure 2.4. Taylor (Taylor et al., 2005) suggests that cement demand is closely linked to economic growth; in Europe and North America this has been relatively constant at 40kg of cement per US$1000 of GDP since the 1970s. However this is far greater in areas such as China who accounted for two-thirds of global growth in cement demand between 1998 and 2004.

The developing markets of China, the Middle East and India where this demand is increasing are more open to innovative technologies that aim to overcome such issues as sustainability, making their increased demand an ideal opportunity to produce innovative "Green Concrete" (Duxson et al., 2007). Furthermore, the discussions of the Copenhagen Conference have put more pressure on nations to reduce emissions (United Nations, 2009).

There are three major proposals for a more sustainable concrete; improving the out-dated production methods, improving the material technology to allow less cement to be used and finally prolonging the working life of structures. These issues are not new in the field of concrete technology and many solutions have been proposed to overcome them. Some are now standard practice in civil engineering, such as pre- and post-tensioning, cement replacement materials and geopolymer cements, which will now be discussed. However if the environmental impact is to be reduced further, a step away from traditional construction methods is required.

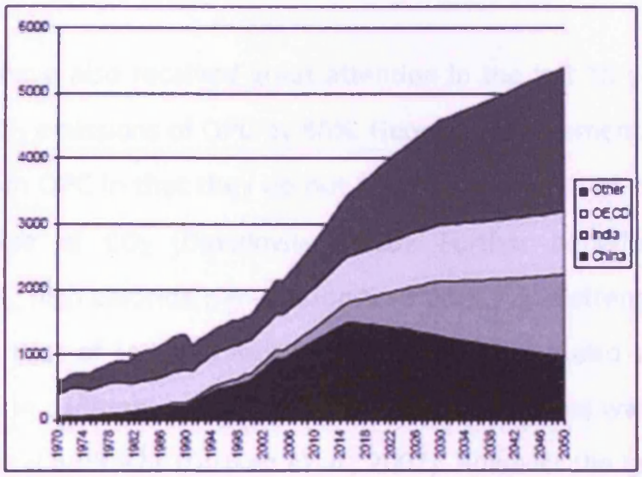

Source: USGS and IEA

Figure 2.4 - Global Cement Demand by Region and Country (1970-2050) (Taylor et al., 2005).

2.2.2 Existing Solutions for a "Green Concrete"

The move toward a more sustainable manufacturing process began following the OPEC oil embargo in the mid-1970s, which forced the cement industry to reduce its dependence on oil and improve its energy efficiency. Since then there have been various advances in the manufacturing process, however not all companies around the world have the capital available to introduce the most energy efficient manufacturing processes. It is likely to be a long process as new equipment replaces old and out of date machinery (Gartner, 2004).

This thesis concentrates on material development and increasing the durability of concrete. Recently cement replacement materials have gained much attention from material scientists. In so-called blended cements a portion of the clinker is replaced with either an industrial by-product such as coal fly ash or blast furnace slag, or a natural pozzolanic material such as volcanic material. These products are blended with the ground clicker to produce a homogenous product. Such blended materials can achieve the same, if not greater strength, than that of OPC and also produce less CO_2 as they are either natural or by-products of industry (Hendriks et al., 1998). However, the issue of availability is a major problem, unlike limestone which is the most widely available material on earth (Gartner, 2004), the location of such by-products and natural materials is sparse. Therefore, the cost of blending and thus economic viability of using cement replacement materials strongly depends on the transportation costs, which can also counter balance the environmental gain of using cement replacement materials (Worrell et al., 2001).

Geopolymer cements have also received great attention in the last 15 years as they have the ability to reduce the CO_2 emissions of OPC by 80%. Geopolymeric cements are manufactured in a different manner from OPC in that they do not rely on calcination of calcium carbonate and the subsequent release of CO_2 (Davidovits, 2010). Further benefits include lower kiln temperatures than OPC, high chloride penetration resistance, rapid strength development (that does not come at the cost of reduced long-term properties) and also superior chemical and mechanical properties. In addition, geopolymer concretes require less water and do not require superplasticising chemical additives (Duxson et al., 2007). However the take up by industry has been plagued by a lack of durability data and difficulties of compliance with regulatory standards in Europe and North America regarding cement content (Duxson et al., 2007). The lack of practical acceptance of such an innovative solution is rooted in the conservative nature of the construction industry, something that may affect new developments in the construction industry, such as LatConX. This conservative nature was not helped by the issue of High Alumina Cement Concrete (HACC) in the early 1970s which saw a seemingly innovative new material concept end in disaster, with several collapses (Currie & Crammond, 1994).

Scientists at Imperial College London have developed a concrete which actually absorbs CO_2 from the atmosphere. The cement used contains magnesium oxides and scientists have developed a method for converting magnesium silicates which are readily available into the required magnesium oxide. The production process requires lower temperatures and does not produce any CO_2 during the reaction process. Although OPC itself does absorb CO_2 as it hardens, this only amounts to between 0.2 and 0.5 tonnes per tonne of cement which itself generates 1 tonne of CO_2 during manufacture. Whereas the cement developed at Imperial College London absorbs 1.1 tonnes of CO_2 during hardening and only emits 0.4 tonnes during manufacture (Kennett, 2009).

McLeod (McLeod, 2005) describes numerous alternatives to cement which have the same properties but reduce the CO_2 produced. Such examples include Limecrete, which is made by mixing lime with a suitable aggregate and has the ability to reabsorb CO_2 by carbonation during their prolonged setting process. A further example includes CeramiCrete which combines magnesium oxide with a phosphate, which although still emits CO_2, it is much stronger and hence less is required.

A more widely accepted method of crack prevention and hence enhanced durability is that of pre-stress by pre or post tensioning. These pre-stressed structures are designed to be uncracked under serviceability loading, although in recent times there have been problems with the durability of such structures (Richardson, 2002). The major problem with the pre-stressed system is that steel tendons are relatively expensive and require expensive anchors and jacking operations, which themselves also pose a health and safety issue. Recently a solution to overcome these safety issues has been to employ shape memory alloys, which, if embedded in the concrete, can generate the required stress to post tension the concrete without the need for expensive and dangerous jacking operations (Saiidi et al., 2007) (El-Tawil & Ortega-Rosales, 2004) (Janke et al., 2005) (Maji & Negret, 1998). A detailed explanation of this system along with its benefits and drawbacks will be given in a later section.

A final area of research into a more sustainable concrete has been that of self-healing cementitious composites.

2.2.3 Self-healing Cementitious Composites

The development of self-healing cementitious materials has recently generated significant interest, which to this date has focused both on the natural ability of hydrates to heal cracks over time (autogenic) and artificial means of crack repair that are man-made inclusions (autonomic) (RILEM, 2009).

2.2.3.1 Autogenous Healing of Cementitious Composites

Knowledge of the natural healing within concrete, termed autogenous healing, has been understood for many years and dates back to studies at the French Academy of Science in 1836

(Hearn, 1998). Cracks in old concrete structures such as Roman aqueducts and gothic churches have been seen to heal when moisture interacts with unhydrated cement clinker in the crack. The hydration of the cement pastes causes precipitation of calcium carbonate which subsequently blocks the flow paths and thus heals the crack (Edvardsen, 1999). However in recent structures the cement content is reduced due to modern construction methods and hence the amount of available unhydrated cement is lower (van Tittelboom & De Belie, 2009).

Numerous authors have investigated the effect of differing conditions on the ability of cementitious materials to undergo autogenous healing. One of the main focuses has been on the use of cement replacement materials to enhance autogenous healing (van Tittelboom & De Belie, 2009) (Ahn & Kishi, 2009) (Copuroglu et al., 2009) (Qian et al., 2009) (Ramm & Biscoping, 1998) (ter Heide & Schlangen, 2007) (Reinhardt & Jooss, 2003).

Ahn & Kishi (Ahn & Kishi, 2009) have investigated the use of a three part system which incorporates 90% OPC, 5% geo-materials and 5% expansive agent in healing a 0.2mm crack in 28 days as seen in Figure 2.5. It was found that aluminosilicate materials and various modified calcium composite materials significantly affected the self-healing ability.

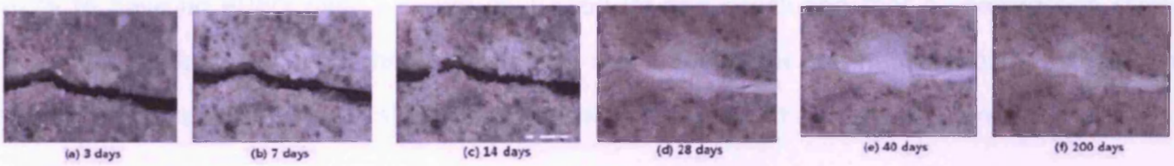
(a) 3 days (b) 7 days (c) 14 days (d) 28 days (e) 40 days (f) 200 days

Figure 2.5 - Development of Autogenous healing in three component system by Ahn (Ahn & Kishi, 2009)

Van Tittelboom & De Belie (van Tittelboom & De Belie, 2009) investigated the effect of blast furnace slag (BFS) and concluded that increased self-healing can be achieved by both increasing the ratio of BFS and also reducing the water to binder ratio. Ter heide & Schlangen (ter Heide & Schlangen, 2007) also investigated the use of BFS as a replacement to OPC, however they found that the healing process in OPC occurred much quicker than in BFS, although following a curing period of 15 days both achieved a similar recovery.

Qian et al (Qian et al., 2009) investigated the effect of water and air on the self-healing abilities of 'Engineered Cementitious Composite (ECC)' developed by Li et al (Li et al., 1998). They found that water curing (65%-105% recovery) was more successful than air curing (40%-62%) with regard to deflection capacity. Qian et al proposed that it is the lack of ability of air-cured samples to leaching of calcium carbonate and/or calcium-silicate-hydrate (CSH) from the bulk material into the crack that is responsible for its inability to self-heal. Earlier studies by Edvardsen (Edvardsen, 1999) and Clear (Clear, 1985) agreed with the requirement of water to enhance autogenous healing.

Ramm & Biscoping (Ramm & Biscoping, 1998) studied the water permeability of reinforced concrete and proposed that the reduction in water permeability with time was due to further hydration of concrete, expansion of concrete in the cracks and crystallisation. Further reduction in permeability was proposed by Ramm & Biscoping as being due to solid matter in the water and particles from the crack face which act to block the flow paths and enhance autogenous healing. However ter Heide & Schlangen (ter Heide & Schlangen, 2007) defined this as "self-tightening", a mechanical action, as opposed to "self-healing" which they refer to as the chemical action.

Studies carried out by Reinhardt & Jooss (Reinhardt & Jooss, 2003) found that lower crack widths and increased temperatures enhanced the self-healing ability of concrete. Comprehensive studies by ter Heide & Schlangen (ter Heide & Schlangen, 2007), found the crack width to have no effect over a range of 20-150μm and concluded that a compressive stress across the crack face of 0.5N/mm^2 is beneficial in increasing the self-healing ability, but further compressive strength although slightly beneficial has little effect as seen in Figure 2.6.

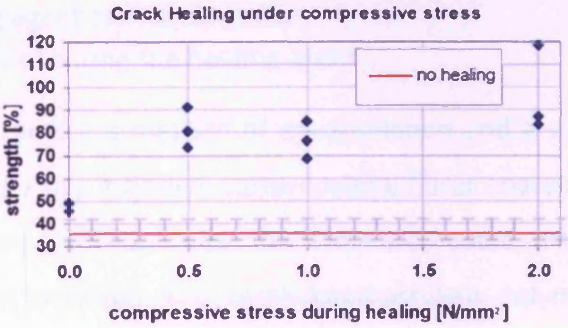

Figure 2.6 - Relative Strength after Crack Healing for Various Compressive Stress Values (ter Heide & Schlangen, 2007)

The effect of the age of the first crack was found to also influence the self-healing potential of concrete, with a decrease in strength recovery with age of first crack (ter Heide & Schlangen, 2007). It is reasoned that this is due to the level of hydration that has already taken place and although older concrete still has potential for hydration it is very limited relative to "fresh" concrete.

In summary, the self-healing capability of the LatConX concept can be enhanced by ensuring that a small crack width preferably under compression (approx 0.5N/mm^2) in a wet environment and at an early age is present. Cement replacement material may also benefit LatConX.

2.2.3.2 Autonomic Healing of Cementitious Composites

Manufactured, man-made self-healing materials are known as autonomic materials and fall into two classes; active or passive; depending on the healing mechanism employed. 'Passive Mode' structures have the ability to react to an external stimulus without the need for human intervention, whereas 'Active Mode' structures require the intervention of humans in order to undertake the healing process. Both modes have benefits and drawbacks relating to the economic benefits of excluding human interaction and the higher degrees of control exercised by humans. Autonomic self-healing cementitious systems were pioneered by Dry at University of Illinois who proposed 6 components of such materials (Dry, 1994):

a. An internal deterioration, e.g. a crack
b. A stimulus to release healing agent
c. A fibre
d. A coating or fibre wall which responds to the stimulus
e. A healing agent contained in fibre
f. A method of curing the healing agent

Such systems therefore require a method of encapsulation and a suitable healing agent. The active system proposed by Dry included polypropylene fibres coated with wax and filled with methylmethacrylate. Upon crack formation the fibres are heated, melting the wax coating and releasing the methylmethacrylate. The methylmethacrylate polymerises during secondary heating and thus heals the crack. The passive system proposed by Dry utilised the release of "crack-adhering adhesives" from brittle vessels upon crack formation due to rupturing of the vessel. In the years following the proposed concept in cementitious materials by Dry, various authors (Joseph, 2008) (van Breugel, 2009) (Mihashi et al., 2000) (van Tittelboom & De Belie, 2009) (Li et al., 1998) have investigated a variety of encapsulation methods and healing agents.

A variety of healing agents have been proposed in the literature, many of which are "off the shelf" due to their low cost and availability. The main healing agents used have been cyanacrylatates, alkali-silica solutions and epoxy resins. Joseph (Joseph, 2008) states that, such healing agents should be of "a low enough viscosity to enable them to spread over a wide area, but also strong enough to bond the surfaces of the crack." Two part healing agents have been investigated by van Tittelboom (van Tittelboom & De Belie, 2009) with each part in a separate brittle vessel that upon crack formation both rupture and cause mixing and subsequent healing.

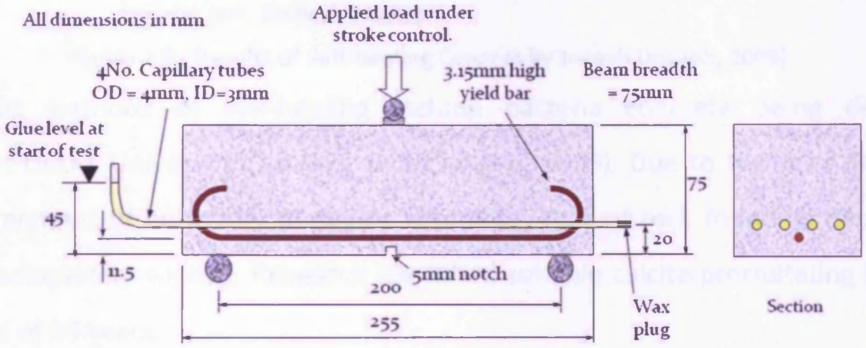

Figure 2.7 - Testing Arrangement for Continuous Flow System (Joseph, 2008)

Mihashi et al (Mihashi et al., 2000) proposed the use of glass pipes containing a crack repairing agent embedded in the cementitious matrix and also the use of microcapsules similar to those used in polymers (White et al., 2001). Li et al (Li et al., 1998) utilised glass capillary tubes containing cyanacrylycate and sealed with silicon. This concept was also investigated by Joseph (Joseph, 2008) who undertook a detailed series of experiments on a continuous flow arrangement, consisting of glass capillary tubes and a cyanoacrylate healing agent. The testing arrangement is seen in Figure 2.7 and consists of 4No. 4mmOD, 3mmID glass capillary tubes cast into a reinforced concrete beam. Joseph carried out a series of three-point bend tests in a three stage process; Stage 1 involved damaging the specimen with a 0.3mm crack which ruptured the glass capillary tubes and released the healing agent, Stage 2 was a 24 hour healing period after which Stage 3 loading was undertaken. Stage 3 loading involved loading the beam to a central deflection in excess of 3mm, hence to failure.

It was found that the beams were capable of additional load during Stage 3 damage, highlighting that not only had the beam healed but had also gained strength. These results are seen in Figure 2.8 and highlight its success.

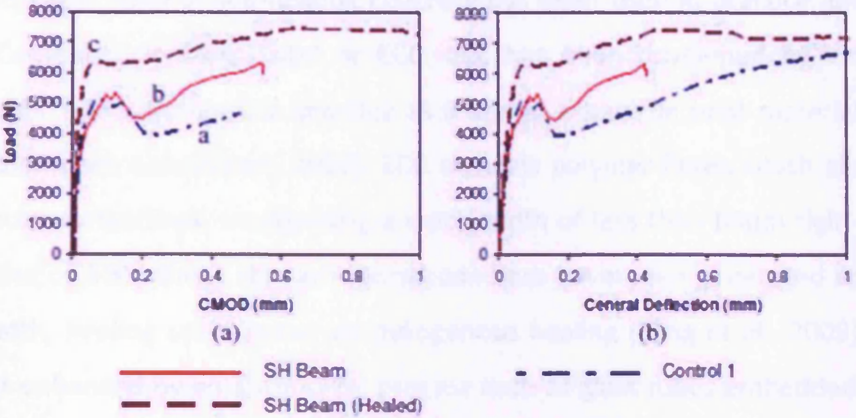

Figure 2.8 - Results of Self-healing Concept by Joseph (Joseph, 2008)

Other notable methods of self-healing include bacteria concrete being developed by researchers at DELFT University (Jonkers & Schlangen, 2009). Due to the very dry and highly alkaline environment of concrete, it closely resembles that of rock found at depth on which bacteria can adequately survive. Research identified suitable calcite-precipitating bacteria that had a life span of 50 years.

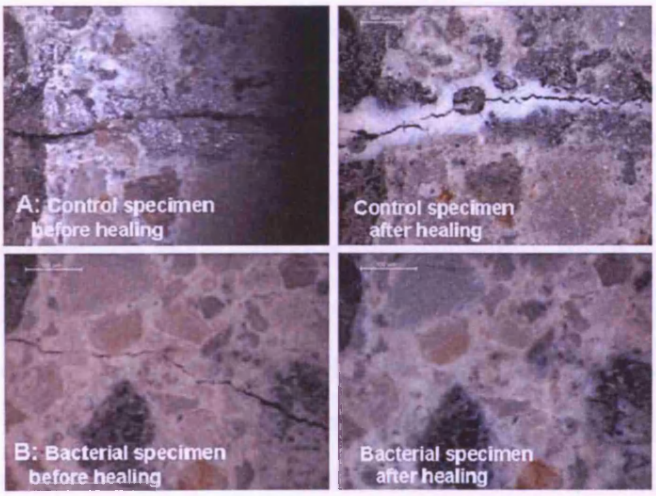

Figure 2.9 - Results of Bacteria Self-Healing Concrete (Jonkers & Schlangen, 2009)

Initial studies showed that this life span was reduced when embedded in concrete and therefore the bacteria were encapsulated within expanded clay particles to prolong their life. These expanded clay particles then replaced the 2-4mm aggregate in the concrete mix and upon formation of a crack were ruptured and released the bacteria. The bacteria then react with the oxygen in the crack and precipitate calcium carbonate (calcite) which acts as a bio-cement and heals the crack as seen in Figure 2.9.

At present, only one form of self-healing concrete has been used in practice and is known as 'Engineered Cementitious Composite' or ECC. ECC has been developed by Victor Li at the University of Michigan and used in practice as a bridge expansion joint material in Michigan, USA (Portland Cement Association, 2010). ECC contains polymer fibres which allow it to bend and crack in narrow hairlines, maintaining a crack width of less than 60μm right up to failure. Strain capacities of 300+ times that of normal concrete have been generated and due to the tight crack width, healing could occur via autogenous healing (Yang et al., 2009). This healing can be further enhanced by an autonomic process such as glass tubes embedded in the matrix and filled with a healing agent such as superglue (Li et al., 1998).

2.2.4 Economic Viability of a Sustainable Concrete – Potential and Constraints

As with any new technology there are both potentials and constraints related to its adaption by their particular industry, none more so than the "conservative" construction industry (Foresight Smart Materials Taskforce, 2004). The main driver for the development of a sustainable concrete is the environmental and economic benefits that could be achieved by enhancing the durability of concrete (Duxson et al., 2007). A further driver is that of health and safety, as a sustainable self-healing concrete is likely to be almost 100% maintenance free and hence reduces the risks associated with maintenance of dangerous and difficult structures. Van Breugel discusses the possibility of maintenance free concrete and, although he accepts 100% maintenance free is almost impossible, maintenance can be dramatically reduced (van Breugel, 2007). Despite the reduced maintenance seemingly providing sound economic viability it is difficult to convince owners to outlay a larger initial cost for a long term saving (Foresight Smart Materials Taskforce, 2004). In an industry where low-cost and historical safety data are paramount and the appreciation of life cost is yet to catch on among clients, the introduction of self-healing materials is a challenging one. Self-healing materials also have a high financial risk in their development and implementation (Duxson et al., 2007). Unlike materials in the high technology industries, such as ceramics, where it is low volume and high performance that offset the financial risk (Foresight Smart Materials Taskforce, 2004), the construction industry cannot afford this luxury.

The concept of the life cost of a structure is depicted in Figure 2.10 which highlights that with a more integrated design, construction and maintenance culture; self-healing materials become more attractive. Furthermore, as Figure 2.10 shows, such materials could also increase performance as they continually maintain themselves and do not require the regular maintenance of normal concrete, seen by the cost implications. Figure 2.10 also shows that self-healing materials will require some human maintenance but this will be very infrequent, again shown by the cost implication.

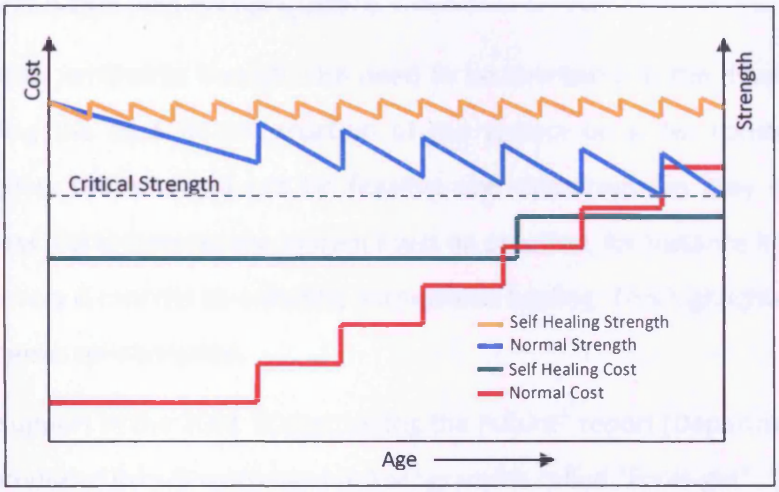

Figure 2.10 - Life Cost of Structures

Further benefits of zero or low maintenance structures include the decrease of indirect costs due to the loss of use during maintenance and a reduction, or even eradication, in monitoring and inspections (van Breugel, 2007). This will also lead to the requirement of fewer new structures and hence less raw materials and the associated sustainability issues. With the reduced requirement for new builds comes the reduced requirement for disposal of rubble from demolished structures, which has a beneficial environmental and economic impact (van Breugel, 2007).

The lack of long term data and the difficulties of compliance with regulatory standards in the Western world is a major constraint in the development of a sustainable concrete (Duxson et al., 2007). Such standards have been developed over many years in conjunction with companies supplying OPC based concretes, who for political/commercial reasons, may be adverse to the new materials.

The materials themselves must be capable of maintaining their self-healing ability throughout the life of the structure which is 50 years for buildings and 120 years for highway structures. It is therefore important that appropriate standards are developed for the new materials to aid their acceptance and encourage the construction industry to specify them in designs (Duxson et al., 2007). The potential for such opinion change is more likely in the Middle East, China and India where acceptance of new technologies is greater and the requirement for high performance materials is higher. There is also a big potential in cases where failure is extremely dangerous for example nuclear waste (van Breugel, 2007).

Non-market related constraints though, still need to be overcome in the development of such materials, including the ease of construction of the system on a live construction site. For example brittle glass tubes would not be feasible and microcapsules may break during the compaction process. Furthermore, the system must be practical, for instance it is not feasible to soak a structure every 6 months to enhance autogenous healing. This highlights the importance of industrial-academic collaboration.

There was great support in the 2001 "Constructing the Future" report (Department of Trade and Industry, 2001) produced by a Government led programme called "Foresight". The report stated as the first of its major recommendations, "the promotion of 'smart' buildings and infrastructure" and encouraged industry to "accelerate the introduction of new technologies, 'intelligent' products, standardised pre-assembled components and advanced materials into every level of the built environment."

2.2.5 Time dependent concrete behaviour

Although poor construction can have immediate effects, it usually leads to reduced durability and therefore causes problems in later years. Such methods of failure can include plastic shrinkage, drying shrinkage and thermal effects as will be discussed in the following section; notably creep and shrinkage.

2.2.5.1 Concrete Creep

Creep is the time-dependent strain development occurring in concrete placed under constant load conditions. The dual mechanism of creep is relaxation which is the time dependent stress reduction occurring in concrete held at constant deformation. Creep also shares many of its mechanisms with drying shrinkage which will be described in a later section. The theory of concrete creep has been understood for over a century with the work of Hatt in 1907 (Bazant, 2001) marking a beginning to an area of research that has received a great deal of attention. Particular attention was seen in the 1970's and 1980's when nuclear containment was a major concern (Idiart, 2009). Despite this detailed attention it is not yet fully understood (Bazant, 2001) (Idiart, 2009) and several mechanisms for creep have been proposed and some were later disregarded. Bazant and co-workers have been leaders in the field and have produced by far the most work on the subject. In his paper titled "Prediction of Concrete Creep and Shrinkage: Past, Present and Future" (Bazant, 2001), Bazant details long lists of proposed creep mechanisms and models to simulate the behaviour, such as the RILEM B3 model.

Such is the interest in predicting concrete creep, that a RILEM committee was established with the aim of collating all work on the topic, such as the "RILEM data bank". All numerical simulations must, in addition to conformation with physical phenomena, agree with this data bank. A detailed study into the accuracy of a variety of models in comparison to this data was carried out by Fanourakis (Fanourakis & Ballim, 2003), who concluded that of all code type models, the RILEM B3 model was the most successful and that the model provided in BS8110 (1985) accounted for extrinsic factors such as age, applied stress and relative humidity but not intrinsic factors such as concrete type, W/C ratio and air content.

Creep itself can be split into two superposed strains as summarised by Idiart (Idiart, 2009):

1. *Basic Creep*: Time dependant deformation under constant load occurring at relative humidity.
2. *Drying Creep*: Deformation in excess to basic creep strain observed when there is movement due to the lack of thermodynamic equilibrium in the environment.

Basic creep can be further split in to a short-term (approximately 1 year or less) and a long-term component to simulate the decrease in creep with age at loading (Bazant et al., 2004). It is the drying creep that has proved more difficult in its understanding. Initial work was carried by Pickett in 1942 to which the effect lends its name, "The Pickett Effect" (also known as drying creep) is the increase in creep in specimens undergoing drying (Altoubat & Lange, 2001). Various modifications of Pickett's work have since been undertaken and new theories proposed, however it has been the subject of much disagreement in the academic world. It is now though generally accepted that drying creep is the sum of two components; an intrinsic drying creep and a structural drying creep resulting from micro-cracking (Idiart, 2009) (Bazant et al., 2004) (Altoubat & Lange, 2001).

In addition to the two superposed strains proposed by Idiart (Idiart, 2009), Bazant et al (Bazant et al., 2004) also discuss a third creep component, that can be captured by the microstress buildup and relaxation, and is named the transitional thermal creep (transient creep increase with temperature change).

Two notable models are those of Bazant & Chern (Bazant & Chern, 1985) and Benboudjema (Benboudjema et al., 2005), although detailed reviews will not be given as they are out of the scope of this thesis. A review of code related derivations of creep has highlighted Eurocode 2 (BSI, 2004) as offering a simpler yet adequate determination of creep, seen in Appendix A.

2.2.5.2 Shrinkage in Concrete

There are four main classifications of shrinkage in concrete (Construction Civil, 2010), namely; (i) Plastic Shrinkage, (ii) Drying Shrinkage, (iii) Autogenous Shrinkage and (iv) Carbonation Shrinkage. Plastic shrinkage occurs early on when concrete is still in a plastic state and is believed to be caused by the evaporation and absorption of water causing a reduction in volume. Autogenous shrinkage accounts for approximately 10-15% of shrinkage and is really only applicable in the construction of mass concrete, such as dams (Neville, 1995). Such shrinkage occurs where no moisture movement is permitted and where temperature is constant. Carbonation shrinkage is a newly understood phenomenon in which CO_2 in the atmosphere reacts in the presence of water with hydrated cement to form calcium carbonate and causes shrinkage. Although at the same time it increases the strength and reduces permeability. It is however drying shrinkage that is of highest importance, especially in the LatConX system where temperature activation will increase the drying shrinkage of the concrete specimens.

Concrete gains and looses moisture with changes in the surrounding environment. Such a change causes the concrete to swell and shrink which if restrained, results in stresses in the material due to a variety of factors (Pickett, 1946) (Bisschop, 2002) (Asad et al., 1997) (Abbasnia et al., 2009). It is known that creep does act to relieve these stresses (Al-Gadhib et al., 2008). The rate and magnitude at which this moisture loss occurs is a function of the drying conditions (relative humidity, temperature and air-flow) (Bisschop, 2002). It is in particular the drying shrinkage of the cement paste that causes the overall drying shrinkage as the aggregate particles are generally of a greater stiffness than the cement paste and is generally only an issue in "green" concrete or in a condition of high moisture content (Sakata, 1983).

Bisschop (Bisschop, 2002) describes the various restraining effects that cause stresses to develop on three different length scales. The first is at the macro level where structural constraint due to construction causes restraint, the second at a mesoscale includes the steel reinforcement, aggregate restraint and self-restraint. Finally at a micro level the cement paste matrix itself is restrained internally by 'hard' phases such as unhydrated cement grains. The self-restraint is described by various authors and is the result of differential shrinkage throughout the section which itself is caused by the moisture gradient that develops in concrete specimens (Benboudjema et al., 2005) (Bisschop, 2002) (Abbasnia et al., 2009). The experimental measurements of drying shrinkage are very sensitive to specimen size and shape (Benboudjema et al., 2005) and the drying process begins at the exposed surface and gradually penetrates the concrete (Abbasnia et al., 2009).

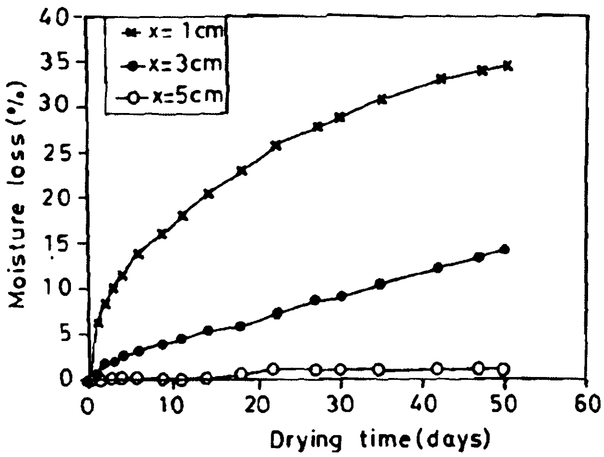

Figure 2.11 - Moisture Loss versus Drying Time at Different Levels (Asad et al., 1995)

Figure 2.11 shows the development of moisture loss with time for three different levels in the specimen and clearly highlights that at any given time moisture loss is considerably larger nearer the surface (Asad et al., 1997) (Asad et al., 1995). Similar results were recorded by Sakata

(Sakata, 1983), which shows that shrinkage (and hence moisture loss) increases rapidly near the exposed surface at early age and the rate decreases at 120 days while shrinkage at lower levels continues to increase.

The moisture contained within the concrete can be divided into three different types; (i) chemically bonded which has reacted with cement and part of the cement gel, (ii) physically adsorbed water occupies the gel-pores and (iii) free water which occupies capillary pores. The sum of (ii) and (iii) accounts for the evaporable water which can be removed from the cement paste by heating to 105°C (Bisschop, 2002). The main factors that affect the amount of evaporable water include W/C ratio, degree of hydration and whether the cement paste was allowed to absorb water. It is generally accepted that the loss of evaporable water is one of the major sources of moisture loss and hence shrinkage (Abbasnia et al., 2009). These can be manipulated to produce a mix composition that suits high temperature environments, such as in LatConX, to minimize shrinkage. Other sources of drying shrinkage include bulk shrinkage of the cement paste, capillary stress, changes in surface free energy and disjoining pressures. However, Bisschop (Bisschop, 2002) concludes that the basic nanoscale mechanisms of drying shrinkage have yet to be fully established.

The major relationship of importance to this thesis is that between moisture loss and shrinkage. It is widely accepted that shrinkage is approximately proportional to moisture loss although some authors believe that a linear relationship is sufficient and others propose a non-linear relationship. According to Pickett (Pickett, 1946), the flow of water in concrete is a diffusion equation and he solved a linear diffusion equation using Newton's law of heat transfer with exposed boundary conditions (Sakata, 1983). Benboudjema (Benboudjema et al., 2005) also adopts a linear relationship between drying shrinkage and moisture content, which he claims enables "a major part" of experimental results by Granger (Granger, 1996) to be described. However, many other authors propose a non-linear relationship due to the moisture diffusivity, a material property defined as the rate at which moisture flows through the material when a unit moisture gradient exists. The moisture diffusivity is highly moisture dependant and hence renders the equation non-linear (Asad et al., 1997) (Asad et al., 1995) (Abbasnia et al., 2009) (Al-Gadhib et al., 2008) (Sakata, 1983) (Bisschop, 2002). Furthermore, Suwito describes in detail the coupling effect of drying shrinkage and moisture diffusion (Suwito et al., 2006) and proposes a model in which the moisture capacity and humidity diffusivity are modified to include the effect of drying shrinkage on moisture diffusion. The effect of drying shrinkage on the humidity diffusivity is introduced using a Kachanov damage parameter and the effect on the moisture capacity utilises an analytical model based on non-equilibrium thermodynamics and minimum potential energy principle for a two-phase composite. Finally, the mechanical part of drying shrinkage is modelled as an elastoplastic damage problem and simulated using a finite element simulation.

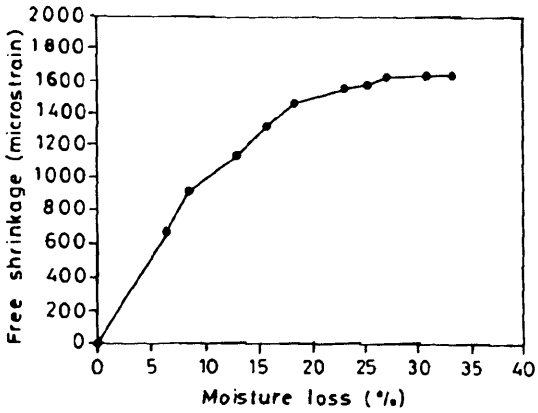

Figure 2.12 - Relationship Between Moisture Loss and Free Shrinkage Strain (Asad et al., 1995)

The moisture diffusion in a cementitious repair material as discussed by Asad et al (Asad et al., 1997) (Asad et al., 1995) and Al-Gadhib et al (Al-Gadhib et al., 2008) obeys the moisture diffusion equation given by Fick's second law, a key component of which is the previously mentioned moisture diffusivity. The authors go on to describe the undertaking of a free shrinkage versus moisture loss experiment at a depth of 1cm and found the relationship to be non-linear and based on a regression model which takes the following form equation (2.1) and is seen in Figure 2.12:

$$\varepsilon_{sh}(t) = \frac{M^{1.5}}{195 + M^{1.5}}(\varepsilon_{sh})^{\infty} \tag{2.1}$$

In which $\varepsilon_{sh}(t)$ is the free shrinkage strain at time t, M is the percentage loss of moisture and $(\varepsilon_{sh})^{\infty}$ is the ultimate free shrinkage strain. Both authors also give more detailed equations for moisture content at depth and develop finite element simulations of the moisture diffusion and stress development in restrained cementitious patch repair systems. Such a method was also discussed by Bazant and Najjar (Bazant & Najar, 1971).

Although Sakata (Sakata, 1983) also studied the moisture diffusion problem using non-linear diffusion theory, they concluded from experimental results that the relationship between moisture loss and shrinkage strain can be assumed linear in the vicinity of the exposed surface as seen in Figure 2.13. This does contradict the findings of Asad (Asad et al., 1997) (Asad et al., 1995), although this can be attributed to the specimen size and mix proportions. Asad uses cementitious mortar on small repair patches, whereas Sakata uses larger specimens with concrete mix containing OPC, crushed aggregate and marine sand. All the experiments investigating moisture diffusion used the same procedure of rendering the experiment one-dimensional by sealing 4 of the 6 sides with paraffin wax.

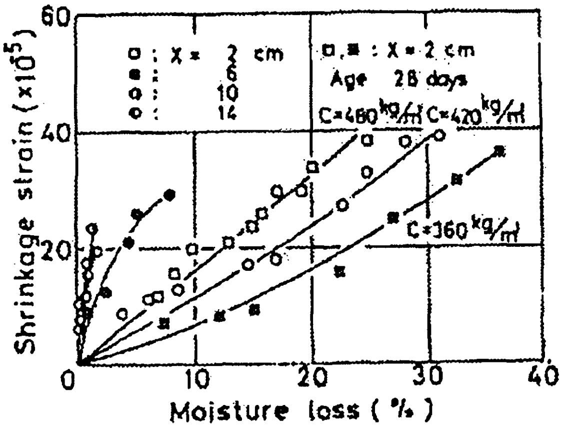

Figure 2.13 - Drying Shrinkage Strain versus Moisture Loss (Sakata, 1983)

A more comprehensive overview is given by Bisschop (Bisschop, 2002) in their PhD thesis which states that shrinkage strains are considerably higher during first period drying when compared to samples that are rewetted and dried for a second time, giving justification for irreversible shrinkage. Although not completely understood, a combination of changes in pore distribution and permanent rearrangements in the packing of CSH particles due to water distribution changes are possible causes. It is also proposed that the use of cement replacements such as blast furnace slag can help in reducing the drying shrinkage of cementitious composites. Bisschop gives a general overview graph for moisture loss versus shrinkage strain (Figure 2.14) which highlights four approximately linear domains. "Domains 1 and 2 are attributed to loss of water from capillary pores, domain 3 represents loss of absorbed water from the surface of CSH gel particles and domain 4 results from loss of water that contributed to the structure of CSH-gels" (Bisschop, 2002).

As seen in Figure 2.14 both relative humidity and moisture loss can be used interdependently when considering free shrinkage. However, most authors use moisture loss as it can be calculated simply by measuring the weight loss of the specimen (Benboudjema et al., 2005) (Bisschop, 2002) (Asad et al., 1997) (Abbasnia et al., 2009) (Sakata, 1983). The strains can be easily measured using a strain gauge or more simply using Demec readings (Asad et al., 1997). The use of weight loss though is only an approximation as the drying behaviour is non-uniform throughout the specimen (Bisschop, 2002).

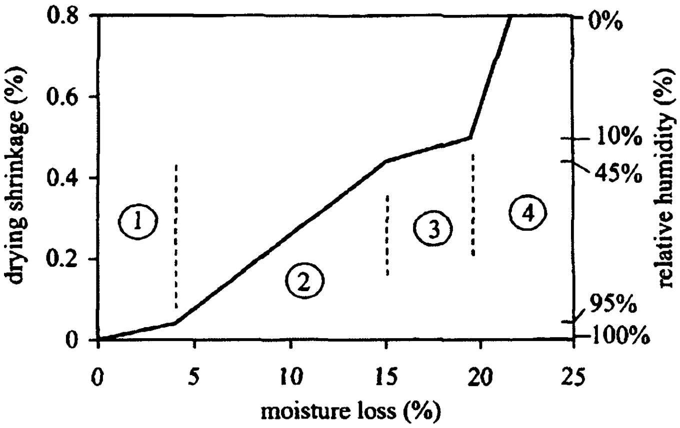

Figure 2.14 - Moisture Loss versus Drying Shrinkage Relationships for Hardened Cement Paste (Bisschop, 2002)

2.3 Polymers

The following section will introduce the important properties relevant to the proposed LatConX system such as orientation and crystallinity, the glass transition region, deformation behaviour, thermal behaviour and shrinkage. Further details into manufacture and processing will be given for polyethylene terephthalate (PET) as this is the chosen material for the LatConX system. An introduction to shape memory polymers (SMPs) is given as these were the motivation for the proposed system. Finally the existing uses in concrete are highlighted and discussed. It should be noted however that the author of this thesis approaches the understanding from a civil engineering background.

2.3.1 Brief History

Polymers have been understood in their natural form since the early 19th Century, with the development of man-made polymers coming in 1862 with Parkensite. The early 20th century saw important developments with Bakelite, nylon and polyethylene. It was not until the 1920s that the full and correct understanding of the structure of polymers was published by Hermann Staudinger (McCrum & Buckley, 1997). Since these early beginnings, polymers have become a vital part of society with materials such as nylon, polyethylene and silicone being produced in mass volumes and used in nearly every industry ranging from children's toys and medical applications to aerospace components and the electronics industry (McCrum & Buckley, 1997).

2.3.2 Factors Influencing Mechanical Properties

There are three factors that affect the mechanical properties of polymers, namely; molecular structure, processing and geometry (Klompen, 2005). Polymers are the result of the polymerization of individual chemical units called monomers (Ward & Sweeney, 2004), which causes the removal of the double bond in the monomer and allows long chains to form. Simple homopolymers which contain only a single repeated monomer, such as poly(styrene), are rarely found. More often they contain additives, such as chemical cross-linking which bonds the chains together to form a network (Sperling, 2006). The resulting polymer is called thermosetting as the cross-linking agent is normally activated by heating and upon further heating the polymer will not soften or flow. It should be noted that temporary cross-linking can also occur in linear polymers when very long molecules entangle, these are known as physical cross-links (Ward & Sweeney, 2004). An example of chemical cross-linking is the vulcanization of rubber with sulphur. A further less extreme complication is chain branching in which a secondary chain initiates from a point on the main chain. These branches can lead to considerable differences in the mechanical behaviour of polymers, for example high density polyethylene (HDPE) and low density polyethylene (LDPE). Another form of modification using additives involves the use of plasticizers which are small molecules added to soften a polymer by lowering its glass transition temperature or reducing its crystallinity and melting temperature. It is also known that the molecular weight has an effect on the flow properties and thus mechanical properties of polymers (Sperling, 2006).

2.3.3 Orientation and Crystallinity of Polymers

The degree of orientation and crystallinity are both important in determining whether the polymer is amorphous or crystalline or a proportion of both. Amorphous polymers form as the chains are "too irregular to permit regular packing" (Sperling, 2006). Crystalline polymers on the other hand are formed via crystallisation, although it is widely accepted that polymers are never 100% crystalline due to the inability of chains to completely disentangle and line up (Furness, 2001). Crystallization is a first order transition and in order for a polymer to undergo crystallisation the polymer must "have a regular structure, be at a temperature below the crystal melting point and sufficient time must be given for the long molecules to become ordered in the solid state." (Ward & Sweeney, 2004).

Crystal growth can be induced by cooling from melt or from a dilute solution (Cheremisinoff, 1989). Cooling slowly from melt tends to form sphere-shaped crystalline structures called spherulites, which grow and coalesce eventually forming "structures that pervade the entire mass of the material" (Sperling, 2006). Those formed from a dilute solution however tend to form lamellar-shaped single crystals whose structure can be varied by altering the concentrations (Cheremisinoff, 1989). The rate of cooling is a key parameter as rapid cooling will form disordered amorphous states, such as rapidly cooled polyethylene terephthalate (Ward & Sweeney, 2004).

The molecules of many amorphous state materials, if stretched, may align in the stretch direction and appear ordered, hence crystalline. This "orientation" must occur between the glass transition (T_g) and melting temperature (T_m) of the polymer (Abdel-Bary, 2003). These so called oriented amorphous polymers should not be confused as being crystalline, although some polymers may produce small regions of crystallites in addition to the molecular orientation. The class of materials containing amorphous and crystalline regions are named semicrystalline and it is the molecular regularity that determines the crystalline fraction. For example oriented PET has 30% crystallinity (Ward & Sweeney, 2004).

Under plastic deformation or drawing the crystalline region breaks down, with the remaining structure being a factor of the initial degree of crystallinity. Furthermore heating polymers above their crystal melt temperature (T_m) will result in an amorphous melt and complete destruction of the crystalline region (Sperling, 2006).

As crystallinity increases the stiffness, density, thermal properties and shrinkage all increase, whereas the impact strength and permeability both decrease (Kenplas Industry Limited, 2010) (Dusunceli & Colak, 2008).

2.3.4 Transition Regions in Polymers

The material properties of amorphous polymers are very dependent on the temperature; and at low temperatures they are glassy, hard and brittle, while at high temperatures they exhibit rubber elasticity (Sperling, 2006) and their chains become more flexible (Ward & Sweeney, 2004) (Cambridge, 2004). The region in between is known as the glass transition region and along with the glass transition temperature (T_g) is regarded as the most important material parameter (Mark et al., 1993). The increased flexibility of the chains at higher temperatures allow polymers to "adopt confirmations that lead to maximum entropy" (Ward & Sweeney, 2004) and thus shrink. The melting temperature is always higher than the glass transition temperature. This effect is also seen in semi crystalline polymers and although to a lesser degree the stiffness can vary by an order of magnitude (Ward & Sweeney, 2004).

Figure 2.15 highlights the 3 key regions; glassy region (1), glass transition (2) and rubbery region (3). Regions (4) and (5) are the rubbery flow and liquid flow regions respectively and along with secondary transitions, such as the liquid-liquid are out of the scope of this thesis (Sperling, 2006).

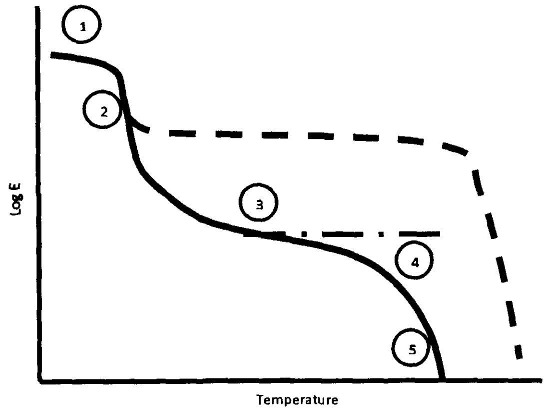

Figure 2.15 - Transition Regions in Polymers

In the glassy region, polymers are brittle and the Young's modulus is constant. The stiffness in this region relates to the changes in stored elastic energy on deformation that are associated with small displacements of the molecules from equilibrium positions (Furness, 2001). As the temperature increases and passes through T_g, the thermal energy within the chains allows them to rotate causing a decrease in Young's modulus and just a few degrees change in temperature will affect the stiffness of the material. Identification of this region is done using the glass transition temperature (T_g), which is often defined as the temperature where the thermal expansion coefficient undergoes a discontinuity (Sperling, 2006). Examples of such glass transitions have been presented by Furness (Furness, 2001), such as PET (T_g = 70°C, T_m = 265°C). Finally, Young's modulus plateaus again and the polymer behaves like rubber and can be stretched several hundred percent and still return to its original length when released. This behaviour continues until the melting temperature is reached. Behaviour does though vary between linear (solid line) and cross-linked (dashed line) polymers as seen on Figure 2.15 with the height of the plateau determined by the degree of crystallinity (Furness, 2001).

It has also been shown that transitions occur in the viscosity of the material as the temperature changes (Buckley et al., 1996) (Morshedian et al., 2005). This can be seen for glass in Figure 2.16 below.

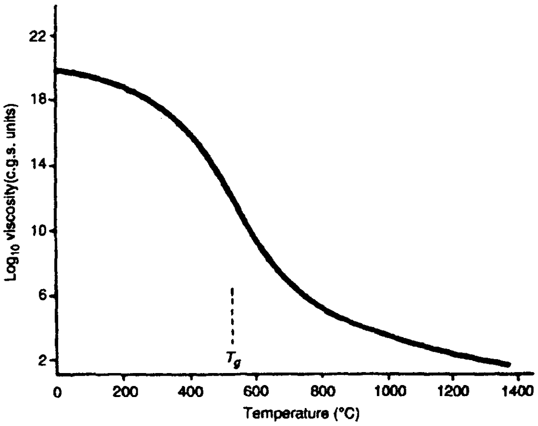

Figure 2.16 - Viscosity-Temperature Relation for Soda-Lime-Silica glass (Sperling, 2006)

2.3.5 Effects on Glass Transition Temperature

The glass transition region is affected by changes that influence the amorphous phase as the crystalline region does not undergo a glass transition temperature (Daniels, 1989).

Such changes include the molecular weight which as proposed by Fox and Flory (Fox & Flory, 1950) will increase T_g with increasing molecular weight. Daniels (Daniels, 1989) proposes that such an increase can be achieved by lightly cross-linking the molecules. Chemical cross-linking for example reduces the free-volume by bringing adjacent chains closer together thus raising T_g (Ward & Sweeney, 2004). Conversely, the use of lightweight polymers will reduce the T_g and can be achieved with the inclusion of a plasticizer (Sperling, 2006) (Ward & Sweeney, 2004).

Furthermore, a range of T_g in a single polymer can be achieved by varying the densities throughout (Daniels, 1989). This highlights the possibility of differential pre-stress within a tendon in LatConX. The density can also be increased by reducing the free volume through increased levels of crystallinity (Daniels, 1989), thus increasing T_g in the amorphous phase and Sperling (Sperling, 2006) therefore proposes a polymer has two values for T_g. One corresponds completely to the amorphous phase and the other to the extent of crystallinity which affects the amorphous phase. Pressure can also be used to decrease the free volume and hence density, therefore increasing T_g and as proposed by Daniels (Daniels, 1989), this is a linear relationship.

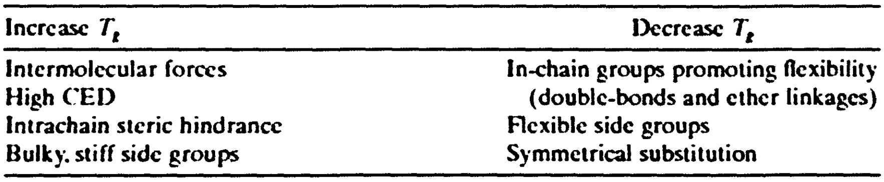

Increase T_g	Decrease T_g
Intermolecular forces	In-chain groups promoting flexibility (double-bonds and ether linkages)
High CED	Flexible side groups
Intrachain steric hindrance	Symmetrical substitution
Bulky, stiff side groups	

Figure 2.17 - Factors Affecting T_g (Sperling, 2006)

In general, anything that reduces the free volume or increases the energy required to onset a molecular motion increases T_g, examples can be seen in Figure 2.17.

It has been proposed though that T_g will alter with time and Sperling (Sperling, 2006) proposes three theories that highlight this; the free-volume theory, the kinetic theory and the thermodynamic theory. The Williams-Landel-Ferry (WLF) equation (Williams et al., 1955) proposes that a change of 6-7°C per decade if the free volume remains constant at 2.5%, which is widely accepted in the literature (Sperling, 2006) (Daniels, 1989).

2.3.6 Deformation Behaviour of Polymers

General deformation characteristics are summarised well by Buckley & Jones (Buckley & Jones, 1995), although the opinions of the most correct method of numerically simulating deformation differ between authors and the type of polymer and manufacturing process being simulated. Some believe that simple rheological models at the macro scale are adequate whereas others believe that microscale models are required. In general a model must account for time dependence, stress dependence and temperature dependence. Furthermore the entire history of stress and temperature are relevant along with the effect of physical ageing and mechanical rejuvenation (erasing the prior history through plastic deformation). The idealised deformation behaviour of a typical polymer can be seen in Figure 2.18. The plastic deformation (drawing) can be recovered by heating the polymer above T_g (Klompen, 2005), however if the polymer remains below T_g then molecules will become orientated and cause strain hardening.

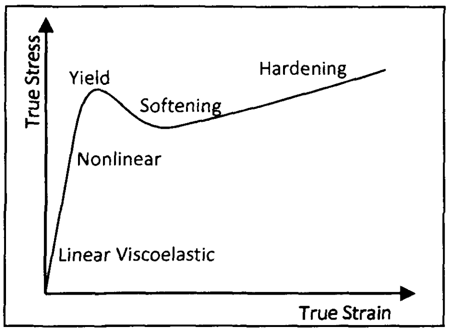

Figure 2.18 - Idealised Deformation Behaviour of Polymers

Klompen (Klompen, 2005) suggests that the most common way to describe the linear viscoelastic region is using the Boltzmann single integral representation and that for short times this reduces to time-independent Hookean elasticity (linear elasticity). However there are large numbers of different constitutive relationships proposed for the nonlinear viscoelastic region, most being based on modifications of the linear Boltzmann integral with non-linear stress/strain, reduced time and higher order stress/strain terms.

The use of molecular flow theories forms the basis of many deformation models, classic examples include the Eyring theory and later Argon double kink theory (Halsey et al., 1945) (Argon, 1973). Further molecular flow theories which makes use of high viscosity dashpots and fluids and are based on these classic works include (Morshedian et al., 2005) (Pakula & Trznadel, 1985) (Bhattacharyya & Tobushi, 2000) (Trznadel & Kryszewski, 1992). However they do not account for strain softening or hardening (Klompen, 2005). Attempts to model the later stages of deformation and large deformations have been proposed by several authors (Adams et al., 2000) (Boyce et al., 2000) (Matthews et al., 2000) (Dooling et al., 2002) (Drozdov & Christiansen, 2003) (Wu & Buckley, 2004) (Makradi et al., 2005) (Dusunceli & Colak, 2008).

Thermal dependency also plays a major part in deformation as increasing thermal energy increases the rate of conformational change and allows greater deformation to occur. This conformational change is restricted by energy barriers which themselves are controlled by intramolecular and intermolecular interactions. In the absence of a physical model for this conformational entropy, statistical theory is used (Buckley & Jones, 1995) (Ward & Sweeney, 2004).

Time dependency is also a major component as longer times allow larger conformational changes, although physical entanglements which act as temporary cross-links can limit this. As with increased temperature the molecular mobility increases with time and the polymer behaves like rubber.

Stress dependency also has a strong influence on molecular mobility and hence deformation (Klompen, 2005). With increased stress the mobility increases, although the effect of physical ageing, due to the non-equilibrium thermodynamic state apparent in polymers, causes this mobility to decrease. Such physical ageing is apparent in both linear and nonlinear viscoelastic ranges, as well as in the plastic range.

Sperling (Sperling, 2006) gives details on the behaviour and simulation of stress relaxation and creep and introduces the basic four-element model as a simple approach. However the problem is complicated by the fact that the viscosity and elastic modulus themselves are not simple values.

2.3.7 Thermal Behaviour of Polymers

Temperature dependence is widely discussed in the literature, in particular in the area of shape memory polymers (SMPs). SMPs will therefore be given their own section. Other papers deal with the thermal effect of polymers in general such as thermal expansion/shrinkage and the changes in material properties with temperature (Ward & Sweeney, 2004). Extensive research into the numerical modelling of the thermal effects has been carried out by Tobushi (Tobushi & Hashimoto, 1997) (Tobushi et al., 2001), Shih (Shih, 1994), Liu (Liu et al., 2006), Eyring (Halsey et al., 1945), Trznadel (Pakula & Trznadel, 1985), Morshedian (Morshedian et al., 2005) and Buckley (Buckley & Jones, 1995).

There are a variety of theories proposed in the literature to simulate temperature dependence, a simple example is the "Gaussian Network" (Sweeney et al., 1999) which proposes G = NkT. (G is shear modulus, N is number of chains per unit volume in the network, k is Boltzmann's constant and T is the temperature (Sweeney & Ward, 1995).

In its simplest form the viscoelastic behaviour at one temperature can be related to that at another temperature by a change in the time scale (Sperling, 2006) (Ward & Sweeney, 2004). This can be seen Figure 2.19 taken from (Ward & Sweeney, 2004) where α_t is the shift factor.

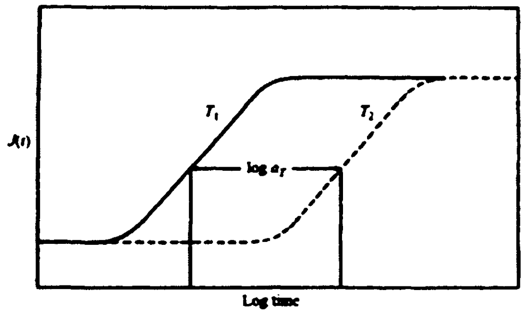

Figure 2.19 - Viscoelastic Behaviour Shift Factor (Ward & Sweeney, 2004)

A more advanced formulation that has been widely reported is the work of Williams et al (Williams et al., 1955). The so called WLF equation highlights how polymers soften and flow at temperatures near and above T_g and stems from the work of Doolittle on the viscosity of non-associated pure liquids (Doolittle, 1951). Despite it being limited to the region T_g to T_g+100 (Ward & Sweeney, 2004) the WLF equation has been widely used by polymer scientists (Sperling, 2006).

The site nodal theory has also been widely accepted by polymer scientists and consists of two sites separated by an equilibrium free energy difference as seen in Figure 2.20 where ΔG_1 and ΔG_2 are the barrier heights (Ward & Sweeney, 2004). The population of each site varies with changes in energy difference which can be brought on by the application of stress. The site population can be directly related to strain and the frequency of molecular "jumps" related to conformational changes. The frequency of molecular conformational changes is given by the "Arrhenius equation" derived by Arrhenius to describe the influence of temperature on the velocity of chemical reactions (Ward & Sweeney, 2004). The site nodal theory is limited to constant activation energy, such as the localised motions of crystalline regions in semicrystalline polymers.

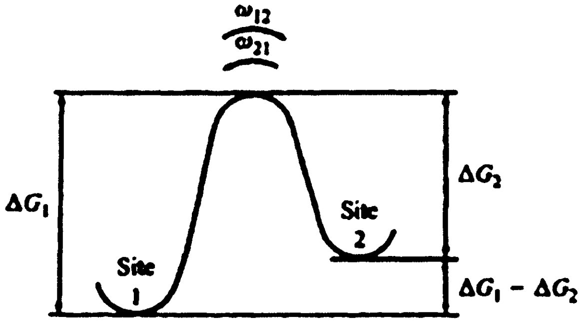

Figure 2.20 - The Two-site Model (Ward & Sweeney, 2004)

Another important thermal effect is that of thermal contraction/expansion which is affected by several factors such as geometric shape (Figure 2.21), annealing, thermal cycling and mechanical preloading. Annealing in the presence of stress has been observed to decrease the linear thermal expansion coefficient. (Baschek & Hartwig, 1998).

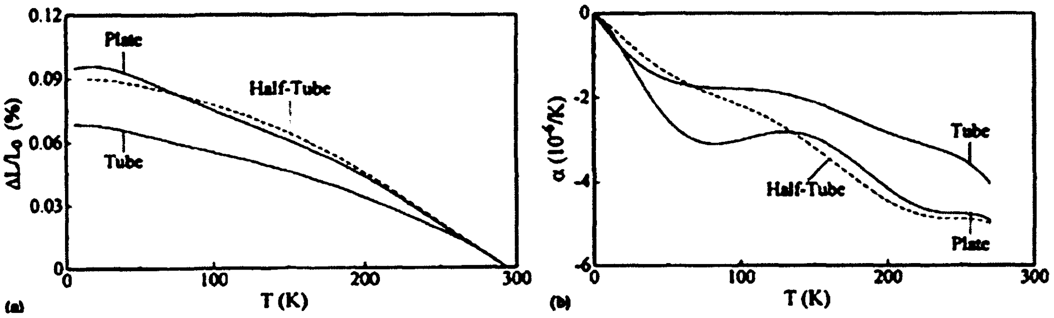

Figure 2.21 - Effect of Shape on Thermal Properties of Carbon Reinforced Polymers (Baschek & Hartwig, 1998).

The coefficient of thermal expansion of oriented PET in the stretch direction is also seen to drop sharply with increasing orientation (Bhushan, 2000), although it shows a slight increase in the transverse direction. Such an affect is caused by the chain alignment in the crystalline regions, although at very high stretch ratios of 300+% the crystalline orientation becomes saturated and the coefficient plateaus. The effect of increasing crystallinity on thermal expansion was investigated by Uematsu and by Uematsu and Choy et al as reported in (Bhushan, 2000).

Tobushi & Hashimoto (Tobushi & Hashimoto, 1997) discuss the inclusion of a coefficient of thermal expansion in the development of the constitutive equation, proposing that it is independent of mechanical behaviour. The experimental work carried out by Tobushi & Hashimoto highlighted that an initial drop in stress with temperature increase at low temperatures up to approximately 55°C is attributed to the "compressive stress against thermal expansion".

2.3.8 Shrinkage Properties of Polymers

Heat shrinkable materials have a wide range of applications, ranging from the packaging industry to the cable industry. These heat shrinkable materials, on application of heat, return to almost their original dimensions, such materials have, what is termed, elastic memory (Morshedian et al., 2005). The process of manufacture is based on the shape memory phenomenon that will be described in detail in a later section (Khonakdar et al., 2003). However, the generalised manufacturing process of shrinkable polymers involves the initial compound being made by extruding it into the required form and chemically cross-linking it. Secondly the "elastic memory" is induced by drawing a specimen to an elongated desired length at a certain temperature; following this the temperature is removed whilst the specimen is held at this length, thus "freezing in" the elastic restoring force. When the specimen is later returned to this temperature it returns to its original length, this occurs through the melting of the plastic crystalline domains (Morshedian et al., 2005) (Khonakdar et al., 2003) (Liu et al., 2006).

The generation of shrinkage-stresses is a well-known property of drawn polymers, associated with the orientation of the long chain molecules in the direction of drawing (Ward & Sweeney, 2004) (Trznadel & Kryszewski, 1992). Trznadel and Kryszewski suggest that the shrinkage-stress potential of the partially extended polymer chains is associated with the "entropic tendency of the chains to assume more coiled conformations" (Trznadel & Kryszewski, 1992) (Mody et al., 2001).

Mody et al. (Mody et al., 2001) state that "resistance to shrinkage increases with increased levels of material crystallinity". The process of orientation can be used to develop strain induced crystallisation (Bhushan, 2000). The history of previous stretching and annealing of a polymer also has an effect on the amount and onset temperature of shrinkage (Chandran & Jabarin, 1993) (Chandran & Jabarin, 1993a). Trznadel and Kryszewski (Trznadel & Kryszewski, 1992) explain that the shrinkage that has occurred previously, associated with molecular coiling, is permanent and non-recoverable, but that the independent molecular action of thermal expansion is recoverable.

Various authors have proposed different mechanisms for polymer shrinkage; formation of taut tie molecules (Peterlin, 1971), chain folding (Dismore & Statton, 1966) and combinations of two amorphous domains (Prevorsek et al., 1974). Depending on level of contraction depends on which of these mechanisms apply. It is fair to assume that the behaviour in amorphous polymers can be related to semi crystalline polymers as many authors believe that shrinkage is related mainly to changes in amorphous phase (Pakula & Trznadel, 1985).

The processing conditions of PET were studied by Sharma and Mishra (Sharma & Mishra, 1987) who concluded that high shrinkage values were achieved at low draw ratios (2x1) and that there was a reduction in shrinkage at high draw ratios. This though was contradicted by the work of Khonakdar et al (Khonakdar et al., 2003) on high-density polyethylene, who concluded that the higher the draw ratio the higher the ultimate shrinkage. Similiar observations were made by Gupta et al (Gupta et al., 1994) and Haworth et al (Haworth et al., 1993). Khonakdar et al (Khonakdar et al., 2003) also observed that the stretch ratio had no effect on shrink temperature, although this was affected significantly by the draw temperature, with those stretched above the melting point having a higher shrink temperature than those below it.

2.3.9 Application of Polymers in Concrete

The use of polymers in construction is by no means new, in fact their use dates back to the 4th Century when the clay brick walls of Babylon were built using the natural polymer, asphalt, in the mortar. The first use in concrete however came in 1909 when a patent was filed by L.H. Backland in USA and later in 1922 by M.E. Varegyas in France. The first patent in Britain was by L. Cresson for a rubber-modified road surfacing material in 1923, followed by a latex modified cement in 1924 (Kardon, 1997).

The first use of polymer concrete, as we know it today, was in the 1950s and their use in concrete has both broadened and become more innovative since that period (Fowler, 1989). Ranging from polymer-impregnated cement (PIC) and polymer concrete (PC) (Hing, 2007) (Kardon, 1997) to the use of polymer fibres to make bendable concrete in the form of engineered cementitious composite (ECC) (Li et al., 1998). A comprehensive overview of the use of polymers in concrete has been undertaken and a report produced in 2009 by an ACI committee (ACI Committee 548, 2009).

In a move to produce more sustainable polymer concrete, recycled PET, from common waste products such as plastic bottles, can be chemically modified to produce unsaturated polyester which can be mixed with aggregate and fly ash to produce a good quality polymer concrete. Such concrete, not only reduces the cost of PC, but also provides a long term disposal opportunity for PET waste (Rebeiz, 1995) (Jo et al., 2008) (Rebeiz et al., 1991) (Li et al., 1998).

A more recent development has been that of polymer fibre reinforced concrete and in order to allow the use of such a concrete in construction, the British Standards Institute released a standard (EN 14889-2-2006) (BSI, 2006) in 2006. The most notable polymer fibre reinforced concrete is ECC developed at Michigan University by Prof. Victor Li (Li, 2008). As described previously, ECC makes use of polymer fibres randomly distributed in the concrete matrix to maximise the tensile ductility by development of closely spaced multiple microcracks. The development of ECC has grown exponentially since its conception by Li, with researchers around the world now investigating its use and enhancing its properties (Li, 2008). Another popular use of fibre reinforced polymer (FRP) composites is in the strengthening of existing concrete structures via external bonding of FRP plates (Benyoucef et al., 2007).

2.4 Shape Memory Materials

Shape memory materials are materials that have the ability to memorize a macroscopic shape, while being manufactured into a temporary shape. The stress-free memorized shape can later be recovered from the temporary shape via an actuation method such as thermal or electrical (Liu et al., 2007). The shape memory effect has been demonstrated in metals, polymers, ceramics and gels and the mechanisms for shape memory have been found to be different in each. A well-defined crystalline phase change at a specific temperature in metals generates the shape memory effect whilst in polymers the effect is related to a variety of molecular interactions (Abrahamson et al., 2003). Shape memory alloys (SMAs) are the most prominent and widely used shape memory materials (Liu et al., 2007). Polymers on the other hand did not receive any significant attention until 1960's with the development of polyethylene as heat-shrinkable tubing. However the development of new technologies and polymers in the 1980's, along with their relative ease of manufacture and programming, saw shape memory polymers (SMPs) gain much greater interest (Liu et al., 2007). An overview will now be given of SMPs and SMAs along with a brief mention of other shape memory materials.

2.4.1 Shape Memory Polymers

Polymeric materials can have an elasticity that is somewhere in the range from hard such as glass to soft such as rubber. SMPs on the other hand have the characteristics of both hard and soft, with their elasticity modulus showing reversible change. The glass transition temperature (T_g), discussed previously, defines the border between glass and rubber responses (Hayashi et al., 2004). In the glass phase the material is rigid and cannot be easily deformed, whilst above T_g the material becomes soft and easily deformable. In this later phase, the polymer can be deformed and upon subsequent cooling, whilst this deformation remains, a locked-in stress is generated in the polymer. Upon removal of the deformation at the lower temperature, the polymer remains in the deformed "temporary" shape. When the polymer is heated again beyond T_g, the locked-in stress is released and the polymer returns to its previous "memorized" shape (Lendlein et al., 2005).

Figure 2.22 shows this process for a shape memory material (a) and compares it to natural rubber (b) which does not show this effect. The rubber example clearly shows the sample returning to its equilibrium strain during unloading at low temperatures (Liu et al., 2007).

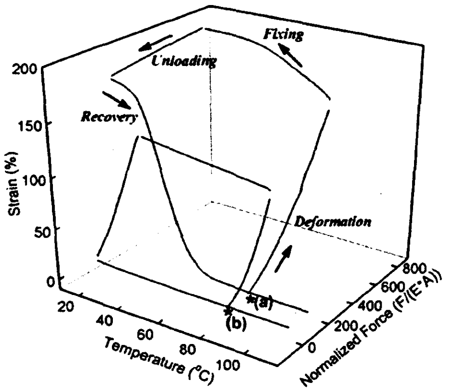

Figure 2.22 - Shape Memory Material Programming Process (Liu et al., 2007)

Liu et al (Liu et al., 2007) describes what makes a good SMP as a material that has; (i) a sharp transition used to promptly fix temporary shape and recover memorized shape, (ii) superelasticity above the transition temperature leading to shape recovery and avoids residual strain, (iii) complete and rapid fixing of the temporary shape by immobilising the polymeric chains without creep thereafter. A comprehensive review by Liu et al (Liu et al., 2007) highlights four main categories of SMPs divided according to their "differences in fixing mechanism and origin of "permanent" shape elasticity." These are (i) Covalently cross-linked glassy thermoset networks, (ii) Covalently cross-linked semi-crystalline networks, (iii) Physically cross-linked glassy copolymers and (iv) Physically cross-linked semi-crystalline block copolymers.

There are a number of key research groups around the world investigating new SMP materials and applications (Liu et al., 2007) ranging from the medical industry to space exploration. One aspect that gives rise to the variety of applications is the ability of SMPs to be activated by different methods and more significantly at specifically designed points. Examples include the use of body temperature activation for medical applications such as self-retaining needles (Hayashi et al., 2004), self-tightening surgical suture and microactuators used to remove blood clots (Liu et al., 2007). Larger applications can be seen by morphing plane wings which can adjust wing surface area according to flying conditions for optimal flight (Volk, 2005) and flat packed spacecraft wheels that expand on exposure to the sun's heat (Mitsubishi Heavy Industries, 2002).

Further actuation methods are described in depth by Behl (Behl & Lendlein, 2007) who describes methods of indirect heating using irradiation and the possibility of lowering the transition temperature at which activation takes place through the diffusion of low molecular weight molecules into the polymer, which act as a plasticizer. The effect of this is the ability for the temperature to remain constant and the transition temperature lowered to reach the current temperature and create activation. The lowering of the transition temperature can also be initiated by the diffusion of moisture into the polymer which will act as a plasticizer, so submersion in water can activate the shape memory effect. Heating can also be produced through use of infrared light and this has been demonstrated in a laser-activated polyurethane medical device. Light induced activation has also been investigated using UV light of a different wavelength to activate the shape memory effect (Lendlein et al., 2005). Additives such as conductive ceramics, carbon black and carbon nanotubes can also be added to the polymer which on application of an electrical current will raise in temperature due to high ohmic resistance and activate the shape memory effect. The incorporation of magnetic nanoparticles can enable the shape memory effect to be induced using a magnetic field (Conti et al., 2007).

Following activation and by further programming, including mechanical deformation, the SMP can be made into a temporary shape again, which does not necessarily have to be the same as the previous temporary shape (Lendlein et al., 2005).

2.4.2 Shape Memory Alloys

The shape memory effect in shape memory alloys (SMAs) such as Ni-Ti (nickel-titanium) was first discovered in 1968 by Buehler et al (Otsuka & Kakeshita, 2002) with other materials soon discovered to exhibit the same effect, namely Fe-Mn-Si (iron-maganese-silicon) in 1982 by Sato et al (Sato et al., 1986). Since their discovery SMAs have seen application in a variety of industries such as aerospace, medical equipment and structural control.

It terms of structural control it is the consequence of the phase change from low temperature martensite phase to a high temperature austenite phase under restrained conditions which can be used to introduce forces in structures (Janke et al., 2005). Likewise a constant temperature phase transformation from austenite to martensite phase can occur by increasing the external stress, called superelasticity.

Within the civil engineering industry SMAs hold many benefits, such as having a coefficient of thermal expansion close to that of concrete ($11.0\text{x}10^{-6}$ °C) (Saiidi et al., 2007) and being suitable for outside applications as the transition temperature can be set outside of the ambient temperature range defined as between -20°C in winter and 60°C in extreme summers (Janke et al., 2005). They also have a relatively high internal friction giving good damping capacities making use in seismic retainers in structures appealing (Johnson et al., 2004).

There are however some drawbacks with the use of SMAs as a construction material, the biggest and most documented is that SMAs are relatively expensive and are therefore only suitable for the most specialist of situations. Liu et al (Liu et al., 2007) report that SMAs cost approximately $250 per pound, whereas SMPs cost less than $10 per pound. They also have poor functional fatigue properties and therefore their use should be limited to fairly small numbers of shape memory transformation cycles (Freed & Aboudi, 2008). Actuation time is also relatively slow in construction terms and although this can be increased by using a greater electrical current, the size of the power source can become very large, making them unsuitable for fast changing loads such as wind.

SMAs do though offer an alternative to the conventional pre- and post-stressing methods (Janke et al., 2005) (Maji & Negret, 1998) (Freed & Aboudi, 2008) (Saiidi et al., 2007) (El-Tawil & Ortega-Rosales, 2004). Moser et al (Moser et al., 2005) also investigated the use of stretched SMA fibres embedded in the concrete at low temperatures and activated upon curing. Janke et al (Janke et al., 2005) discusses the use of SMA in confinement of reinforced concrete members by utilising the shape memory effect for tensioning the wrapping placed around columns thus enhancing the confinement and has been termed "active confinement". Freed and Aboudi (Freed & Aboudi, 2008) have carried out numerical simulations of such SMA-cementitious systems.

It is clear that such systems could be undertaken by SMPs although the one major drawback is the stress that SMPs are able to generate, which currently is only in the order of less than 80MPa (Gupta et al., 1994) (Long & Ward, 1991).

2.4.3 Other Shape Memory Materials

Materials known as martensitic ceramics experience a martensitic phase transition from a tetragonal to monoclinic structure, which is induced thermally or by the application of stress. The transformation back from monoclinic to tetragonal symmetry can occur thermoelastically and hence shows a thermoresponsive shape memory effect. Another category of shape memory material is that of polymer gels. These gels have the ability to react to changes in the external conditions and show considerable changes in volume, both swelling and shrinking to 100 times their original size. These changes can be triggered thermally, by variation in pH values or by the quality of the solvent. As with SMPs, light and electrical current can also be used, however gels differ from SMPs in that they have poor mechanical stability (Lendlein & Kelch, 2002).

2.5 Polyethylene Terephthalate

Polyethylene terephthalate (PET), as seen in Figure 2.23, is a hard, stiff, strong and dimensionally stable material (Azom, 2003). It is a thermoplastic resin belonging to the polyester family and may exist as an amorphous or semi-crystalline polymer depending on its manufacturing process (Plastics Federation of South Africa, 2009). PET absorbs very little water and has generally good resistance to chemicals, although alkaline environments and superheated steam can cause issues of degradation (Plastics Federation of South Africa, 2009).

It has a variety of uses ranging from the textile industry, where it is often referred to simply as polyester, to the packaging industry where it is generally called PET (Bower, 2002).

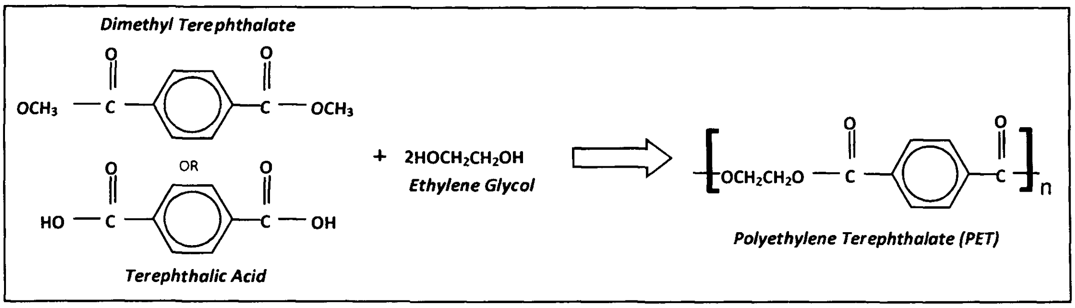

Figure 2.23 - PET Structure

2.5.1 Manufacture

There are two methods of producing PET, both begin with the conversion of ethylene glycol (EG) into bis-hydroxyethyl-terephthalate (BHET). The first method then uses pure terephthalic acid (TA) and distils out excess EG and water to form PET; while the second uses dimethyl terephthalate (DMT) and undergoes polycondensation which releases excess EG (Brandrup, 1996). The properties can be further enhanced by additional processing such as a second stage of polymerisation, drawing and the use of chemical additives or heat treatment (International Life Sciences Institute, 2000).

Drawing above the glass transition temperature and cooling in the stretched condition allows fibres and films to be manufactured (Global Association of Manufacturers of Polyester Film, 2009). Alternatively if the stretched PET is held above 72°C it slowly crystallises and the material becomes opaque, more rigid and less flexible and is known as crystalline PET (CPET) (International Life Sciences Institute, 2000). There are many other manufacturing processes including extrusion blow moulding, injection blow moulding and injection stretch blow moulding. The chosen process very much depends on the desired end product and mechanical properties

2.5.2 Applications

The main areas of application for PET films have been the food packaging industry and as a carrier for magnetic tapes (American Chemistry Council, 2009), whereas the textile industry have made great use of PET fibres (Azom, 2003).

The shrink film industry is one that has seen substantial growth in the last decade, as Mitsubishi Industries highlighted in a food industry publication in 2002, which signalled their movement away from "the already oversupplied traditional PET film business and into the rapidly growing shrink film market" (Food Production Daily, 2002).

PET requires 2kg of oil to produce 1kg of the polymer and although incineration returns an equivalent 0.5kg of oil, however it is possible to recycle PET (Shyam Plastic Machinery, 2009). A simple method of recycling PET is to crush moulded PET products and mix them with crushed PET granules from virgin PET resins. The percentage of regrind proportion should be limited to approximately 20% to ensure the melt viscosity, colour and odour is not adversely affected (Kenplas Industry Limited, 2010).

2.6 Experimental Investigations of Polymers

Experimental studies investigating the shrinkage behaviour of polymers and in particular PET are wide and varied, however very few pieces of work investigate the development of shrinkage with temperature and the subsequent change in material properties. In their comprehensive review of shrinkage in oriented polymers, Trznadel and Kryszewski (Trznadel & Kryszewski, 1992) say that the measurement of shrinkage in polymers is widely understood for the qualitative determination of orientation and locked in stress and that although shrinkage depends on much more than the orientation, this technique is suitable for amorphous polymers as well as semi-crystalline polymers due to the amorphous component dominating shrinkage. It should be noted though that the crystalline phase does affect shrinkage in that it restrains the amorphous phase, such an affect has been used to estimate the crystallinity of oriented PET samples by Smith and Steward (Smith & Steward, 1974).

Notable work was carried out by Tobushi et al (Tobushi et al., 2001), who investigated changes in material properties with temperature in a thin polyurethane SMP film. Seven types of tests were carried out in the temperature region $T_g \pm 20K$, namely (i) dynamic mechanical tests, (ii) thermal expansion tests, (iii) uniaxial tensile tests, (iv) creep tests, (v) stress relaxation tests, (vi) thermomechanical tests and (vii) recovery-stress tests. Tobushi et al found that the behaviour of stress and strain varied a great deal between $T_g \pm 15K$ and was relatively constant outside this region. They determined the range of the glass transition region to be 30K and that the material properties varied exponentially throughout this region.

Morshedian et al (Morshedian et al., 2005) undertook a similar series of experiments using a low density polyethylene (LDPE). The LDPE was mixed with peroxide and various additives and cast into dumbbell shaped flat sheets followed by a shape fixing procedure to produce a heat shrinkable material. The shape fixing procedure involves stretching the specimens to 200% strain at 160°C at which point they were cooled instantly using salt-ice water. The rapid quenching locked in the build-up of molecular orientation, such that when unclamped the specimens they did not contract. Further investigations by Morshedian et al found that if the specimens are left for a period of time before allowing crystallisation to occur (i.e. cooling), they experienced some stress relaxation. It was found that if the elapsed time before crystallisation is in excess of 30 hours then the shrinkage capability is lost completely and no shrinkage occurs upon reheating. Upon reheating the specimens shrunk and the stress-strain behaviour was monitored using a tensile testing machine.

In understanding the total shrinkage of oriented polymers, Trznadel and Kryszewski (Trznadel & Kryszewski, 1992) define the "molecular draw ratio" (MDR) as $(\Delta L + L_0)/L_0$ where ΔL is the length change after shrinkage and L_0 is the original length of the undrawn sample, to describe the shrinkability of oriented polymers. Trznadel and Kryszewski also emphasize the importance of shrinkage force measurements in determining the magnitude of internal entropic stresses fixed in an oriented polymer. They propose two types of test; (i) constant load (free-shrinkage) and (ii) constant length; and detail constraints of both types of experiment. Their method of heating, previously used by other investigators, was to use an oil bath and submerse the polymer into the oil at the required temperature (Trznadel & Kryszewski, 1992) (Capaccio & Ward, 1982). Other authors propose the use of water baths and heater plates (Gupta et al., 1994).

Capaccio and Ward (Capaccio & Ward, 1982) note the importance of removing the effect of thermal expansion/contraction of the apparatus on the stress/strain measurements and propose gripping the specimen perpendicular to the apparatus. Such a method is also beneficial if the specimen is to be heated by submersion in an oil bath. Other methods of overcoming the thermal expansion/contraction issue include the use of materials of known thermal expansion so that results can be adjusted accordingly (Trznadel, 1986) or the use of two materials such as steel and brass, with the length of the brass chosen to compensate that of the steel (Pakula & Trznadel, 1985).

Further care should be taken when measuring the initial stages of shrinkage, especially at higher temperatures when the delay in heating the polymer to the same temperature throughout becomes critical, as the external parts will contract before the rest of the sample. The thermal expansion of the polymer itself can also cause slight errors in the results, especially at high temperatures. At low temperatures the relaxation of the shrinkage-stresses can be another source of errors (Trznadel & Kryszewski, 1992).

Early experiments carried out to investigate the free shrinkage of polymers were burdened with serious errors due the difficulty of the measuring samples which had the tendency to coil, twist and fold (Trznadel & Kryszewski, 1992). One method to overcome this was proposed by Andrews (Andrews, 1955) which involved placing the sample in a glass pipe. Another method proposed by several authors was the use of an initial preload (Tanabe & Kanetsuna, 1979) (Kambe & Kato, 1973) (Ribnick, 1969). Both methods though did introduce additional forces such as surface friction and external tension which ultimately disturb the free shrinkage and must therefore be accounted for in the analysis. In experiments carried out by Haworth et al (Haworth et al., 1993) it was found that the percentage shrinkage decreases with increasing load, although preloads less than 10g produce accurate and reliable results. An additional problem with length measurement is the initial slow development and later fast development, such that measuring at constant time intervals is not sufficient and a continuous measurement method is more suitable.

It is much more successful to investigate the development of stress at constant length as it is much more sensitive and can give more accurate results even at initial stages. Such experiments were undertaken by Gupta et al (Gupta et al., 1994) on oriented PET strips of 2mm width and 5cm length clamped with a slight pretension between two grips, one of which was fixed and the other attached to a load cell. The sample was then heated using a cylindrical heating device set at the desired temperature and the shrinkage force was recorded with time. This was carried out at a variety of temperatures to enable a peak stress versus temperature graph to be plotted.

The results showed that a peak stress increased with temperature and stabilised at approximately 120°C when crystallisation can occur and crystallites stabilise the oriented state, making relaxation difficult. Gupta et al also investigated the effect of draw ratio of shrinkage-stress concluding that shrinkage-stress increases with draw ratio.

A similar series of experiments was carried out by Haworth et al (Haworth et al., 1993) using a thermo-mechanical analyser (TMA) with a built-in linear variable differential transformer to enable rapid measurement of length. Haworth et al also undertook digital scanning calorimetry (DSC) studies. They found that significant shrinkage developed around the glass transition temperature (approx 85°C for this sample). Haworth et al also investigated the effect of heating rate on shrinkage with heating rates of between 10°C and 50°C per minute. The results showed that shrinkage is typically 5% greater at higher temperatures with the 20°C/min rate in comparison to 10°C/min rate and that at 50°C/min rate anomalous results were seen due to the rapid onset of shrinkage. Such results were also reported by Bhushan (Bhushan, 2000). The development of stress in an isothermal test at 150°C was presented by Haworth et al and showed very rapid shrinkage for the first 10 minutes with an equilibrium being reached after approximately 30 minutes (10.45%) which is very close to the final shrinkage after 60 minutes (10.57%).

TMA and DSC was also used by Volk (Volk, 2005) in an investigation into thermomechanical behaviour of SMPs. Volk used both to determine the glass transition temperature, coefficient of thermal expansion and Young's modulus. A series of constant stress recovery and constant strain rate recovery experiments were undertaken at an increasing temperature. In order to control the materials temperature an oven was used to heat and liquid nitrogen to cool the specimen.

The work of Pakula and Trznadel (Pakula & Trznadel, 1985) produced a series of stress versus temperature and time results for PET with different drawing conditions using a thermal chamber. PET drawn at 20°C to a draw ratio of 6 at a rate of 50cm/min achieved the highest stress of approximately 32MPa at 120°C before slowly decreasing with increasing temperature. Lower draw ratios and rates achieved lower stress levels although all showed decreasing stress levels from 120°C onwards.

Dooling et al (Dooling et al., 2002) propose a method of determining load-displacement data and alluded to the issue of grip slippage causing a 2.43% error and stated that care should be taken to protect the load cell from heat variation.

A series of experiments were reviewed and summarised by Khonakdar et al (Khonakdar et al., 2003), who stated that "shrinkage is usually measured using specimens submerged in an oil/water bath or hot air oven at a constant temperature, although the most popular method of measuring shrinkage under a constant heating rate is to use TMA, which is also used to study the shrinkage mechanism and shrinkage modelling." Furthermore, Sperling (Sperling, 2006) suggested that in order to investigate the stress relaxation and creep in polymers two simple experiments can be undertaken. For stress relaxation the sample is rapidly stretched and stress is required as a function of time at constant length and temperature. For creep experiments a constant stress is applied and the dimensions are recorded as a function of time.

2.7 Numerical Modelling of Polymers

The numerical simulation of polymers is a wide and varied area of research with models differing depending on the type of polymer and behaviour required. Due to the wide variety of models the author refers the reader to the comprehensive review paper by Trznadel and Kryszewski (Trznadel & Kryszewski, 1992) which gives a good overview of existing models and a paper by Buckley and Jones (Buckley & Jones, 1995) which details well the requirements of a unified polymer model and discusses existing solutions. Further details of models have also been discussed previously in Sections 2.3.6 and 2.3.7. A detailed summary of the relevant models will be given in Chapter 5 as their components will form the basis of a numerical model developed by the author. Further literature on modelling polymers can be found in Ward and Sweeney (Ward & Sweeney, 2004), Morshedian et al (Morshedian et al., 2005), Sperling (Sperling, 2006), Klompen (Klompen, 2005), Dooling et al (Dooling et al., 2002) and Dusunceli and Colak (Dusunceli & Colak, 2008).

Chapter Three: **LatConX System - Experimental Studies**

The following chapter gives a brief overview of the initial experimental work carried out to prove the concept of the LatConX system. It also describes a subsequent study undertaken to investigate how the system could be used to enhance the autogenic healing of cracks. Full details of these experimental programmes are given by Jefferson et al. (Jefferson et al., 2010), Isaacs et al. (Isaacs et al., 2010) and Isaacs (Isaacs, 2010), but since these studies provide the data used to validate the numerical model presented in Chapter 6, a brief overview will be given here. The work described here also draws upon the techniques developed for the testing of the polymer tendons discussed in the next chapter and published in Dunn et al. (Dunn et al., 2011).

3.1 Experimental Procedure

The experiments used small hollow prismatic mortar beams through which the polymer tendons were threaded and anchored at either end. Small specimens (145mm x 25mm x 25mm) were used due to the size of polymer tendons available. The polymer tendons consisted of 75No. individual strips of PET tape (each strip being 6mm x 0.046mm) bonded together at their ends. The tendons were placed and anchored after curing the specimens for 4 days and constituted 3.9% of the cross-sectional area of the un-notched mortar beam (20.7mm^2). The polymer tendons used were PET Shrinktite, which had been shown to develop a shrinkage-stress of approximately 33MPa at 90°C. Further details of the polymer behaviour will be given in the next chapter.

The mortar beams were cast using a mix ratio of Water:Cement:Sand of 306kg/m^3:510kg/m^3:1530kg/m^3 of mortar respectively, or 0.6:1:3 by weight. The cement used was Portland-fly ash cement, designation CEM II/V-V32.5 R supplied by Lafarge Aberthaw which contained 7% fly ash. The sand used was 0/4mm, EN12610 complaint concrete sand, dredged from Nasia, Swansea. The sand was though passed through a 1mm sieve prior to mixing. The mixing was undertaken in a CreateAngle® Multiflow Pan Type Mixer Model 'S'.

The mortar beams used in the experiments are shown in Figure 3.1 and contain a 10mm x 10mm cavity running the full length through the centre of the beam. The specimens were prefabricated with a 3mm deep notch at their centre to ensure the crack formed at a known location. The mortar in the specimens was placed in 3 stages and compacted on a vibrating table between each stage. The first stage formed a bed for a polystyrene cavity former, the second being to the upper surface of the former and the third to the top surface of the mould.

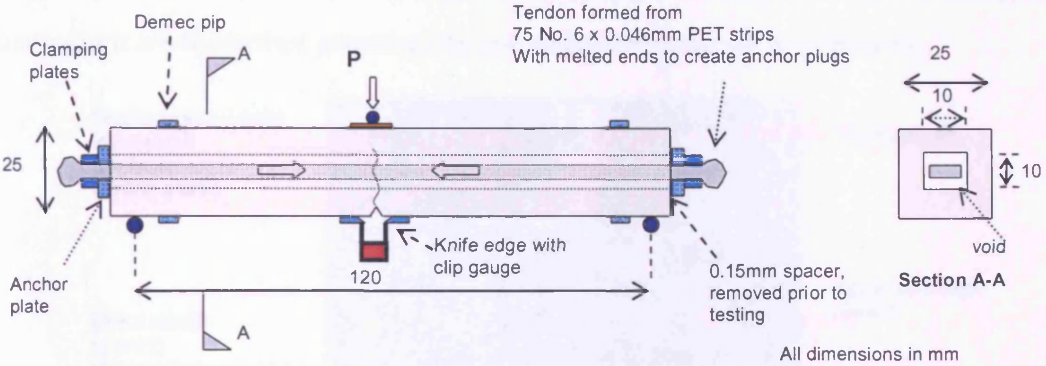

Figure 3.1 - Testing Configuration (Jefferson et al., 2010)

The polystyrene former was used to create the axial cavity that the polymer would pass through. The former was removed during demoulding on day 2. Immediately after casting the beams were covered in wet hessian and wrapped in cling film to maintain moisture within the specimens and simulate curing in a wet environment.

The polymer tendons were inserted on day 4, immediately prior to testing. The anchorage system comprised clamping plates and a plug of melted material as shown in Figure 3.1 and ensured limited slip in comparison with the shrinkage potential of the polymer. Further details of the method of gripping are presented in Chapter 4. It was required that the tendons be consistently loose at the start so as not to affect initial loading and damage. This was achieved by anchoring one end of the tendon and holding the beam vertically with a 1kg weight hung on the other end of the tendon. A 0.15mm spacer was placed between the anchor plate and the clamping plate prior to tightening. Heat was then applied to the excess polymer to create a mechanical anchor plug and the spacer was removed.

Testing was carried out in 3-point bending and in three stages using an Avery-Denison testing machine as shown in Figure 3.2. The three stages were:

Stage 1: Loading specimen until crack formation

Stage 2: Activation of PET shrinkage to initiate healing

Stage 3: Reloading to failure.

A lightweight clip gauge (CG) was located between two knife edge plates glued to the underside of the specimen either side of the notch (Figure 3.2). This was used to monitor the Crack Mouth Opening Displacement (CMOD). The test was controlled via feedback from a machine stroke displacement transducer thus allowing the softening behaviour to be captured.

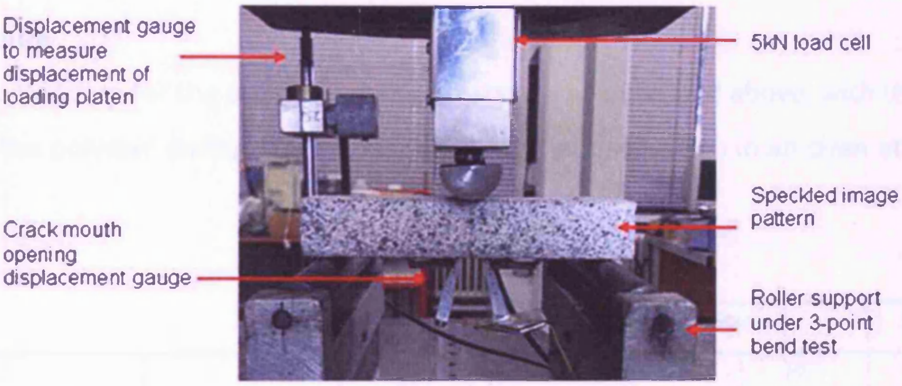

Figure 3.2 - Three-Point Bending Testing Arrangement (Isaacs et al., 2010)

The CMOD was also measured using Digital Image Correlation (DIC), a technique which is relatively new for concrete. This technique captured the full 2D displacement and strain on one side of the mortar beam. The DIC system was supplied by LIMESS and comprises two cameras which tracked a speckled image on the side of the specimen (Limess, 2010) (Bornert et al., 2009). The system had an accuracy of 1µm for displacements using the chosen grid size of 120mm x 25mm (Limess, 2010).

The first method of finding the CMOD used the clip gauge to identify the unloading point, as it gave real-time results, whereas the DIC measurements required post processing. The DIC CMOD ($CMOD_{DIC}$) values were measured across the 3mm deep notch at a height of 1.8mm above the underside of the beam. The clip gauge CMOD ($CMOD_{CG}$) was measured across the knife edges at approximately 4mm below the underside of the specimen.

The above procedure was used to undertake two different studies; the first to investigate the ability of the LatConX system to close cracks and heal the specimens (Proof of Concept tests) and the second to study methods of enhancing the autogenous healing process, which ultimately will increase the effectiveness of the LatConX system. The data obtained using the above procedure enabled the load to be plotted against the CMOD for both stage 1 and stage 3.

3.2 Proof of Concept Tests

The proof of concept tests were carried out as part of a Royal Society of Engineering Brian Mercer Feasibility Award. The aim of the tests series was to prove that the LatConX system could close and subsequently "heal" a crack in a cementitious composite.

3.2.1 Procedure

The testing procedure for the proof of concept tests was as described above, with the activation method for the polymer during Stage 2 loading being heat activation in an oven at 90°C for 18 hours.

Table 3-1 - Summary of Specimen Details

			Stage 1	**Stage 2**		**Stage 3**
GROUP	**DESIGNATION**	**PET tendon inserted prior to day 4 test**	**Day 4** **3-point bend test**	**Heated at 90°C for 18hrs**	**PET tendon removed prior to day 8 test**	**Day 8** **3-point bend test**
3 Control beams, tested on day 4	CTRL1_a-c	No	Yes, to failure	N/A	N/A	N/A
3 Control beams, tested on day 8	CTRL2_a-c	No	No	Yes	N/A	Yes, to failure
3 post-tensioned beams with PET tendon throughout	PET_a-c	Yes	Yes, to 0.3mm CMOD_{CG}*	Yes	No	Yes, to failure
3 post-tensioned beams with PET tendon removed after activation	PETr_a-c	Yes	Yes, to 0.3mm CMOD_{CG}*	Yes	Yes	Yes, to failure

*Notes: **1**:Day 1 is taken as the day of casting,

2:An opening of 0.3 mm measured by the clip gauge 4mm below the underside of the specimen equates approximately to an opening 0.22mm measured by the DIC equipment at 1.75mm above the base of the specimen at the end of the softening branch in the unprestressed stages.

3:CMOD_{CG} = Crack Mouth Opening Displacement by clip gauge.

Twelve 145mm x 25mm x 25mm specimens were cast and divided into 4 groups of 3 beams as summarised in Table 3-1. In addition, material tests were carried out on the mortar to determine its key material properties, namely compressive strength, fracture energy, tensile strength and Young's modulus as detailed in Table 3-2.

The control specimens were used to ensure that the response of the specimens with loose tendons was the same as that for specimens without tendons (CTRL1) and also to assess the effect of the heating and additional curing time on the strength of the specimens (CTRL2). The group with the tendons removed prior to stage 3 loading (PETr) was used to quantify the amount of autogenous healing that had taken place.

Table 3-2 - Measured Material Properties

	E	f_{cu}	$f_{t\,(Stage\ 1)}$	$f_{t\,(stage3)}$	G_f
	kN/mm^2	N/mm^2	N/mm^2	N/mm^2	N/mm
Mean	*24.8*	*23*	*2.0*	*0.09*	*0.025*
CoV %	*1.6*	*8.3*	*7.3*	*10.6*	*11.7*

E = Young's Modulus, f_{cu} = cube strength, f_t = tensile strength, G_f = fracture energy

3.2.2 Results

Comparison of the control (CTRL) specimens and the PET specimens in which the tendon remained loose shows that the loose tendons have an insignificant effect on the response of the beams during Stage 1 damage, as illustrated in Figure 3.3.

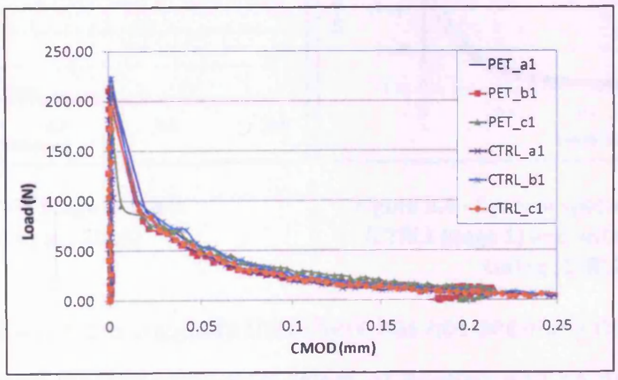

Figure 3.3 - Stage 1 Load-CMOD Results (Jefferson et al., 2010)

Figure 3.3 also shows that there is good consistency between the results of both the PET and CTRL1 specimens, for which the peak loads ranged from 193 to 223N. It should be noted that the CMOD readings presented are taken from the DIC readings as they exhibited less 'noise' but are consistent with the clip gauge readings if the different depths of the CMOD measurement are considered (note that the beams were loaded until a 0.3mm crack registered on the clip gauge which corresponds to a 0.22mm crack at the DIC measurement position).

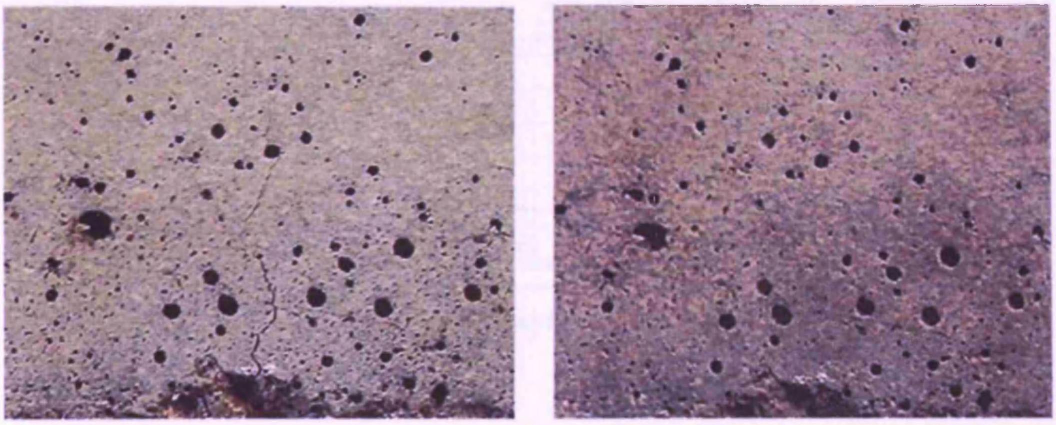

Figure 3.4 - Specimen from Group PET after (a) Stage 1 Loading and (b) Stage 2 Activation

The visual results following stage 1 damage and stage 2 healing can be seen in Figure 3.4(a) and (b) respectively. As the crack is no longer visible in Figure 3.4(b) it is reasonable to assume that the activation of the polymer system has caused full crack closure for the group PET specimens.

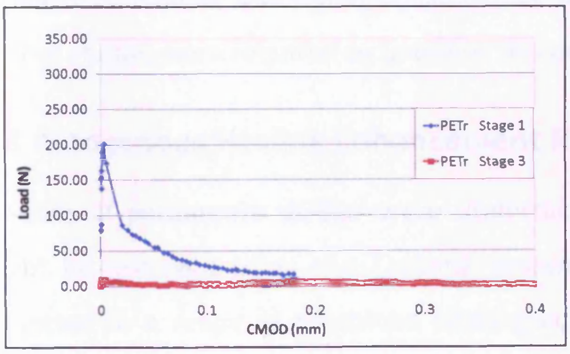

Figure 3.5 - PETr Stage 1 and 3 (Jefferson et al., 2010)

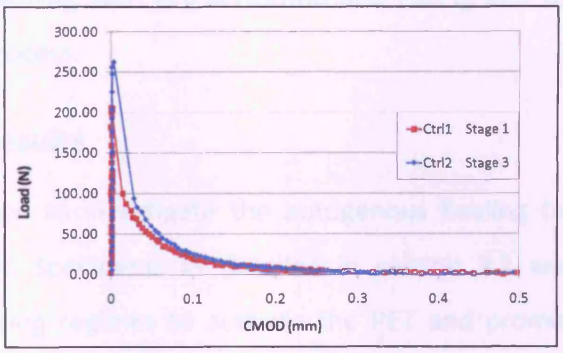

Figure 3.6 - Control specimens without heating (CTRL1 Stage 1) and with heating and further curing (CTRL2 Stage 3)

However, despite this, Figure 3.5 suggests that there has not been any measurable crack healing other than that generated by the combined effect of heating and an additional 4 days curing, which resulted in an increase in peak load and associated tensile strength of approximately 25%, as shown in Figure 3.6.

The effect of the polymer tendons when retained in the beam in their activated state during Stage 3 loading, was to act as pre-stressing tendons. In this condition the softening response of the specimens exhibited a greater apparent post-peak ductility, as illustrated in Figure 3.7.

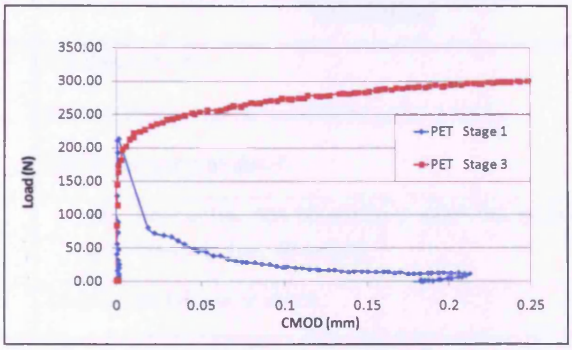

Figure 3.7 - PET Stages 1 and 3 (Jefferson et al., 2010)

3.2.3 Conclusions

The proof of concept experiments that have been presented demonstrated that the LatConX system is a viable solution for crack closure and low-level pre-stressing. The effect of the polymer following activation was to close a preformed crack and to contribute to the post peak ductility of the system by its action as a pre-stressing member. The studies did however highlight that there was no significant crack healing with dry activation and curing and that further studies were required to optimise this process.

3.3 Autogenous Healing Enhancement Results

A series of parametric studies were undertaken to investigate the autogenous healing that might be achieved using the LatConX system. Specimens as detailed in section 3.1 were subjected to a range of combined heating/curing regimes to activate the PET and promote autogenous healing prior to Stage 3 loading to failure.

3.3.1 Procedure

The hollow prismatic mortar beams were prepared as detailed in Section 3.1 with the experimental procedure again being divided into three stages as shown in Table 3-3. Studies were carried out during early age conditions, as previous investigations have shown this to be the period when autogenous healing is most likely to occur (ter Heide et al., 2005). The testing procedure was undertaken in the same manner as detailed in Section 3.1.

Table 3-3 - Stages of Experimental Procedure (Isaacs et al., 2010)

Stage	Description
1	Casting (day 1) Curing under sealed conditions (days 1 to 4) Initial cracking at day 4
2	(a) heat activation (Starting on day 4 for 18 hours) (b) 'healing' (for 48 hours)
3	Loading to failure at day 8

In order to investigate the effect of the activation and curing method on the ability for of the system to undergo autogenous healing, three activation-healing (AH) regimes were investigated as detailed in Table 3-4. For each of the AH regimes twelve specimens were tested; again being divided into four groups of three beams as detailed in Table 3-1 in the 'Proof of Concept Tests'

Table 3-4 - Heat Activation Methods and Healing Regimes (Isaacs et al., 2010)

AH regime	Heat activation method			Healing regime	
	Description	Temp. (°C)	Time (Hrs)	Description	Time (Hrs)
CTRL	Dry heat activation	90	18	Dry healing	48
AH1	Dry heat activation	90	18	Cured in water at ambient temperature	48
AH2	Steam heat activation	90*	18	Specimens remain in the steam chamber with the steam production turned off and the chamber allowed to return to ambient conditions	48
AH3	Water heat activation	90	18	Specimens cured in the water tank with the temperature allowed to return to ambient conditions	48

Note: *the atmospheric temperature was measured at 90 °C and the water in the tank was heated to 100 °C in order to produce steam conditions

3.3.2 Results

In order to compare the different regimes, the 'Load Recovery' (LR) was determined having been defined as LR = (Stage 3 Load) / (Stage 1 Load) x 100%. The results of the mean peak load and LR are presented in Table 3-5. Further to these results, the gradient of the pre-peak loading curves was measured for both Stage 1 and Stage 3 loadings to give an indication of stiffness recovery. The mean gradient for Stage 1 of all the tests was 78N/m and the corresponding gradient recovery for Stage 3 for each of the tests is presented in Table 3-6.

Table 3-5 - Mean Loads, Coefficients of Variance and Load Recovery Percentages for Specimens Tested (Isaacs et al., 2010)

Treatment regime	Specimen	Stage 1		Stage 3		Load Recovery (1) (%)
		Mean Peak Load (N)	Coefficient of Variance (±)	Mean Peak Load (2) (N)	Coefficient of Variance (±)	
Dry heat at 90°C and dry healing (Previous tests)	6 Control beams	207	7	296	10	-
	3 PET beams	204	9	222	12	109
	3 PETr beams	194	5	9	13	5
AH1 Dry heat at 90°C and water healing	6 Control beams	235	2	230	9	-
	3 PET beams	236	13	299	16	127
	3 PETr beams	225	7	176	10	79
AH2 Steam heat and healing	6 Control beams	170	15	254	3	-
	3 PET beams	151	10	294	8	194
	3 PETr beams	159	19	125	10	79
AH3 Water heat at 90°C and water healing	6 Control beams	254	3	311	6	-
	3 PET beams	233	7	216	4	93
	3 PETr beams	255	16	42	16	17

(1) No load recovery because these were control specimens tested to failure at stages 1 and 3

(2) In most cases this was a first peak load and was associated with cracking of the mortar however, where no first peak existed, this load was taken as the point at which the stiffness first changed significantly.

Table 3-6 - Mean Gradient Recovery for Loading Curves of Typical Specimen's Pre-peak at Stage 3 Testing (Isaacs et al., 2010).

	AH1 (%)	AH2 (%)	AH3 (%)
PET specimens	125	104	102
PETr specimens	95	72	35

The DIC system described previously was used to plot a series of load versus CMOD graphs, which when adjusted for their relative positions, were comparable to the clip gauge readings and were also less susceptible to 'noise'. These graphs are shown in Figure 3.8 - Figure 3.11.

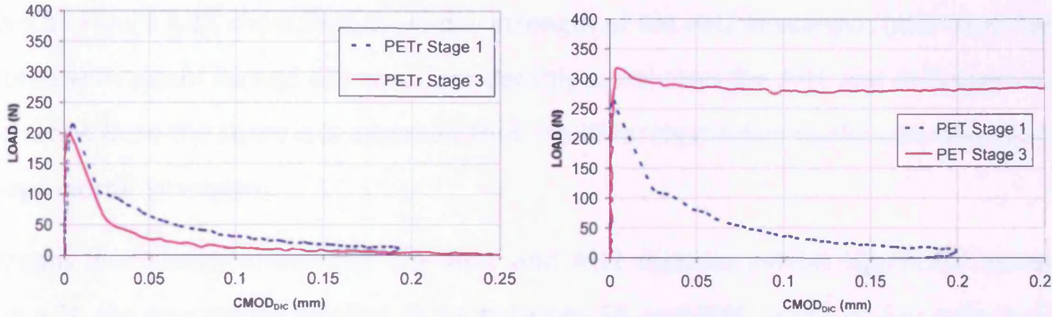

Figure 3.8 - AH1 Specimens (Water Ambient) (a) PETr and (b) PET (Isaacs et al., 2010)

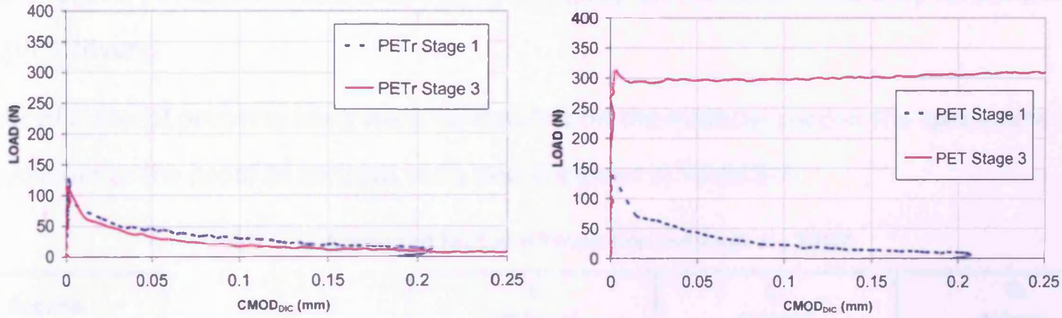

Figure 3.9 - AH2 Specimens (Steam) (a) PETr and (b) PET (Isaacs et al., 2010)

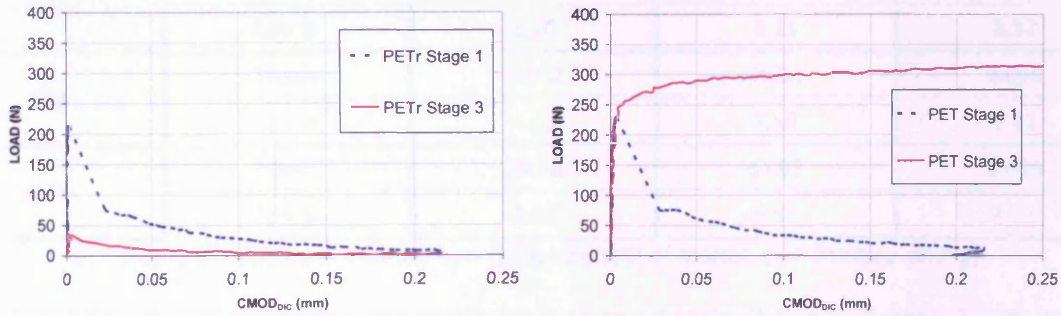

Figure 3.10 - AH3 Specimen (Water 90°C) (a) PETr and (b) PET (Isaacs et al., 2010)

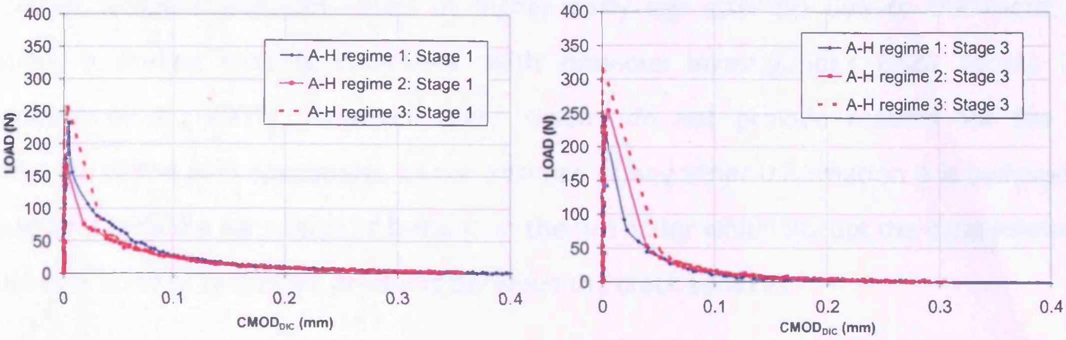

Figure 3.11 - CTRL Specimen for all AH regimes at (a) Stage 1 and (b) Stage 3 (Isaacs et al., 2010)

Figure 3.8 - Figure 3.11 show that the 4-day strength of the AH2 specimens (activated by steam and cured with steam turned off) was considerably lower than the AH1 and AH3 specimens. As all mix ratios were the same it is assumed that the difference is due to the natural variations in early-age mortar strengths.

The graphs also clearly show that the AH1 and AH2 regimes exhibit significant autogenous healing with the percentage healing being between 68 and 80%, which is also reflected in the stiffness recovery results in Table 3-6. The AH3 regime on the other hand only resulted in 17% strength recovery.

A series of material property tests were carried out on the material used in the specimens in the same manner as the proof of concept tests and are given in Table 3-7.

Table 3-7 - Measured Material Properties (Isaacs et al., 2010)

Regime		E kN/mm²	f_{cu} N/mm²	G_f N/mm
AH1	Mean	20.80	23.00	0.017
	CoV %	3.20	8.31	8.32
AH2	Mean	20.72	25.64	0.025
	CoV %	4.59	8.60	1.22
AH3	Mean	24.28	34.83	0.025
	CoV %	2.11	6.62	4.11

E = Young's modulus of mortar, f_{cu} = cube strength of mortar, G_f = fracture energy.

A further series of investigations were carried out on small scale 25mm x 25mm x 25mm mortar cubes which were cured under the same regimes as in AH1 – AH3 in order to isolate the effect of the curing regime on the hydration process. These results are shown in Table 3-8 and suggest that higher temperatures can result in higher early age strength due to the more rapid hydration; a finding that is consistent with previous investigations (Lura et al., 2001) (Lothenbach et al., 2007). However these results do not provide reasons for the poor performance of the AH3 specimens. In the absence of any other information it is believed that this may be due to the formation of bubbles in the hot water which disrupt the establishment of a continuous layer of hydration products between the crack surfaces.

Table 3-8 - Compressive Strength of Small Scale Mortar Specimens

	AH1	**AH2**	**AH3**
Av. strength of cubes (N/mm^2)	16.51	30.67	26.32

Finally, the effect of the pre-stressing effect of the activated polymer is seen in Figure 3.8(b) and Figure 3.9(b) where there is an increase in both load (Table 3-5) and stiffness (Table 3-6). Furthermore the stress drop that follows the peak stress in specimens AH1 and AH2 during Stage 3 loading indicates the formation of new cracking and hence the occurrence of autogenous healing during Stage 2.

3.3.3 Conclusions

These tests have highlighted that both (i) dry heat activation and water based healing (AH1) and (ii) steam activation and healing (AH2) are effective in promoting autogenous healing. In the former, a strength recovery of approximately 80% was achieved having removed the polymer following the healing stage and 125% when the polymer was left in place enabling the system to act as a pre-stressed member. In the latter, the strength recovery was also 80% with the polymer removed and 200% with it remaining as a pre-stressing tendon.

3.4 Significance of Experiments – Future Work

Despite the success of the 'Proof of Concept' experiments and subsequent investigations into the enhancement of autogenous healing, it is suggested that further work is required to develop a system that regains 100% of its strength. As detailed in Chapter 2, possible investigations could include variations in mix proportions and admixture content, water content variations, age of healing and studies into the effect of the curing and healing environments.

Investigations into the development of the polymer shrinkage-stress when activated in both water and steam are also required to understand how the system behaves during the AH2 and AH3 healing regimes.

Finally, the development of polymers that generate a higher shrinkage-stress is also required to enable the potential of the LatConX system to provide full pre-stress to be investigated.

3.5 Conclusions

- This investigation into the LatConX system has shown that the concept is feasible and has the potential for further development.
- Currently, strength recovery of 80% has been achieved and it has been demonstrated that the polymer strands act as pre-stressing tendons.
- It is clear however, that the activation and curing regimes are critical to the success of the system, with both 'dry heat activation followed by water curing' and 'combined steam activation and curing' Activation-Healing regimes providing comparable levels of pre-stress and autogenous healing.

Chapter Four: **Polymer Experimental Studies**

An experimental series was carried out initially to investigate suitable polymers for the LatConX system and subsequently to understand the transient thermo-mechanical behaviour of the chosen polymer. It was first necessary to establish criteria for the polymer to be used as tendons in the LatConX system (Jefferson et al., 2010) and then conduct screening tests in order to find a suitable polymer. This initial work was undertaken as part of a Royal Society of Engineering Brian Mercer Feasibility Award.

The review of literature (Chapter 2) revealed insufficient work on the transient thermo-mechanical behaviour of shrinkable polymers. Therefore a series of trial experiments were carried out to develop a suitable testing procedure and to understand better the behaviour of shrinkable polymer materials. The screening exercise comprised a series of experimental studies investigating the development of stress with temperature. Initial tests were carried out by NetComposite as part of the Brian Mercer Award and were followed by a series of more detailed investigations by the author. These are summarised in Table 4-1.

Upon completion of the material screening and trial experiments, a series of parametric studies were carried out on the chosen material, the results of which are presented in this chapter and are summarised in Table 4-1.

Table 4-1 - List of Experimental Procedures

	Section	Series	Material	Type	Undertaken By
Preliminary Investigation	4.1.1	NCST	PURE PP	Stress Development with Temperature	NetComposite
	4.1.1	NCST	Armordon PP	Stress Development with Temperature	NetComposite
	4.1.1	NCST	Lotrak PP	Stress Development with Temperature	NetComposite
	4.1.1	NCST	Certran PE	Stress Development with Temperature	NetComposite
	4.1.1	NCST	Multiprof PP	Stress Development with Temperature	NetComposite
	4.1.1	NCST	Shrinktite PET	Stress Development with Temperature	NetComposite
	4.1.2.1	CUST	PP Tapes	Stress Development with Temperature	Author
	4.1.2.2.1	CUST	Woven PP Strips (WPP)	Constant Displacement	Author
	4.1.2.2.2	CUST	Woven PP Strips (WPP)	Constant Load	Author
	4.1.2.3.1	CUST	Glass Fibre Reinforced PP Strips (GFRPP)	Constant Displacement	Author
	4.1.2.3.2	CUST	Glass Fibre Reinforced PP Strips (GFRPP)	Constant Load	Author
	4.1.2.4.1	CUST	Shrinktite PET Tapes (PET)	Constant Displacement	Author
	4.1.2.4.2	CUST	Shrinktite PET Tapes (PET)	Constant Load	Author
	4.1.3.3	CUPD	Shrinktite PET Tendons (PET)	Specimen Preparation	Author
	4.1.3.4	CUPD	Shrinktite PET Tendons (PET)	Procedure Development	Author
Material Property Study	4.2.1.1/4.2.2.1	-	Shrinktite PET Tendons (PET)	Study of Geometric Properties	Author
	4.2.1.2/4.2.2.2	-	Shrinktite PET Tendons (PET)	Study of Stress Development with Temperature	Author
	4.2.1.3/4.2.2.3	-	Shrinktite PET Tendons (PET)	Study of Effect of Soak Time on Stress Development	Author
	4.2.1.4/4.2.2.4	-	Shrinktite PET Tendons (PET)	Study of Effect of Temperature on Young's Modulus	Author
	4.2.1.5/4.2.2.5	-	Shrinktite PET Tendons (PET)	Study of Free Shrinkage Development with Temperature	Author

* For "Series" definitions see section 4.1.1 (NCST), section 4.1.2 (CUST) and section 4.1.3 (CUPD)
* For "Type" see subsequent sections.

4.1 Preliminary Investigations

The polymer to be used in the LatConX system (Jefferson et al., 2010) presented in Chapter 1 has the following requirements:

1. A minimum value of shrinkage-stress (20MPa) which is governed by the stress required to close cracks and put the crack into a compression of at least 1MPa. This was chosen to be twice the value required for enhancing autogenous self-healing proposed by ter Heide (ter Heide et al., 2005). Calculations were carried out and showed that if a tendon area of 2% of the cementitious cross-section for tendons placed at an eccentricity of depth/4, a tendon shrinkage-stress of 20MPa will be required to produce an extreme fibre pre-stress of 1MPa (Jefferson et al., 2010). These calculations are presented in Appendix B (Jefferson et al., 2010).
2. An activation temperature for stress development occurring between 70-90°C to prevent premature activation during the hydration process of the cementitious material or damage to surrounding concrete.
3. The material should be inert to an alkaline environment; and;
4. Should maintain >70% of the shrinkage-stress for the working life of the structure.

The preliminary investigation comprised three test series highlighted in Table 4-1 and summarised as follows:

1. Screening tests undertaken by NetComposite (NCST)
2. Screening tests undertaken at Cardiff University (CUST)
3. Experimental Procedure Development at Cardiff University (CUPD)

4.1.1 Screening Tests Undertaken by NetComposite (NCST Series)

The brief for NetComposite in the NCST series was to identify an "off the shelf" polymer that would require little or no modifications in order to be suitable for the LatConX system. It should be noted that no new material development was carried out, as this is beyond the scope of this thesis. NetComposite identified six candidate materials which are summarised in Table 4-2 (Jefferson et al., 2010).

Table 4-2 - Candidate Materials Identified for NCST

Name	Polymer	Description	Form	Area (mm^2)	Supplier
PURE	PP	Oriented PP tape coextruded with PP-PE copolymer	Tape	0.126	Lankhorst
Armordon	PP	Oriented PP tape coextruded with PP-PE copolymer	Tape	0.224	Don & Low
Lotrak	PP	Oriented PP tape	Tape	0.10	Don & Low
Certran	PE	Gel spun PE continuous filament yarn	Yarn	0.061	University of Leeds
Multiprof	PP	Oriented PP tape coextruded with heat sealing layer, fibrillated	Fibrillated Tape	0.24	Lankhorst
Shrinktite	PET	Oriented PET tape	Tape	0.10	Aerovac

The results of the NCST series are presented in Figure 4.1 which highlights PET Shrinktite as the material generating the highest stress, although at a temperature suitable for the LatConX system (70-90°C), the PP MultiProf generated a similar stress.

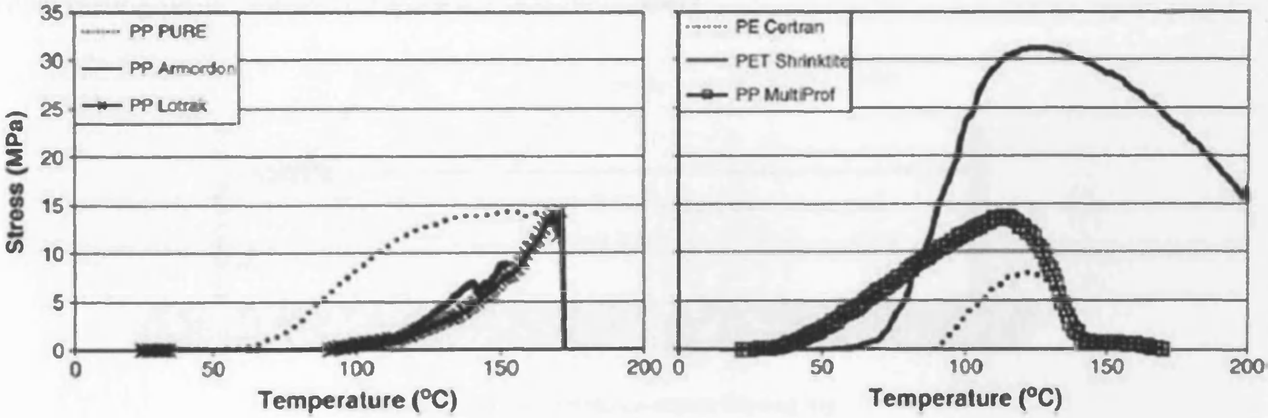

Figure 4.1 - Results of NCST Series

4.1.2 Screening Tests Undertaken by Cardiff University (CUST Series)

The screening tests undertaken at Cardiff University by the author investigated further the shrinkage behaviour of the materials identified in the NCST series and developments thereof and include:

1. Polypropylene Tapes (PP)
2. Woven Polypropylene Strips (WPP)
3. Glass Fibre Reinforced Polypropylene Strips (GFRPP)
4. Polyethylene Terephthalate Tapes (PET)

4.1.2.1 Polypropylene Tapes

Small polypropylene (PP) tapes, 3mmx0.046mm in cross-section and 300mm in length were investigated to understand their shrinkage behaviour with temperature. The method of testing was developed as part of the investigation and will also be presented.

The specimens were initially put in an oven and heated to a temperature of 120°C, as this was known to be well above the transition temperature for this material. By measuring their length before and after heating it would be possible to calculate their free shrinkage. However, when unrestrained, they coiled up at this temperature.

In order to overcome this issue of coiling, the tapes were restrained at both ends which resulted in no coiling, but also no method of understanding the shrinkage behaviour. Therefore the simple testing set-up shown in Figure 4.2 was developed.

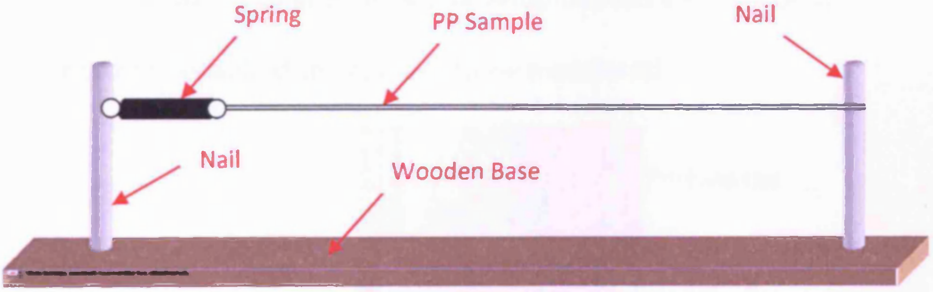

Figure 4.2 - Initial Shrinkage-stress Testing Rig

The specimen was attached between a spring of known stiffness and a fixed support. The length of the spring was measured before and after heating at 120°C for 2 hours (2 hour soak time). In order to overcome thermal expansion issues the post-heating measurement was taken after a period of cooling. The shrinkage force could then be determined from the change in length and spring stiffness.

Further enhancements were made by using multiple strips and a method of gripping that minimised slipping via clamping between steel plates. This test yielded more reliable results, although the PP tapes only produced approximately 4-5MPa of shrinkage force which was too low for the LatConX system and at an undesirable temperature.

4.1.2.2 Woven PP Strips (WPP)

The WPP strips shown in Figure 4.3 were 3mm x 10mm in cross-section and 300mm in length. They were manufactured by weaving PP tapes to form woven strips which were bonded with an adhesive.

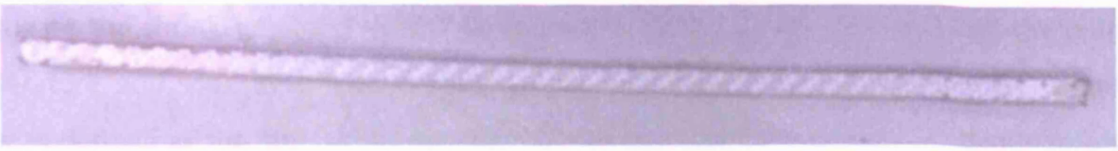

Figure 4.3 - WPP Specimen

The size of these specimens were suitable for a Dartec tensile testing machine with a 5kN load cell retrofitted. This machine also had an Instron environmental chamber, capable of temperatures ranging from -50°C to 250°C. Two testing procedures were developed and undertaken whilst varying the temperature:

1. *Constant Displacement* to enable load development to be monitored
2. *Constant Load* to enable displacement to be monitored.

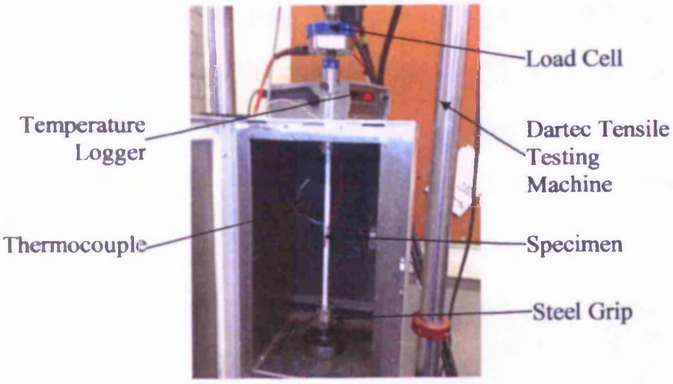

Figure 4.4 - Preliminary Experimental Setup

The general setup consisted of attaching the specimens to the steel grips and placing the gripped specimen into the machine under a pre load of 30N, as seen in Figure 4.4. A thermocouple was located inside the oven, which was linked to a digital recorder to ensure the temperature could be monitored throughout the test.

4.1.2.2.1 Constant Displacement Tests

The constant displacement test measured the overall load development at a desired temperature whilst restraining the shrinkage. The procedure involved heating the specimen to the desired temperature and waiting for the stress to plateau before removing the temperature and returning to ambient temperature. Throughout this process the time, load and temperature were monitored. A variety of selected temperatures and soak times were considered in order to investigate the shrinkage-stress versus temperature behaviour and thereby find the optimum temperature and soak time with respect to the maximum shrinkage-stress. The 'shrinkage-stress' is defined as the stress that develops under restrained conditions i.e. under zero strain change, assuming a specimen to be taut at the start of testing.

The results of the experiments are shown in Figure 4.6 and highlight that as temperature increases, the maximum shrinkage-stress increases. However the maximum stress achievable was only 3.5MPa at a temperature of 155°C, which is not suitable for the LatConX system. The graphs do however highlight an initial issue with the testing procedure; namely, the thermal expansion of the experimental equipment. This is identified by the rapid drop in stress as the temperature is removed, illustrated by the red circle on Figure 4.6.

A significant problem that was noticed during the testing of the WPP specimens was that of delamination and bulging during the heating which may cause damage to the concrete in the LatConX system. This can be seen below in Figure 4.5. Further development seen in section 4.1.3.3 shows a technique adopted for the manufacture of non-laminated specimens which overcomes this issue.

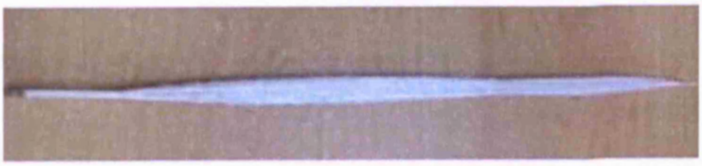

Figure 4.5 - Delamination Issues with WPP

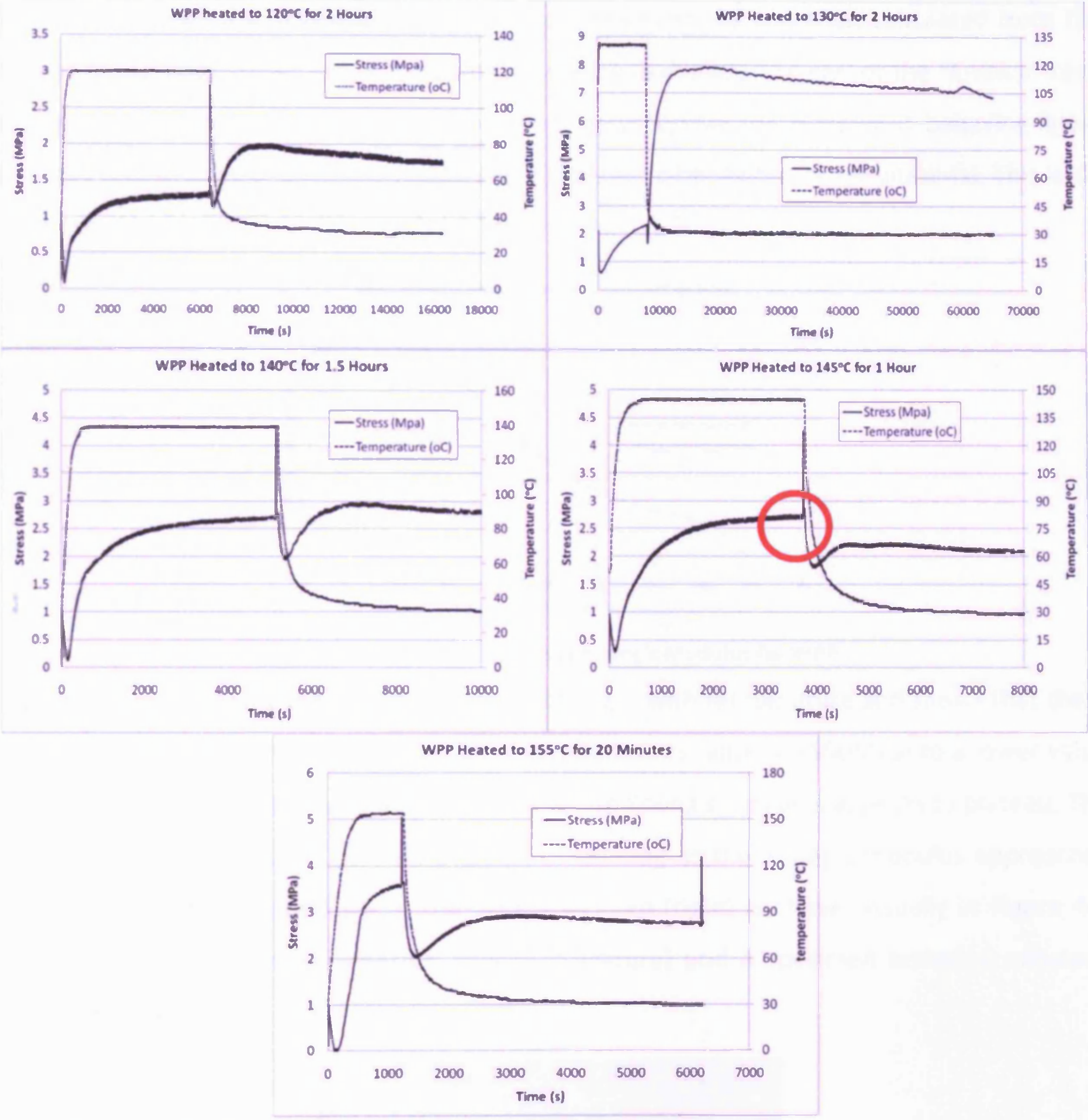

Figure 4.6 - WPP Stress Development with Temperature for Various Temperatures and Soak Times

4.1.2.2.2 Constant Load Tests

The constant load tests were used to investigate the change in Young's modulus with temperature by carrying out "E-value" tests. An "E-value" test comprises a load increase of 50N followed by a load decrease of 50N at each temperature increment, whilst monitoring the load and displacement. The specimen was preloaded with 80N and kept constant at this load during the test whilst monitoring time, temperature and displacement. The temperature was raised in 10°C intervals from 30°C to 160°C with a soak time of 5 minutes at each temperature, following which an "E-value" test was undertaken. The Young's modulus was then calculated from the gradient of the stress-strain graph for both the loading and unloading part of the "E-value" test, thus giving an average value. This does however assume that the material is behaving linear elastically and ignores ongoing shrinkage and visco-elastic behaviour of the material. This issue is addressed in detail for the later tests on PET.

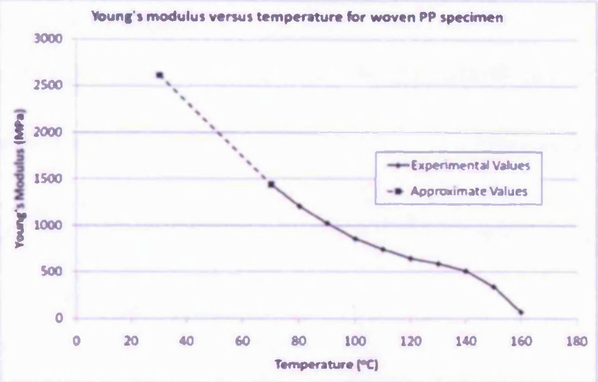

Figure 4.7 - Temperature versus Young's Modulus for WPP

Figure 4.7 illustrates how the Young's modulus changes with temperature and shows that there is a transition from a higher value at ambient temperatures (approx 2500MPa) to a lower value at higher temperatures (500MPa at 140°C) where the Young's modulus appears to plateau. The subsequent drop after 140°C is an indication of melting as the Young's modulus approaches zero. The level of free shrinkage in the WPP specimen (right) is shown visually in Figure 4.8 where it is compared to an untested specimen (centre) and a specimen tested at constant displacement (left).

Figure 4.8 - Visual Shrinkage of WPP

4.1.2.3 Glass Fibre Reinforced PP Strips (GFRPP)

The GFRPP strips as shown in Figure 4.9 were 3mm x 10mm in cross-section and 300mm in length. The specimens were tested as part of the CUST series using the same procedure as the

WPP specimens for the *constant displacement* and *constant load* experiments. The results of which will now be presented.

Figure 4.9 - GFRPP Specimen

4.1.2.3.1 Constant Displacement Tests

The results of the constant displacement experiments for GFRPP are presented in Figure 4.10.

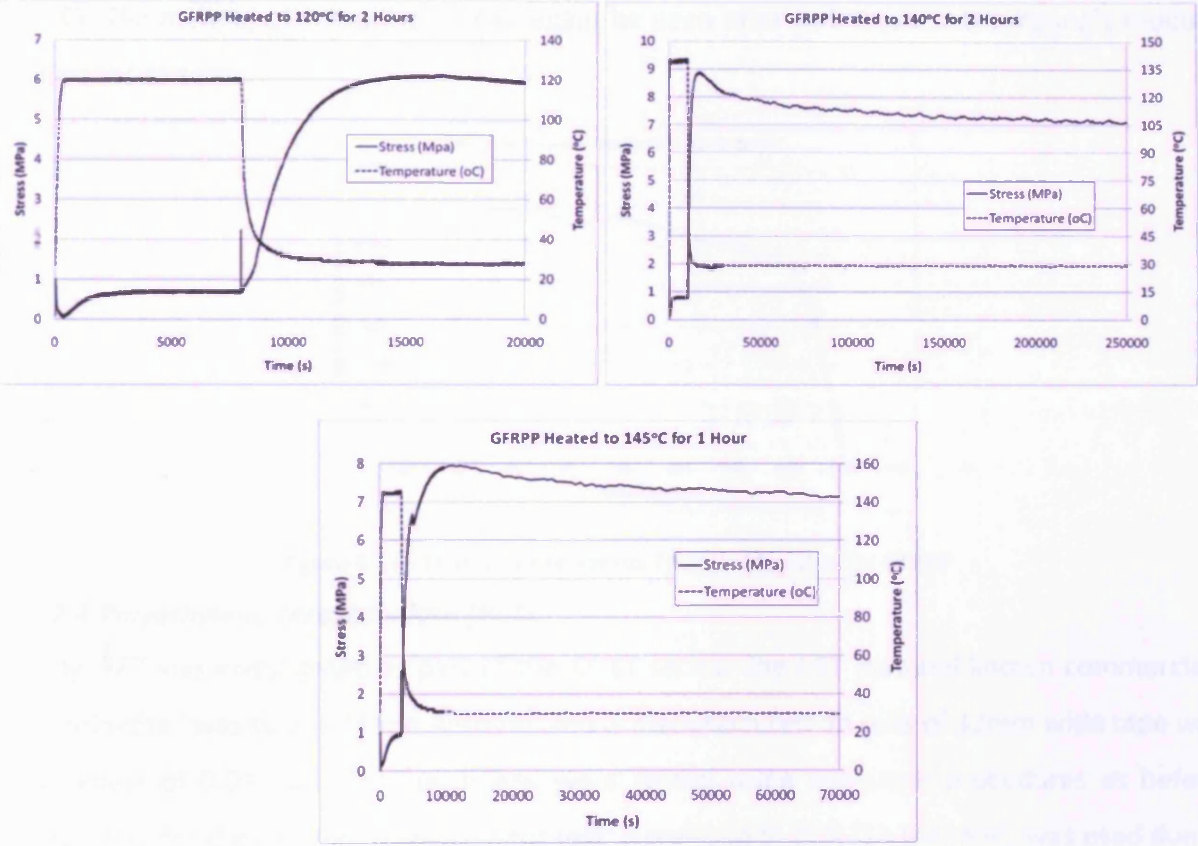

Figure 4.10 - GFRPP Stress Development with Temperature for Various Temperatures and Soak Times

The results show that only a 1MPa stress was generated during the soak time at the chosen temperature, however upon removal of the temperature the stress jumped dramatically to a maximum of 9MPa after being exposed to a temperature of 145°C for 2 hours. The cause for the rapid jump is believed to be the thermal contraction upon cooling of the glass fibres. This stress however does then diminish to 7MPa after 70 hours which equates to approximately a 25% loss in stress over a relatively short period of time, and is potentially due to the relaxation of the glass fibres. These results suggest that glass fibre reinforced specimens may encounter issues of long term stress relaxation due to the relaxation of the glass fibres and therefore do not meet the criteria for the LatConX system.

4.1.2.3.2 Constant Load Tests

The change in Young's modulus with temperature is shown in Figure 4.11 and, as with the WPP, highlights a transition from a higher Young's modulus at ambient temperatures (approximately 12000MPa) to a lower Young's modulus at higher temperatures (approximately 10000MPa at 140°C). The melting of the polymer can again be seen after 140°C when the Young's modulus diminishes to zero.

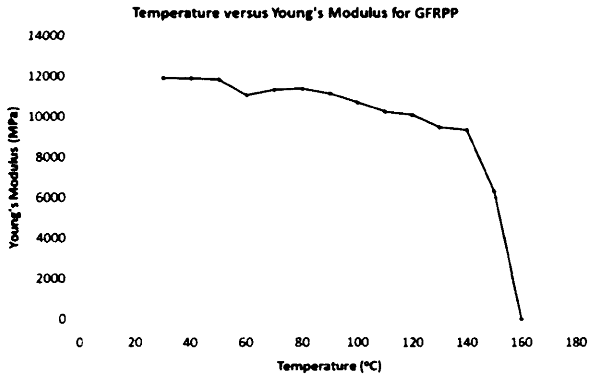

Figure 4.11 - Temperature versus Young's Modulus for GFRPP

4.1.2.4 Polyethylene Terephthalate (PET)

Finally, PET was investigated as part of the CUST series. The PET material known commercially as "Shrinktite" was sourced from AeroVac and is manufactured on rolls of 32mm wide tape with a thickness of 0.046mm. The specimens were tested using the same procedures as before, except that, for the *constant displacement* test, a pre-load of 20N (13.6N/mm^2) was used due to the smaller cross-section and two different pre-loads (20N (13.6N/mm^2) and 30N (20.4N/mm^2)) were used for the *constant load* tests.

4.1.2.4.1 Constant Displacement Tests

The specimens were tested at 3 different heating rates:

1. *Instant Heating to 90°C*

The specimen was heated to 90°C (the maximum temperature specified in the Criteria for the LatConX system) and, following a 3 hour soak time, the temperature was returned to ambient.

2. *ASAP Heating*

   The specimen was heated in 10°C temperature increments from 30°C to 120°C. As soon as the temperature reached the chosen increment, it was raised to the next increment, hence ASAP (i.e. As Soon As Possible).

3. *5 Minute Soak Time*

   The specimen was soaked for 5 minutes at each 10°C temperature increment from 30°C to 120°C; between increments the temperature was raised at the maximum available rate.

The results of the constant displacement tests are shown in Figure 4.12 - Figure 4.14 and highlight a clear effect of heating rate on stress development. The instant heating test, illustrated in Figure 4.12, shows that a maximum stress during heating of 40MPa was generated. Following the peak during heating, the stress then reduced slightly. Upon removal of the heat, a sharp increase in stress was noticed. This can be attributed to the thermal contraction of the specimen and testing equipment as cooling occurs which will be discussed in more detail in section 4.2. The stress finally plateaus at 30MPa and remains at this level for the remainder of the test (14 hours).

The ASAP heating rate seen in Figure 4.13, and the 5 minute soak time seen in Figure 4.14, highlight that at 120°C the stress reaches a maximum and begins to diminish. Both show approximately the same maximum stress of 33MPa. The 5 minute soak time also highlights an interesting trend that sees the stress begin to plateau to a maximum at each temperature increment before rising again as the temperature is raised by a further 10°C.

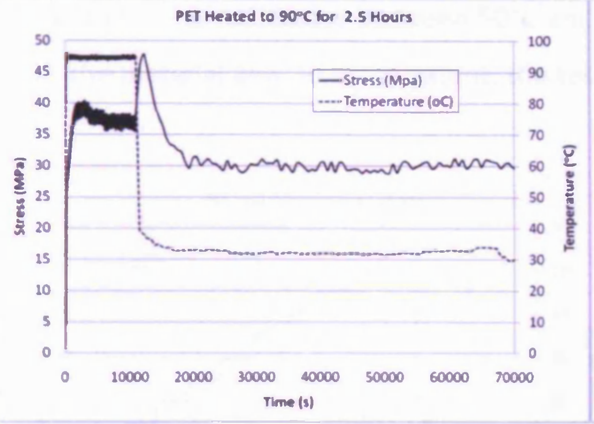

Figure 4.12 - PET Stress Development with Temperature for Instant Heating to 90°C

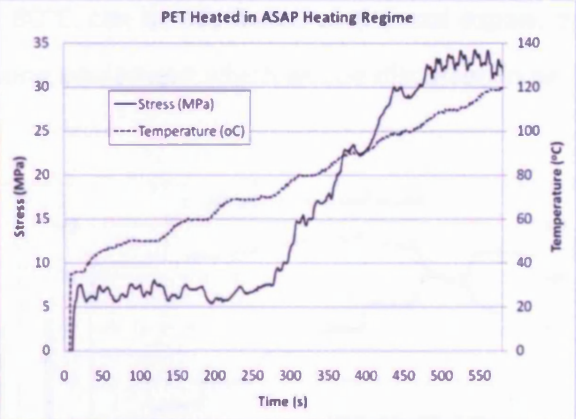

Figure 4.13 - PET Stress Development with Temperature for ASAP Heating Regime

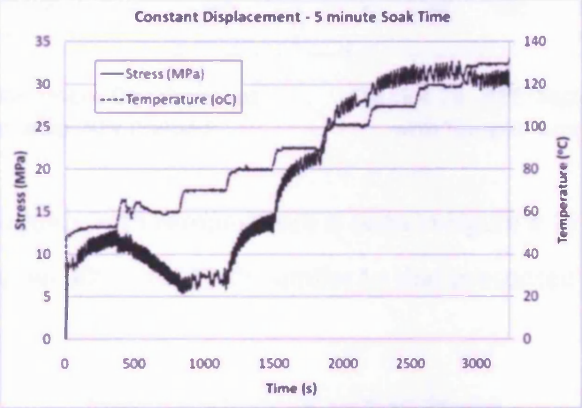

Figure 4.14 - PET Stress Development with Temperature for 5 Minute Heating Regime

4.1.2.4.2 Constant Load Tests

In order to investigate the change of Young's modulus with temperature, a constant load test was undertaken using the same procedure as for the WPP and GFRPP. However, 2 different preloads were used to investigate the effect of preload; these were 20N and 30N. The displacement was also monitored throughout the test which enabled the onset of shrinkage in the specimen to be monitored. Figure 4.15 shows that shrinkage begins to occur at around 80°C and that the specimen continues to shrink until the temperature is removed. The specimen loaded with 30N, seen in Figure 4.16, failed at 110°C and this failure is assumed to be due to the excessive preload. Therefore all future pre-stress will be based on not exceeding 13.5MPa which equates to a 20N preload on the tapes tested. The initial lengthening of the specimen, seen by the graph rising noticeably between 50°C and 80°C, can be attributed to thermal expansion of both the material and, to some extent, the testing equipment which will be discussed in section 4.2.

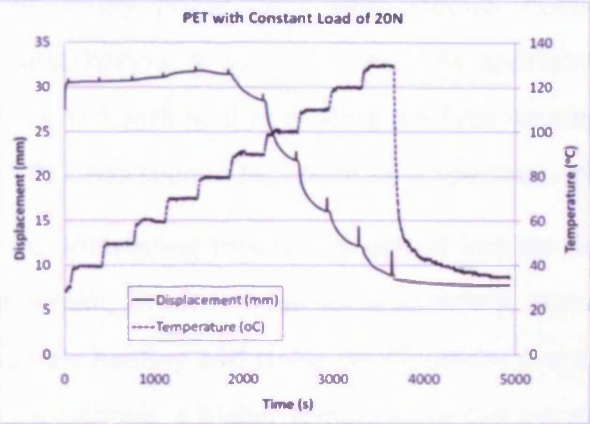

Figure 4.15 - PET Displacement Development with Temperature using 20N Preload

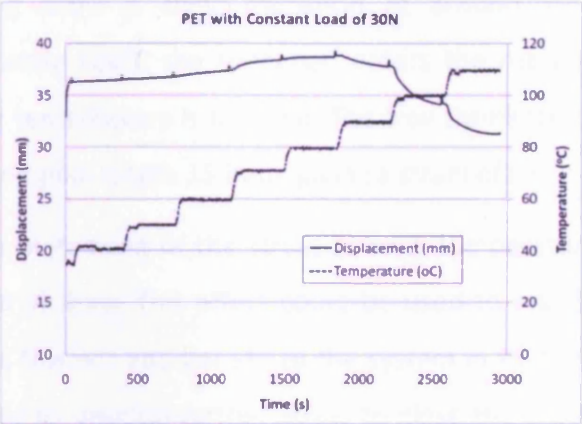

Figure 4.16 - PET Displacement Development with Temperature using 30N Preload

The change in Young's modulus with temperature is seen in Figure 4.17 and clearly shows a tanh type transition zone between 50°C and 120°C similar to that presented by Tobushi et al (Tobushi et al., 2001).

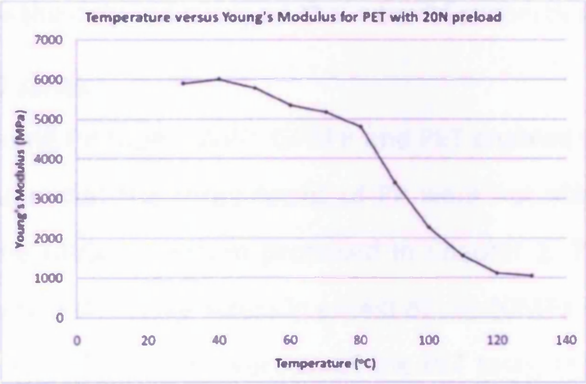

Figure 4.17 – Young's Modulus Development with Temperature for PET with 20N Preload

4.1.2.4.3 Summary of PET Results

PET achieved a maximum shrinkage-stress of 30MPa at 90°C which is not only a suitable stress to close cracks in concrete but also was achieved at an operating temperature that will cause minimal damage to the concrete itself and not be affected by hydration temperatures. The experiments have also highlighted that the PET stress development reaches a maximum at 120°C after which the stress reduces until complete failure due to melting of the specimen. This clearly reflects the theory shown in the literature review in that the specimens are received in their glassy phase, and with gradual heating show a clear transition at around 70°C (Bhattacharyya & Tobushi, 2000). At approximately 120°C the specimen enters the rubbery phase and with further heating the final melting temperature is reached. The free shrinkage of the PET was seen to be 22mm for a specimen of original length 350mm, giving a strain of 6%.

Other interesting trends highlighted include the plateauing of the stress at each temperature increment, if left to soak for a sufficient period of time. This effect could be used to enable multiple heating and stress development events, this will add benefit to the system in that if a crack reforms, a higher temperature can be used to develop further stress to close the crack. The Young's modulus versus temperature relationship also appears to follow a tanh function between 50°C and 120°C, with plateau values before and after the transition corresponding to the glass and rubber regions respectively.

It was however noted that during certain experiments, the PET was found to break at the grips due to the local heating effects. The thin tapes also posed a gripping issue in several tests which needed addressing before the detailed study on the material properties was undertaken.

4.1.2.5 Summary of CUST series

The CUST series investigating PP tapes, WPP, GFRPP and PET enabled a basic test procedure to be developed. It was found that the three forms of PP were not able to meet the minimum criteria established for the LatConX system proposed in Chapter 1. The initial studies on PET tapes however did generate a shrinkage-stress in excess of the 20MPa required for LatConX at a suitable temperature of 90°C. Due to the success of the PET tests, the screening studies were concluded. A follow-on series of tests were then undertaken to enable detailed understanding of the transient thermo-mechanical behaviour of PET and to provide data adequate for the development of a numerical model.

4.1.3 Experimental Procedure Development at Cardiff University (CUPD Series))

The CUST series was deemed adequate to identify a suitable material but not accurate enough for detailed experimental data. The problems that gave rise to inaccuracies will now be presented and solutions developed.

4.1.3.1 Issues with Experimental Procedure

One major issue was that of gripping the specimens. Figure 4.18 below shows the centre of the specimen slipping from the grip and in some cases the specimens actually failed at the grips, which can be attributed to a localised heating at the steel grips.

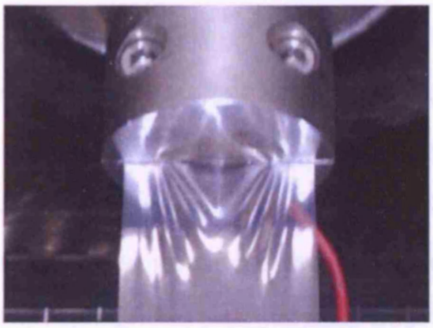

Figure 4.18 - Grip Slip Issues

A major cause of the gripping issues was the small cross-section of the specimen, which in addition also posed difficulties for their use as tendons in the LatConX system. Therefore specimens with larger cross-sections were required to enable accurate testing and efficient use in the combined LatConX system.

4.1.3.2 Solutions to Flaws in Experimental Procedure

A series of investigative experiments were carried out to address the issues highlighted above. After several iterations, a method that both overcame the issue of gripping and was suitable for use in the combined LatConX system was realised. It was decided to use groups of 6mm wide strips, with 25 strips in each group. The number of strips per group could be varied depending on the cross-sectional area required. Initially the strips were bonded together with a spray adhesive, the results of which can be seen in Figure 4.19. The use of a spray adhesive however was found to cause problems with the shrinkage activation and stress development. It was also found that the adhesive melted at the activation employed (i.e. 90 ^{o}C)

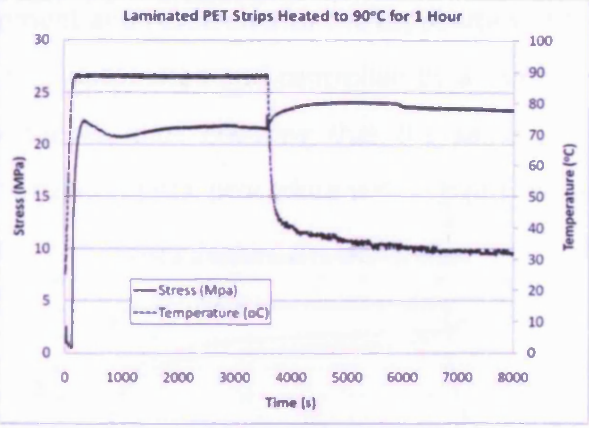

Figure 4.19 - Laminated PET Strips Stress Development with Temperature

The individual strips were therefore grouped together and only bonded at the ends, leaving the individual strips free to shrink independently along the length of the specimen. It was also found that the best method of gripping was to create a mechanical lock within the grips. Preliminary experimental studies using this method are presented in Figure 4.20 and the consistency of the results indicates that the manufacturing method chosen is adequate for the LatConX system. Visual inspection of the grips also highlighted that slippage was no longer apparent. Figure 4.20 shows that a shrinkage-stress of 37MPa at 90°C was generated.

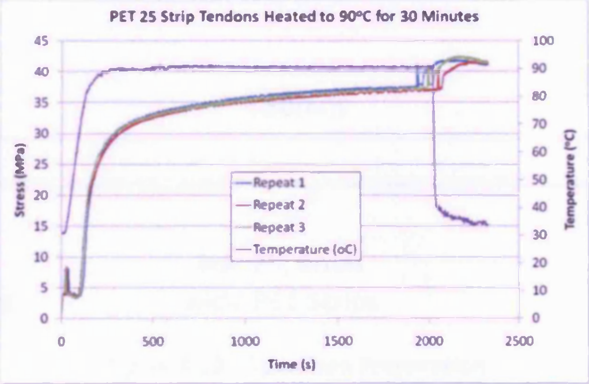

Figure 4.20 - PET 25 Strip Tendons Stress Development with Temperature

As the manufacturing methods consisted of grouping individually cut PET strips, a series of constant displacement tests were also carried out on specimens containing 50 strips to ensure the manufacturing method was adequate. The results of which are presented in Figure 4.21, showing that the chosen manufacturing method does not cause a significant reduction in shrinkage-stress generated.

Following further development and research into the capabilities of the testing equipment, the testing procedures were fully automated and controlled by a computer using the environment chamber's inbuilt thermocouple, thus ensuring that the same procedure was used for all experiments. Details of the experimental procedure will be given in a subsequent section.

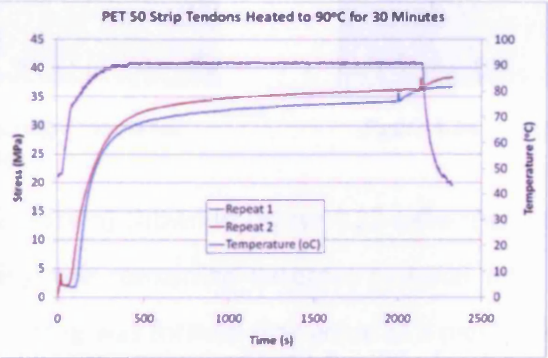

Figure 4.21 - PET 50 Strip Tendons Stress Development with Temperature

4.1.3.3 Specimen Preparation

The specimen preparation has been published in a paper by the author (Dunn et al., 2011) and will now be summarised. Figure 4.22 highlights the specimen preparation which consists of 25No. 6mm wide strips being grouped together and gripped using metal plates and a mechanical plug.

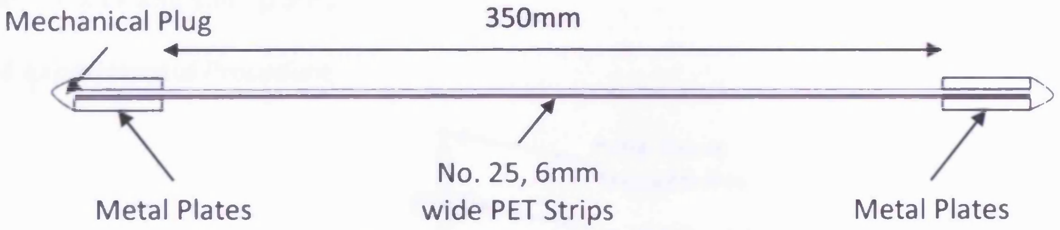

Figure 4.22 - Specimen Preparation

In order to ensure that the individual strips were all of equal tension the setup shown in Figure 4.23 was used. Strips of length 600mm were placed in a specially designed jig which is 450mm in length and which is illustrated in Figure 4.23. The strips are placed one by one, ensuring that each are tensioned equally before compressing in a vice and removing the excess material using a soldering iron. This also bonds together the ends of the 450mm length specimens whilst leaving them as individual strips along their length.

Figure 4.23 - Manufacturing Process for Specimens

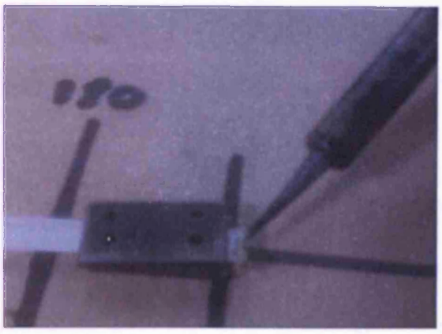

Figure 4.24 - Creation of Mechanical Lock

The metal end plates (10x20x3mm) shown in Figure 4.22 were then attached to the specimen at 350mm spacing. By melting the remaining external material into a single element using a soldering iron, a mechanical plug was formed that acted as a mechanical lock as shown in Figure 4.24.

A series of trials were carried out using this procedure, during which slip at the grips was monitored locally and visual inspections were undertaken at the end of each test. In the preliminary studies, significant slip was evident from the marks at the edge of the gripped region. The system employed in these experiments however was successful in removing the effect of grip slip, with no slip being measured in several trials using this method of a mechanical lock and steel plates.

4.1.3.4 Experimental Procedure

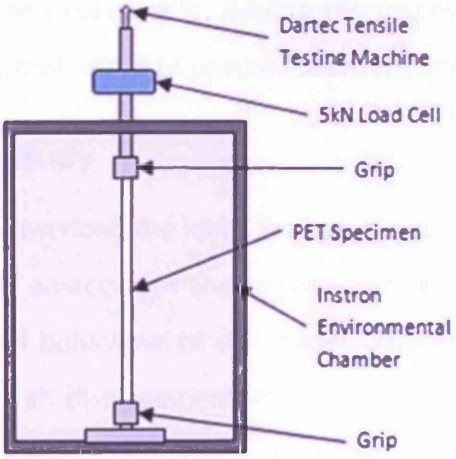

Figure 4.25 - Diagram of Experimental Setup

The experiments were undertaken using a Dartec tensile testing machine fitted with an Instron environment chamber capable of temperatures ranging from -50°C to 250°C. The experimental set up can be seen in Figure 4.25.

The experimental set-up is the result of a series of trial experiments in which iterations were undertaken in order to develop an accurate procedure. The key issues with gripping were overcome through the use of a mechanical lock that both removes grip slipping and prevents differential shrinkage between individual strips.

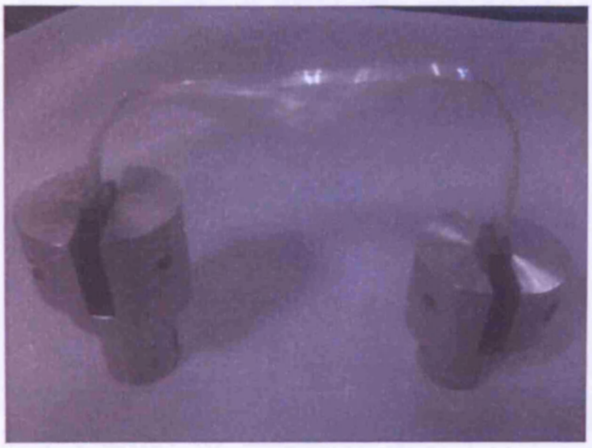

Figure 4.26 - Photograph of Grip Setup

Following the specimen preparation discussed previously, the metal plates are then placed between the machines grips as seen in Figure 4.26. The slack is then removed from the specimens by applying a pre-stress of 2.9N/mm^2 (unless specified otherwise below) using the testing machine. Throughout the experiments, despite the success of the preliminary gripping studies, the grips will be closely monitored to ensure consistent and accurate results.

4.2 PET Material Property Study

The previous subsections have described the identification of a suitable polymer for the LatConX system and the development of an accurate and reliable testing procedure. Therefore in order to understand fully the material behaviour of the chosen PET material a series of parametric studies were undertaken in which displacement at the grips, load and environment chamber temperature were continuously monitored. The maximum monitoring rate of 100 readings per second was used when the temperature or load rate was at a maximum but lower sampling rates were used for other cases. The series of studies were undertaken to explore the following parameters and aspects of behaviour:

1. Geometric parameters
2. Stress development with temperature
3. The effect of soak time on stress development
4. The variation of Young's modulus with temperature.
5. Free shrinkage development with temperature

4.2.1 Parametric Study Procedures

4.2.1.1 Study of Geometric Properties

Sections of different cross-section and length were tested to assess the effect of geometric properties on measured shrinkage-stress. Sections containing 25 strips (6.9mm^2), 50 strips (13.8mm^2) and 75 strips (20.7mm^2) were tested at lengths of 350mm and specimens of length 360mm and 180mm containing 25 strips were also tested. Each specimen was held at constant displacement while the temperature was raised to 90°C at a rate of 0.41°C/s and then soaked for 30 minutes before it was reduced to ambient temperature for 10 minutes.

4.2.1.2 Study of Stress Development with Temperature

A 360mm long specimen containing 25 strips (standard specimen) was held at constant displacement while the temperature was raised to 90°C at a rate of 0.41°C/s and soaked for 3 hours before it was reduced to ambient temperature and soaked for a further 1 hour.

4.2.1.3 Study of Effect of Soak Time on Stress Development

A standard specimen was held at constant displacement while the temperature was increased in 10°C increments from 30°C to 170°C. At each 10°C increment, the temperature was held for the chosen soak time. Three different soak times were investigated; zero soak, 5 minute soak and a 1 hour soak. Between each increment, the temperature was raised at a rate of 0.13°C/s.

4.2.1.4 Study of Effect of Temperature on Young's Modulus – "E-Value Test"

A standard specimen was held at constant load while the temperature was raised in 10°C increments from 30°C to 160°C. At each temperature increment, the specimen was soaked for 5 minutes and then a loading/unloading cycle of amplitude 10N was applied at a specified rate. Three rates were used: 10N/s, 1N/s and 0.1N/s. This loading and unloading cycle is referred to as the "E-Value" test and was repeated for every temperature increment.

4.2.1.5 Study of the Free Shrinkage Development with Temperature

Throughout the Young's modulus study, the displacement of the specimen was recorded and this enabled the shrinkage-temperature relationship to be studied.

4.2.2 Results and Discussion

The results of the parametric studies which are the subject of a journal article by the author (Dunn et al., 2011) will now be discussed and justifications for the behaviour given.

4.2.2.1 Study of Geometric Parameters

The results of the stress development tests for 360mm long specimens with 3 different cross-sectional areas and shorter 180mm specimens of 25 strips can be seen in Figure 4.27 - Figure 4.30. A summary of the averages is presented in Figure 4.31, which indicates that the effect of varying cross-sectional area on stress development is limited (maximum 4%) in the range considered. This further highlights that the chosen manufacturing method for the specimens discussed previously is both accurate and consistent.

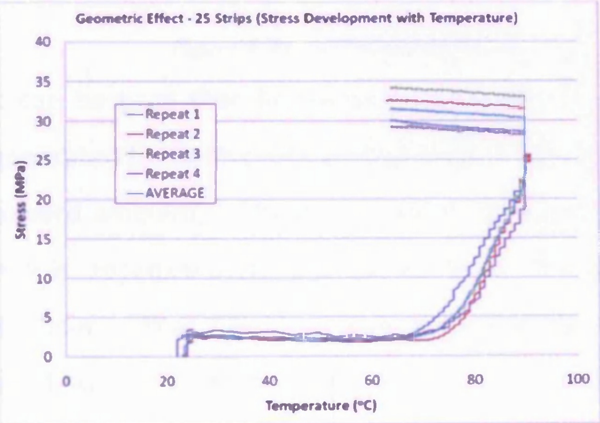

Figure 4.27 - Geometric Effect – 25 Strips (Stress Development with Temperature)

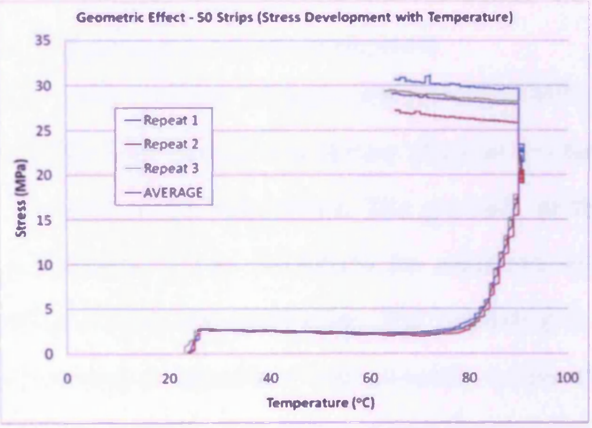

Figure 4.28 - Geometric Effect – 50 Strips (Stress Development with Temperature)

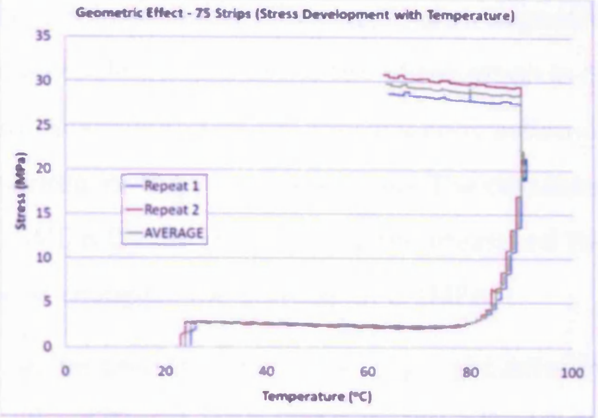

Figure 4.29 - Geometric Effect - 75 Strips (Stress Development with Temperature)

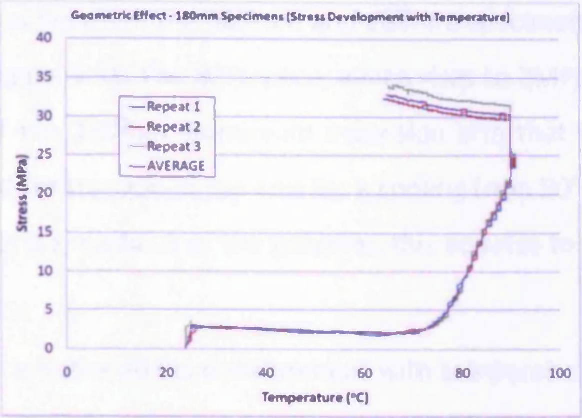

Figure 4.30 - Geometric Effect - 180mm Specimens (Stress Development with Temperature)

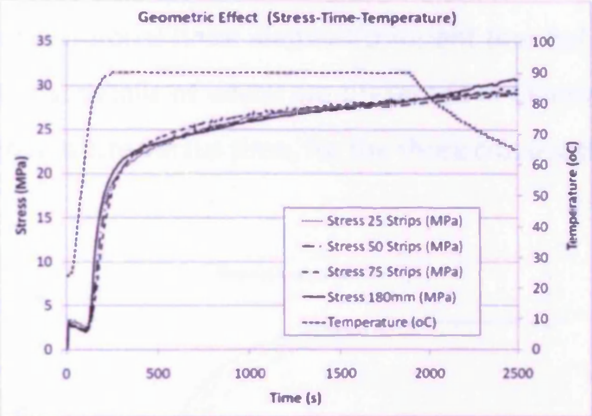

Figure 4.31 - Summary of Effect of Geometric Properties on Stress Development

It can be seen that following a 30 minute soak at 90°C a stress of approximately 28.5MPa is generated for each cross-section tested. Following the reduction of this temperature and return toward ambient, a slight increase in stress can be seen in the specimens. The gradient of this rise is approximately the same for all 3 cross-sections. It can therefore be assumed with confidence that this is a thermal contraction effect due to the steel grips, the bottom grip is fixed to the bottom of the environment chamber and is therefore permanently under the influence of raised temperatures. The top grip is located in the neck of the chamber where heat will also cause thermal contraction effects. In addition, the thermal contraction of the polymer itself will generate an increase in the stress as the thermal contraction is independent of shrinkage and is a reversible effect.

There is a noticeable difference in shrinkage-stress between the 360mm and 180mm specimens in the cooling phase at the top of the graph in Figure 4.31. The difference, which rises to 2MPa, can be attributed to the thermal contraction of the 180mm aluminium extension arm that is required for the shorter specimen. The calculated contraction of the arm for a cooling from 90°C to 64°C is 0.108mm and, using the measured Young's modulus of the polymer, this equates to a stress change in the polymer of 2.1MPa.

It can be seen that there is a very slight difference in the stress development with temperature for the different cross-sections. This effect is expected as the greater the cross-sectional area, the greater the temperature difference between the surface and the centre of the cross-section. To investigate this temperature lag further and to investigate its responsibility for the differences noted, a two-dimensional finite element transient thermal analysis was undertaken for each of the cross-sections, details of which are presented in Chapter 6. The results in terms of centre-of-specimen temperature versus time, for the three cross-sections are shown in Figure 4.32.

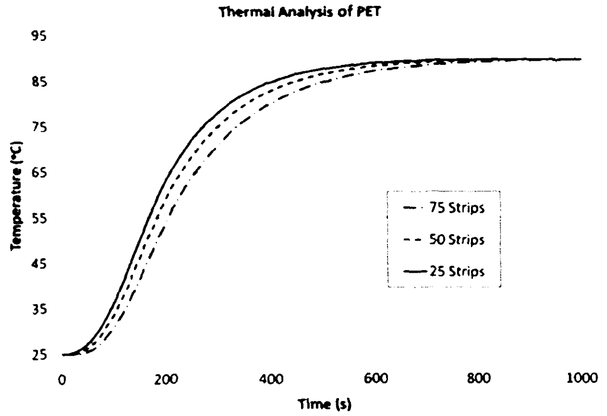

Figure 4.32 - Thermal Analysis of Different Cross-sectional Areas

These results provide justification for the slightly differing stress paths during at the early stages of stress development. The thermal analysis has highlighted that after 930 seconds (15.5minutes) full temperature saturation is achieved for all 3 cross-sectional areas. The details of the thermal analysis are given in Chapter 6.

It is clear that both the cross-sectional area and specimen length have negligible effect on the stress development of the polymer provided that an adequate soak time is provided to enable full saturation of the polymer at a given temperature. Furthermore the LatConX experiments utilise 180mm long specimens and hence the data generated for the 360mm specimens, with corrections, were considered applicable to the behaviour of the tendons in the LatConX specimens.

4.2.2.2 Study of Stress Development with Temperature

Figure 4.33 and Figure 4.34 highlight the stress development with time and temperature respectively. The shrinkage-stress is generated at a decreasing rate reaching a plateau at approximately 32.5MPa following a 3 hour soak at 90°C which is consistent with the magnitude of shrinkage-stress found in (Pakula & Trznadel, 1985). The generation of shrinkage-stresses is a well-known property of drawn polymers, associated with the orientation of the long chain molecules in the direction of drawing (Trznadel & Kryszewski, 1992) (Ward & Sweeney, 2004). Trznadel and Kryszewski suggest that the shrinkage-stress potential of the partially extended polymer chains is associated with the "entropic tendency of the chains to assume more coiled conformations." (Trznadel & Kryszewski, 1992). The stress plateau is consistent with the findings of Gupta et al (Gupta et al., 1994) who suggested that the increase in crystallisation that occurs above the transition temperature (T_g) stabilises the oriented state and reduces relaxation potential, which is seen by the plateau of the shrinkage-stress response (Trznadel & Kryszewski, 1992).

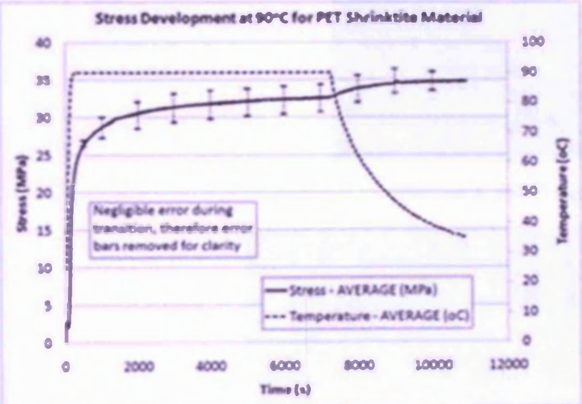

Figure 4.33 – Stress Development with Time

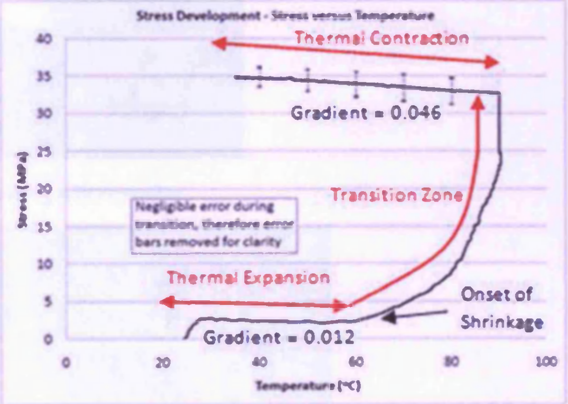

Figure 4.34 - Stress Development with Temperature Showing Highlighted Regions

The stress rise at the end of the test can be attributed to thermal contraction of the polymer upon cooling. Trznadel and Kryszewski explain that the shrinkage that has occurred previously, associated with molecular coiling, is permanent and non-recoverable, but that the independent molecular action of thermal expansion is recoverable (Trznadel & Kryszewski, 1992).

It has been found by others (Trznadel & Kryszewski, 1992) (Bhushan, 2000) that annealing (heating above the transition temperature) acts to increase slightly the coefficient of thermal expansion which provides an explanation for the difference between the 'below T_g' expansion and contraction slopes at the start and end of the graph respectively.

Three distinct regions can be seen in Figure 4.34, namely; an initial thermal expansion zone, a transition zone and a final thermal contraction region upon removal of heat. The initial decrease in stress is attributed to the thermal expansion of the polymer in the pre-shrinkage stage which, under the present constant strain/displacement conditions, gives rise to this decrease in stress. As the transition zone is reached the shrinkage becomes the dominant process and thermal expansion becomes negligible (Trznadel & Kryszewski, 1992). The onset of shrinkage occurs in the region between 60°C and 70°C which is consistent with published values of the glass transition temperature of PET (Gupta et al., 1994) (Ward & Sweeney, 2004).

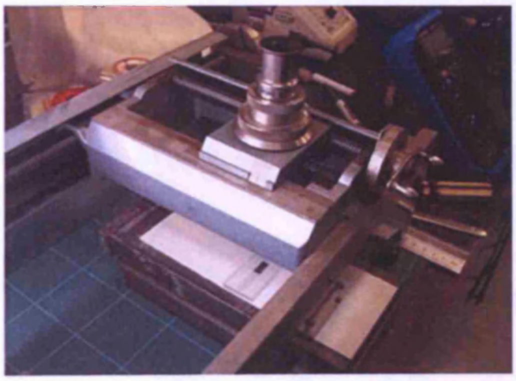

Figure 4.35 - Travelling Microscope

Figure 4.36 - Microscope Slides Containing Specimen for Width Measurement

The error in stress development of a series of experiments is presented in the form of error bars on Figure 4.34. The error is approximately 1.5MPa above and below the average stress calculated. As the calculated maximum stress developed is a function of the cross-sectional area, the error can be attributed to the manufacturing process of the individual strips. A travelling microscope, as seen in Figure 4.35, was used to accurately measure a random selection of strips to an accuracy of 0.01mm. The specimens were coloured black and placed between two microscope slides to enable clear and accurate measurements, as seen in Figure 4.36. The measured mean and standard deviation of the strip widths were 5.77mm and 0.16 respectively. A change in width equal to the standard deviation would equate approximately to the calculated difference in stress.

4.2.2.3 Study of Effect of Soak Time on Stress Development

Figure 4.37 presents the average stress versus temperature trends for the 3 soak times investigated. The graph shows that the maximum stress is achieved at 120°C after which the stress reduces. This approximately matches the recrystallisation temperature identified by Jog (Jog, 1995). Gupta et al (Gupta et al., 1994) also highlight that above 100°C a large increase in crystallinity occurs. It is known that this recrystallisation process affects the ability for shrinkage to occur since when part of a molecular chain is incorporated into a crystallite, during recrystallisation, the stress exerted at the molecule ends is reduced (Gupta et al., 1994) (Trznadel & Kryszewski, 1992).

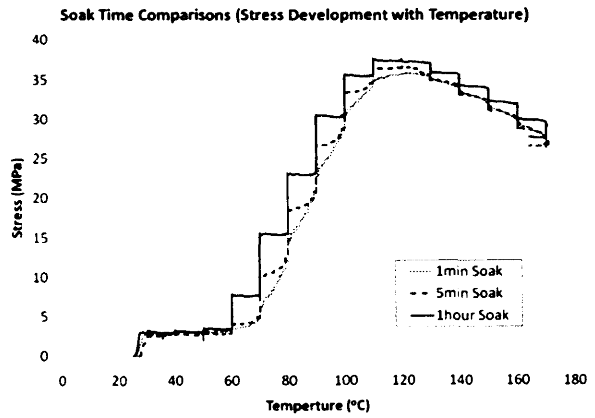

Figure 4.37 - Comparison of Soak Time Experiments (Stress Development with Temperature)

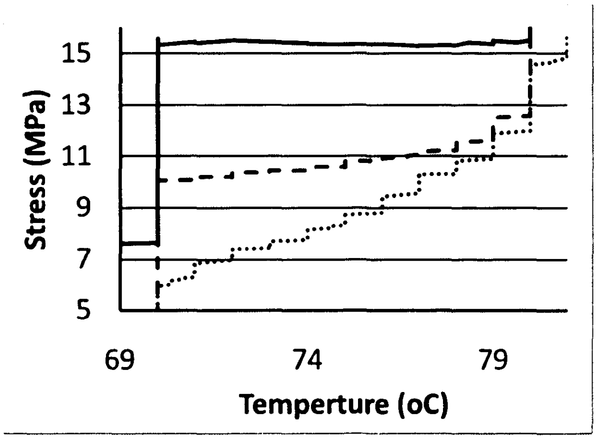

Figure 4.38 - Expanded View of Stress Development with Temperature for 70°C to 80°C Transition

If it is assumed that the glass transition temperature is associated with the onset of shrinkage, then Figure 4.39 suggests a glass transition temperature of 70°C, which is consistent with previous observations of Gupta et al (Gupta et al., 1994) and Ward & Sweeney (Ward & Sweeney, 2004).

The exploded view of the 70°C-80°C transition seen in Figure 4.38 shows that the stress for the 1 hour soak time actually decreases throughout the temperature transition, whereas for the two shorter soak times the stress consistently increases. It appears that two competing mechanisms are occurring at different rates, namely, stress relaxation and shrinkage. The shrinkage is a relatively fast mechanism which stabilises in approximately 5 minutes, whilst stress relaxation is slower and only becomes apparent during the 1 hour soak time tests.

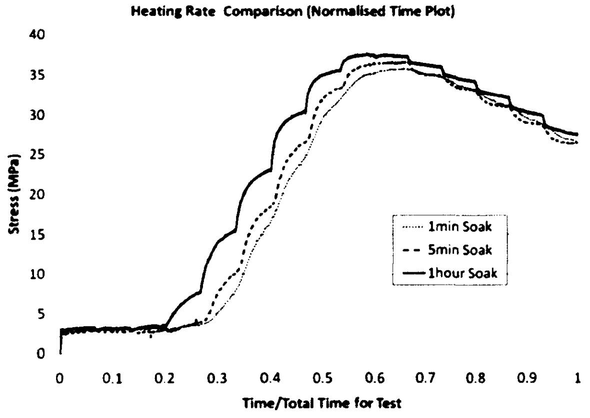

Figure 4.39 - Normalised Time Plot for Three Soak Times

The peak stresses are 35.5 MPa (1 minute soak); 36.5MPa (5 minute soak) and 37MPa (1 hour soak), which suggests that a soak time of 5 minutes is sufficient. The increase in stress between temperature increments remains relatively small until a temperature of 70°C is reached. In the region of 70°C to 90°C, i.e. the glass transition region (Tobushi et al., 2001), the stress increases by approximately 7.5MPa per 10°C increment. In all cases the peak stress is reached at approximately 120°C, beyond which the stress decreases at approximately the same normalised rate.

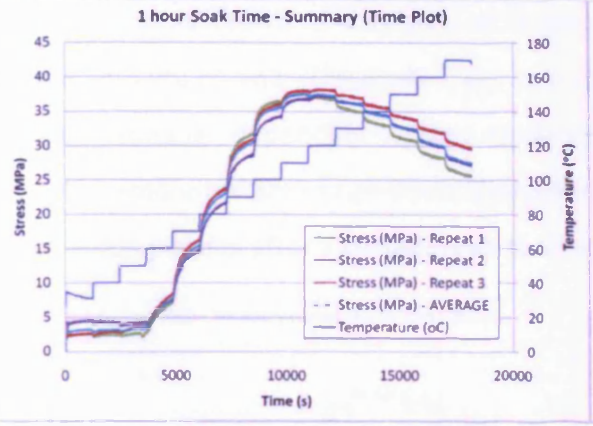

Figure 4.40 – 1 Hour Soak Time Summary
(Stress Development with Time)

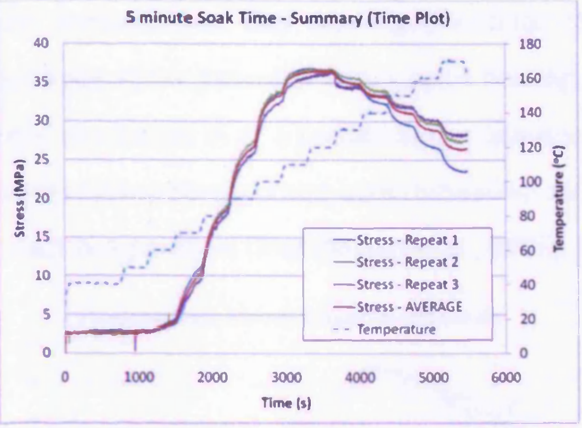

Figure 4.41 - 5 Minute Soak Time Summary
(Stress Development with Time)

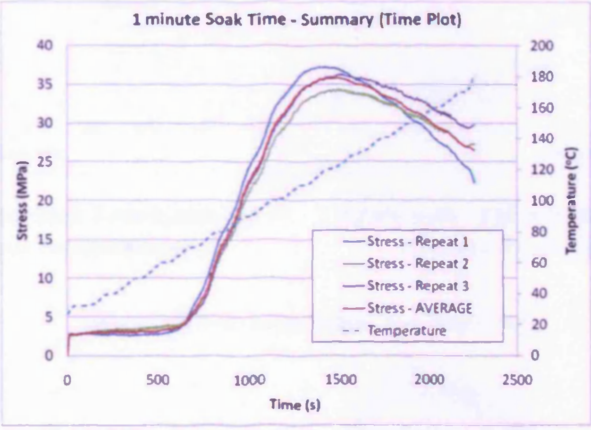

Figure 4.42 - 1 Minute Soak Time Summary
(Stress Development with Time)

The two shorter soak times experience less stress loss than the 1 hour soak time which suggests that the longer a temperature is soaked in this area the more deterioration that is seen in the polymer. Figure 4.40, Figure 4.41 and Figure 4.42 show the time plot of stress and temperature and highlights the stress plateau at each temperature increment, for 1 minute soak time there is no plateau as the time is too short. However the 5 minute soak time shows a plateau beginning to develop and the 1 hour soak time shows a clear plateau. This highlights further that for a given temperature, the polymer can only achieve a certain shrinkage-stress and in order for the stress to increase the temperature must be raised.

The behaviour seen can be attributed to the mechanism which causes shrinkage to occur. As the shrinkage potential is effectively locked in during the manufacturing process in which the polymer melt is drawn and cooled at a certain temperature. This drawing orientates the polymer molecules and effectively locks in a shrinkage-stress potential which upon heating is released. However depending on how much stress was locked in at a certain temperature will affect the amount of shrinkage-stress available at that given temperature upon reheating, seen by the stress plateau after a certain soak time at each temperature (Morshedian et al., 2005).

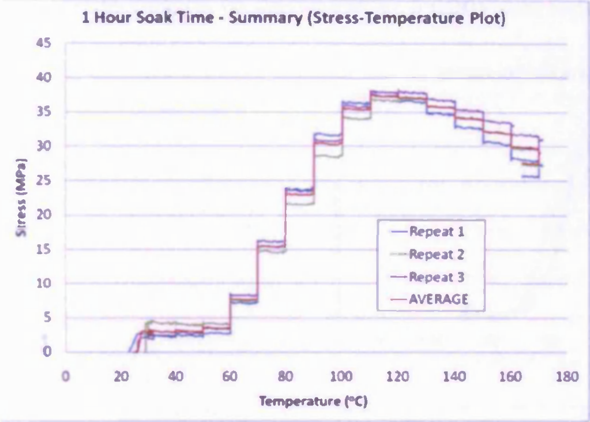

Figure 4.43 - 1 Hour Soak Time Summary (Stress versus Temperature)

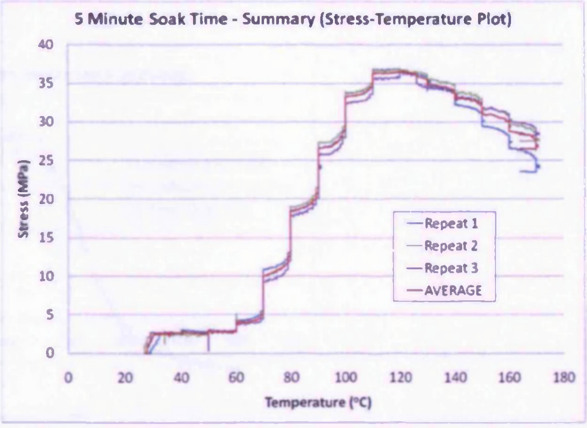

Figure 4.44 - 5 Minute Soak Time Summary (Stress versus Temperature)

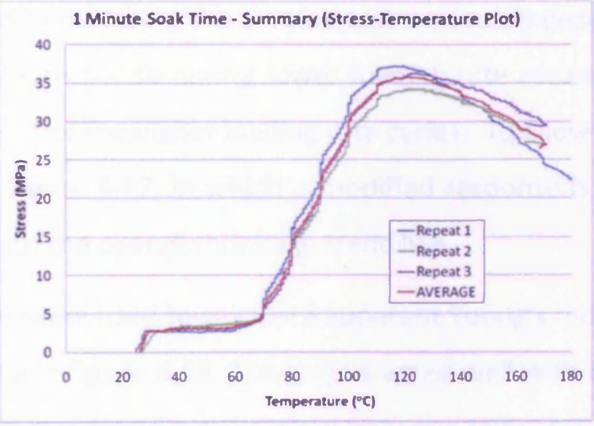

Figure 4.45 - 1 Minute Soak Time Summary (Stress versus Temperature)

Figure 4.43 - Figure 4.45 highlight the spread of results which can therefore be assumed accurate if errors related to the hand manufacture of the specimens discussed previously are considered acceptable.

Figure 4.46 highlights the stress gained/lost at each temperature increment for the 1 hour soak time, the average results are used. The graph clearly shows that the greatest gains occur in the 70°C to 90°C region, where approximately 7.5MPa of stress is gained during the 1 hour soak time, this corresponds to the transition zone. Significant stress gain does not occur until 50°C after which there is a sharp rise in the stress gain. After 90°C the gain reduces up to 120°C when the stress begins to decrease at a constant rate.

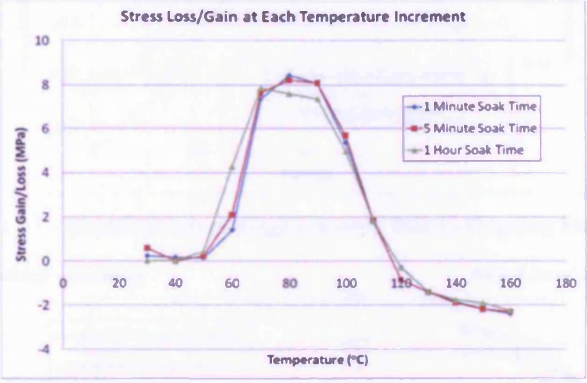

Figure 4.46 - Stress Loss/Gain at Each Temperature Increment

4.2.2.4 Effect of Temperature on Young's Modulus

The response of the specimens during the E-value test was not independent of the continuing overall shrinkage, with the response during lower loading rate cycles being more affected by overall shrinkage than those of the higher loading rate cycles. To allow for this, a correction was applied, as illustrated in Figure 4.47, in which a modified response is obtained by considering the displacement relative to the overall shrinkage trend line.

These modified responses were used to calculate apparent Young's moduli, the results of which are shown in Figure 4.48 and Figure 4.49. The graphs agree well with the work of Tobushi et al (Tobushi et al., 2001) who also found a clear trend between temperature and Young's modulus for PET. The Young's modulus prior to the glass transition region takes the constant value of approximately 6000MPa with the transition beginning at around 60°C-70°C which agrees approximately with Furness (Furness, 2001). This region is known as the glassy region where deformations are associated with small displacements of the molecules from equilibrium positions (Furness, 2001). Following the glass transition a second constant value of approximately 1000MPa was seen, beginning at approximately 120°C, this region is known as the rubbery plateau region (Furness, 2001).

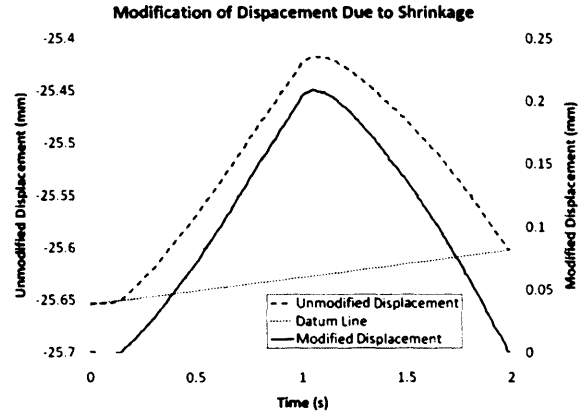

Figure 4.47 - Modification of Displacement Due to Ongoing Shrinkage

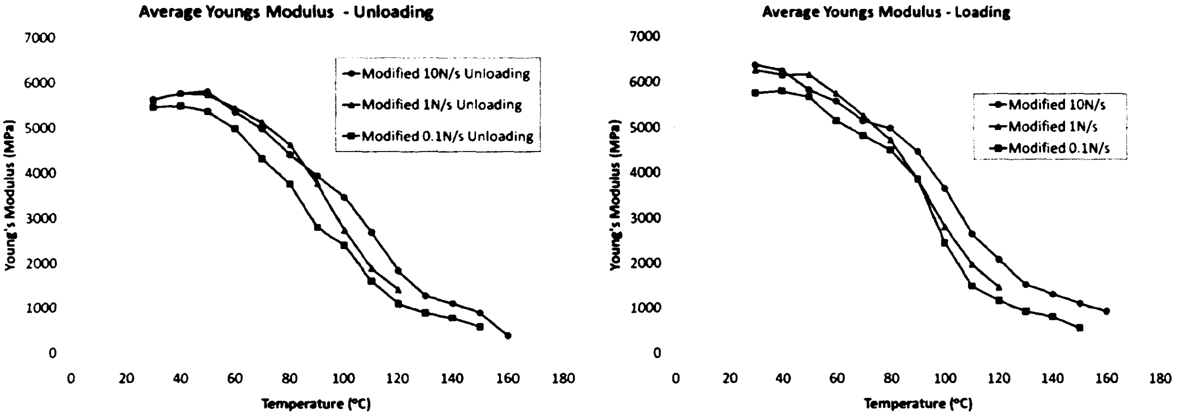

Figure 4.48 - Average Young's Modulus (Unloading)

Figure 4.49 - Average Young's Modulus (Loading)

The trend is the same for the different rates; however, the data suggest a small rate dependency for apparent Young's modulus. It is known that the Young's modulus reduces with increasing crystallisation (Akhmedov et al., 1968) and it is also known that the amount of crystallisation increases with time in the transition temperature range (Jog, 1995). Thus, the observed rate dependency in apparent Young's modulus is explained by differing degrees of crystallisation.

4.2.2.5 Free Shrinkage Development with Temperature

Plots of shrinkage versus temperature for each of the experiments in the previous section are shown in Figure 4.50. The experiments were only continued up to 160°C since at this temperature the testing machine reached maximum travel due to the high levels of shrinkage exhibited by the specimens. The total shrinkage strain achieved at the end of the tests was 18.1%.

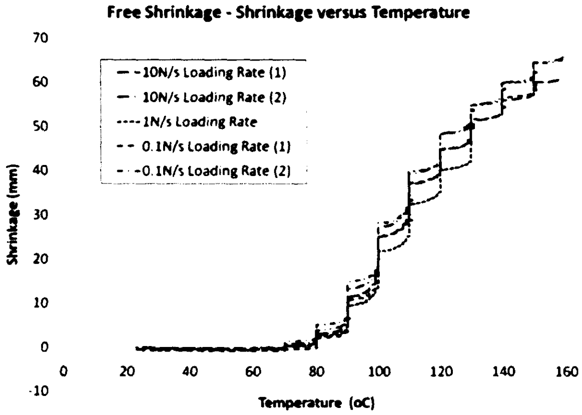

Figure 4.50 - Free Shrinkage versus Temperature

4.2.3 Summary of Parametric Studies

The experimental procedure ensures that the measured material properties are independent of section geometry, such as cross-section or length, provided that a test with a soak time of 15.5 minutes is undertaken. The material has been found to consistently generate a shrinkage-stress of 32.5MPa following a 3 hour soak at 90°C, hence meeting the requirements of LatConX. The Young's modulus has been found to follow a clear transition between the temperatures of 70°C and 120°C and is rate dependant to a small degree. Finally, a free shrinkage of 18.1% was found to develop in heating to 160°C.

4.3 Conclusions

- The use of polypropylene (PP) for LatConX was ruled out by the preliminary studies which highlighted a maximum shrinkage-stress of 8MPa at 130°C.
- Polyethylene terephthalate (PET) was highlighted as the most suitable polymer for LatConX generating on average 32.5MPa following a soak time of 3 hours at 90°C.
- Commercially available PET known as "Shrinktite" is only available in tapes 32mm x 0.046mm, hence further manufacture is required for LatXConX and material testing.

- Investigations into manufacturing techniques found that groups of 6mm wide PET strips would produce suitable tendons for LatConX.
- Investigations into bonding methods found that full length bonding affected the shrinkage behaviour and therefore the specimens are bonded only at their ends, leaving the full length free to shrink individually.
- It was found that geometric properties such as area and length do not affect the development of shrinkage-stress of these manufactured tendons, provided soak time of 15.5 minutes is realised.
- Future work will include the development of polymer tendons that not only generate a greater shrinkage-stress but also in a larger specimen size more suitable to application in civil engineering structures.

Chapter Five: **Polymer Material Model**

In order to fully understand the effect that the polymer will have on the LatConX system and what long term effects may occur, it was necessary to develop a numerical model for shrinkable polymers. An extensive review of the literature was carried out and this highlighted a number of key existing models. These models were assessed, but it was found that no one existing model was able to capture the transient thermo-mechanical behaviour of the shrinkable PET used in the present study. Therefore a new model that simulates this behaviour was developed, based upon elements found in existing models.

The following chapter will introduce and evaluate the existing models and then go on to develop a transient thermo-mechanical model with both validation and simulation experiments also presented and evaluated. Finally, indication will be given of the potential for extension of the model into 3D. The content of this chapter is the subject of a journal paper by the author (Dunn et al., 2011).

5.1 Existing Polymer Models

The literature on numerical simulation of polymers is extensive and an overview of the relevant work begins with that of Eyring, who was a pioneer in polymer modelling and who suggested that "the deformation behaviour of polymers was a thermally activated rate process involving the motion of segments of chain molecules over potential barriers" (Halsey et al., 1945).

A different approach based on similar principles was developed by Trznadel (Pakula & Trznadel, 1985), who proposed a four-state model which qualitatively describes the temperature dependent behaviour of amorphous polymers. Morshedian et al (Morshedian et al., 2005) also developed a mechanical model approach by combining a Kelvin unit and a dashpot modified to simulate "elastic restoring force build up" and its subsequent release to simulate "heat dimensional recovery".

Tobushi et al (Bhattacharyya & Tobushi, 2000) proposed that the isothermal mechanical behaviour of polymers can be described by a four element rheological model consisting of an elastic spring and viscous dashpot in parallel with a friction element and another viscous dashpot. Tobushi's model was aimed specifically at shape memory polymers, as was the work of Liu et al (Liu et al., 2006), who proposed a simplified phenomenological approach to model the temperature dependant shape memory behaviour of viscoelastic polymers. Liu's model splits the polymer into two extreme phases; active and frozen, where the proportion of each reflects the ability of the polymer molecules to flow and deform and is a function of the temperature.

Haward & Thackray (Haward & Thackray, 1968) proposed combining a yield/flow model based on Eyring theory with rubber elasticity to form a non-linear standard linear solid (SLS) model. The SLS model; usually attributed to Zener (Zener, 1948), is the most basic and simplest model found to simulate the basic behaviour of polymers. Mention is given to the SLS model as it forms a sound basis upon which to build a new model that utilises the various components of polymer models proposed by other authors, summaries of which will be given in the subsequent sections.

Finally, with an increased reliance on computers for the analysis of production processes in addition to material behaviour, the development of 3D models has progressed in the last 15 years. Such 3D models include those for glassy polymers (Boyce et al., 2000) (Hasan & Boyce, 1995) (Dooling et al., 2002), the Bergstrom model for cross-linked rubbery polymers (Bergstrom & Boyce, 1998) and finally the "Glass-Rubber" type model of Buckley and Jones for amorphous polymers in the vicinity of the transition region (Buckley & Jones, 1995). The model of Boyce and co-workers (Boyce et al., 2000) is a 3D extension of the Haward-Thackray model in which the Eyring flow model is replaced with the Argon "double-kink" theory (Argon, 1973). This model simulates well the stress-strain behaviour in the glassy region. A more complete 3D model is that of Buckley & Jones (Buckley & Jones, 1995) who developed a glass-rubber constitutive model which combines existing components including linear elasticity, Eyring viscosity, Edwards-Vilgis entropy function and the Vogel-Tamman-Fulcher and Arrhenius viscosity equation.

The following sub-sections provide overviews of the models that were used to develop the 1D transient thermo-mechanical model proposed in this chapter.

5.1.1 Eyring Model

Eyring proposed that a temperature dependant dashpot replace the existing dashpot in the SLS model. This model represents non-linear viscoelastic behaviour and is related to physical parameters in that it requires the input of activation volume and activation energy. As described in Ward & Sweeney (Ward & Sweeney, 2004) the "macroscopic deformation is assumed to be the result of basic processes that are either intermolecular (chain-sliding) or intramolecular (conformation change in chain)" which forms the basis for the 'Eyring Dashpot'. Halsey, White & Eyring (Halsey et al., 1945) proposed that an applied stress alters the potential energy barrier (see Figure 5.1) and thus causes an unequal flow of chain segments in each direction over the potential barrier. The stretch ratio, λ and shearing force, f are indicated on Figure 5.1.

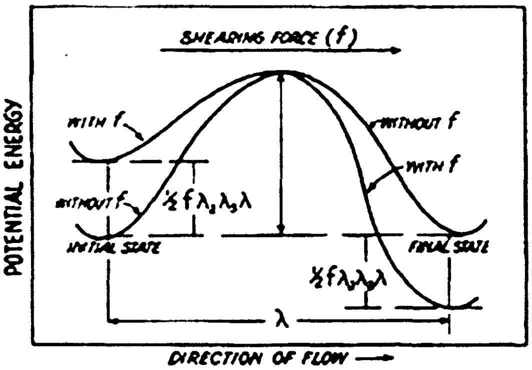

Figure 5.1 - Effect of Applied Stress on Potential Energy Barrier (Halsey (1945) (Halsey et al., 1945))

The general form of the 'Eyring Equation' is seen in equation (5.1), where k is the reaction rate constant, T is absolute temperature, $\Delta H^{\ddagger}$ is enthalpy of activation, R is gas constant, k_B is Boltzmann constant, h is Planck's constant and $\Delta S^{\ddagger}$ is entropy of activation (Anslyn & Dougherty, 2005).

$$k = \left(\frac{k_B T}{h}\right) exp\left(\frac{\Delta S^{\ddagger}}{R}\right) exp\left(-\frac{\Delta H^{\ddagger}}{RT}\right) \tag{5.1}$$

The 'Eyring Equation' can be used to predict the net flow in the direction of the applied stress (σ) and it can be assumed that the "net flow in the forward direction is directly related to the rate of change of strain" (Ward & Sweeney, 2004), which gives an 'activated' viscosity that replaces that of the dashpot in Zener's SLS model (Zener, 1948). The Eyring strain rate, as given by Ward & Sweeney (Ward & Sweeney, 2004), is seen in equation (5.2):

$$\frac{de}{dt} = \dot{e} = \dot{e}_0 exp\left(-\frac{\Delta H}{RT}\right) sinh\left(\frac{v\sigma}{RT}\right) \tag{5.2}$$

Many authors have since adapted the so called 'Eyring Equation' for different characteristics such as creep (Sherby & Dorn, 1958), (Wilding & Ward, 1981), stress relaxation (Guiu & Pratt, 1964), (Sweeney & Ward, 1990) and finally yield behaviour (Sweeney et al., 1999).

5.1.2 Trznadel Model

Trznadel, Pakula and Kryszewski investigated the shrinkage behaviour of oriented polymers in a series of papers (Pakula & Trznadel, 1985) (Trznadel et al., 1985) (Trznadel, 1986) studying the time dependence, temperature dependence and induction time. They considered the effect of orientation due to stretching and proposed that this acted to "increase the effectiveness of intermolecular interactions due to increased alignment". In doing so the potential barriers that must be overcome for shrinkage to occur are too high for molecules to traverse at low temperatures, effectively locking in a shrinkage-stress. In order for these potential barriers to be overcome and shrinkage to occur, the temperature must be raised. They considered a variety of models, notably Tanabe & Kanetsuna and Joseph which utilised a two-state model, but was unable to accurately depict the stress generation with time and temperature (Pakula & Trznadel, 1985). Therefore Trznadel et al referred to the Burgers Model and modified it by replacing the dashpots with two-site elements as shown in Figure 5.2.

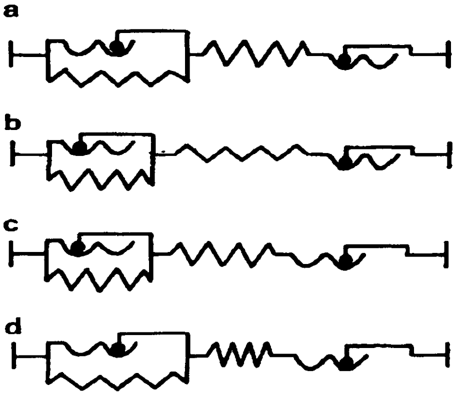

Figure 5.2 - Four-state Model by Trznadel et al (Pakula & Trznadel, 1985)

The model is characterized by two elastic springs and two two-site elements. The left hand spring is related to the chain elasticity and the right hand spring represents the elastic junction of the subunit and matrix. The extension/contraction of the springs is caused by overcoming the potential barriers in the two-site elements. The barriers can assume four states which "differ from one another in the internal stresses and external response sensitive to the change of state at constant length" (Pakula & Trznadel, 1985). The heights of the potential barriers are defined by the "Helmholtz free energy difference related to excitation of local frozen-in molecular configuration" and the behaviour of the model is defined by the probability of jumps between the sites which is also influenced by the local stresses of the springs (Trznadel et al., 1985).

5.1.3 Morshedian Model

The mechanical model proposed by Morshedian et al (Morshedian et al., 2005) comprises a Kelvin unit in series with a dashpot, with the second dashpot having a much larger viscosity. The model is then used in steps to produce the stored stress and subsequent release as seen in Figure 5.3.

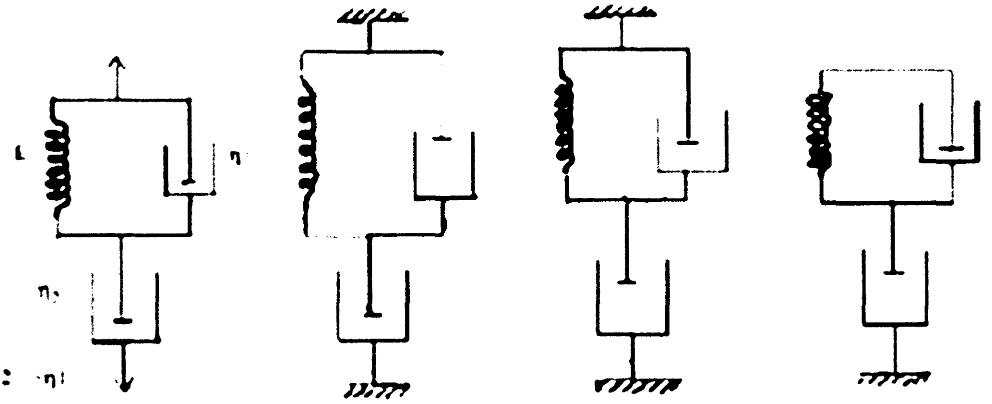

a) Proposed Model

b) Stretched by a fixed strain and cooled

c) Stress relaxation followed by orientation freeze-up to produce a heat shrinkable system

d) Heat shrunk model without full recovery

Figure 5.3 - Proposed Mechanical Model by Morshedian (Morshedian et al., 2005)

The model consists of first stretching at high temperature, such that both dashpots are in a liquid state and then cooling in the stretched condition. In Figure 5.3(c) stress relaxation occurs before complete solidification, as the lower dashpot expands and the Kelvin unit contracts. Upon later increase in temperature the model shrinks at the melting temperature of the Kelvin unit to a "somewhat longer length than its initial length in Figure 5.3(a)". The constitutive relationship proposed by Morshedian (Morshedian et al., 2005) is seen in equation (5.3):

$$\sigma = \frac{E\gamma + \eta_1 \frac{d\gamma}{dt}}{1 + \frac{\eta_1}{\eta_2} + \frac{t}{\tau}} \tag{5.3}$$

In which E is the spring modulus, $\tau = \eta_2/E$ (relaxation time), η_1 is viscosity of Kelvin dashpot, η_2 is viscosity of lower dashpot and γ is the total strain.

Comparisons between numerical simulations and experimental studies are given by Morshedian et al and show success. Of particular note is their representation of the viscosity-temperature relationship for the Kelvin dashpot which is seen in Figure 5.4.

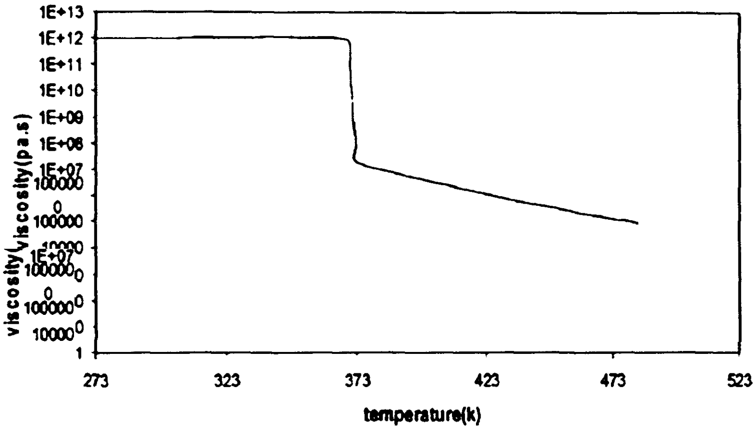

Figure 5.4 - Variation of Viscosity with Temperature by Morshedian (Morshedian et al., 2005)

5.1.4 Tobushi Model

Tobushi et al (Tobushi & Hashimoto, 1997) (Bhattacharyya & Tobushi, 2000) (Tobushi et al., 2001) have developed a thermo-mechanical constitutive model to describe the thermo-mechanical properties of shape memory polymers of polyurethane series. The authors noticed the ability of the Standard Linear Viscoelastic (SLV) model to predict mechanical behaviour of polymers at constant temperature, but like Trznadel and Morshedian realised that it lacks the ability to predict the variation of mechanical properties with temperature. They therefore considered the use of a "slip mechanism due to internal friction" in order to simulate the change in mechanical properties above and below the glass transition temperature (T_g). The proposed four-element rheological model illustrated in Figure 5.5 consists of a spring-dashpot in parallel with a spring-friction element. It is the friction element that models the effect of shape memory strain and the mechanical properties are expressed by a single exponential function of temperature (Tobushi & Hashimoto, 1997).

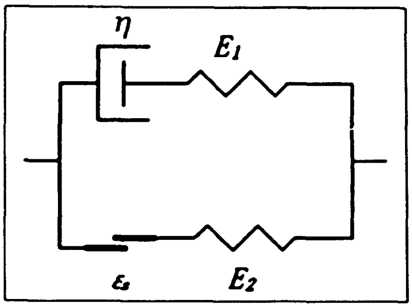

Figure 5.5 - Four-element Model by Tobushi et al (Tobushi & Hashimoto, 1997)

The linear constitutive equation proposed by Tobushi et al (Tobushi et al., 2001) is seen in (5.4) with its non-linear form seen in equation (5.5), the non-linear version being required due to the high levels of strain generated upon recovery by heating in SMPs.

$$\dot{\varepsilon} = \frac{\dot{\sigma}}{E} + \frac{\sigma}{\eta} - \frac{\varepsilon - \varepsilon_s}{\lambda} + \alpha_T \dot{T} \tag{5.4}$$

$$\dot{\varepsilon} = \frac{\dot{\sigma}}{E} + m\left(\frac{\sigma - \sigma_y}{k}\right)^{m-1}\frac{\dot{\sigma}}{k} + \frac{\sigma}{\eta} + \frac{1}{b}\left(\frac{\sigma}{\sigma_c} - 1\right)^{n} - \frac{\varepsilon - \varepsilon_s}{\lambda} + \alpha_T \dot{T} \tag{5.5}$$

In both equations ε_s is the irrecoverable strain and takes the value $S\varepsilon_c$, where S is a proportional coefficient and ε_c is the creep strain. σ, ε and T denote stress, strain and temperature respectively, with E, η and λ representing modulus of elasticity, viscosity and retardation time respectively which are all temperature dependant and α_T is the coefficient of thermal expansion. In the non-linear equation σ_y and σ_c denote "the proportional limits of stress in the time-independent term and the viscous term respectively, and correspond to the yield stress and creep limit" (Tobushi et al., 2001).

The temperature dependent coefficients of the mechanical properties show a clear transition which occurs around the glass transition (T_g). Tobushi et al (Tobushi et al., 2001) state that the reason for this transition is that SMPs are made up of soft and hard segments and that with increased temperature above T_g the soft segments are activated and below T_g are frozen. The expression for E in the region T_g±15K is seen in (5.6) and is "similar to the equation for viscosity derived theoretically by Eyring and empirically by Arrhenius" (Tobushi et al., 2001).

$$E = E_g \exp\left\{a\left(\frac{T_g}{T} - 1\right)\right\} \tag{5.6}$$

The other material parameters (k, σ_y, η, σ_c, λ and S) can also be expressed in the same way by replacing the E and E_g with the relevant material parameter. Figure 5.6 shows the graphical representation for E in the glass transition region both experimentally and numerically and highlights the parameter "a" as the gradient of the transition..

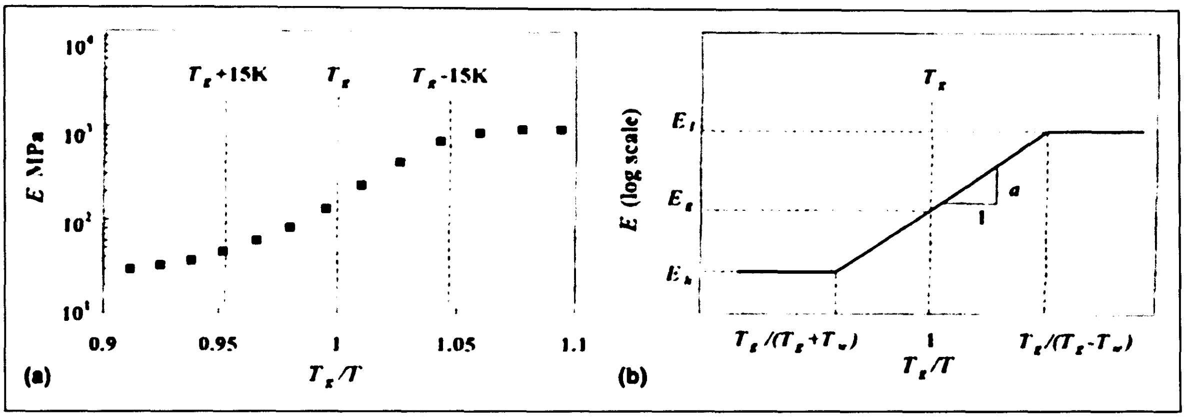

Figure 5.6 - Experimental (a) and Numerical (b) representation of Young's Modulus in Transition Region (Tobushi et al., 2001)

Bhattacharyya and Tobushi (Bhattacharyya & Tobushi, 2000) developed the model in terms of constant stress, constant strain, constant stress rate, constant strain rate and periodic strain to simulate tensile stress states on thin SMP films with good success.

5.1.5 Liu Model

Liu et al (Liu et al., 2006) undertook a comprehensive experimental and numerical study on the thermodynamics of shape memory polymers. A "three-dimensional small-strain internal state variable constitutive model" was developed by consideration of experimental results and the molecular behaviour of the shape memory polymers studied. The model is capable of predicting the development of stress in a uniaxial experiment and includes the effect of thermal expansion. It is based on the assumption that the polymer is a mixture of two kinds of extreme phases; the frozen phase and the active phase as seen in Figure 5.7.

The frozen phase "implies that the conformational rotation corresponding to the high temperature entropic deformation is completely locked (stored), while the internal energic change such as the stretching or small rotation of the polymer bonds can occur". The active phase however consists of active bonds and allows conformational motion to occur and by decreasing the temperature the "large-scale conformational motions in the material are gradually localised in the active phase". The ratios of each phase can be adjusted to embody the glass transition and shape memory behaviour.

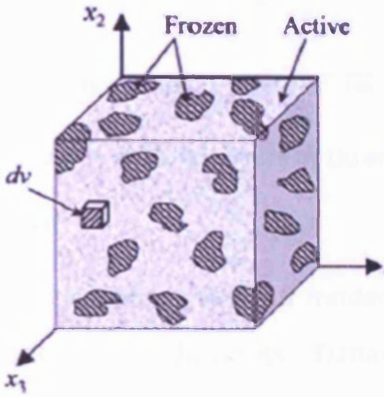

Figure 5.7 - Schematic Diagram of 3D SMP Model by Liu et al (Liu et al., 2006)

The 1D constitutive equation is seen in (5.7) with the temperature derivative of stored strain given in (5.8) (Liu et al., 2006).

$$\sigma = \frac{\varepsilon - \varepsilon_s - \int_{T_h}^{T} \alpha_T \, dT}{\frac{\phi_f}{E_i} + \frac{1-\phi_f}{E_e}} = E\left(\varepsilon - \varepsilon_s - \int_{T_h}^{T} \alpha \, dT\right) \tag{5.7}$$

$$\frac{d\varepsilon_s}{dT} = \frac{\varepsilon - \varepsilon_s - \int_{T_h}^{T} \alpha_T \, dT}{E_e\left(\frac{\phi_f}{E_i} + \frac{1-\phi_f}{E_e}\right)}\left(\frac{d\phi_f}{dT}\right) \tag{5.8}$$

In which the frozen fraction, $\phi_f = 1 - 1/1 + c_f(T_h - T)^n$, the Young's modulus, $E = 1/\left(\frac{\phi_f}{E_i} + \frac{1-\phi_f}{E_e}\right)$, the modulus of entropic deformation, $E_e = 3Nk_BT$, the coefficient of thermal expansion is given by $\alpha_T = d\varepsilon_T/dT$ and the stored strain, $\varepsilon_s = \int_0^{\phi_f} \varepsilon_f^e(x)d\phi$.

A series of one-dimensional experimental studies were used to develop the frozen fraction using a phenomenological approach and it was found that the model predicted well the uniaxial temperature dependant stress development of SMPs. Liu also proposes a numerical prediction for the Young's modulus as a function of temperature which is presented in Figure 5.8.

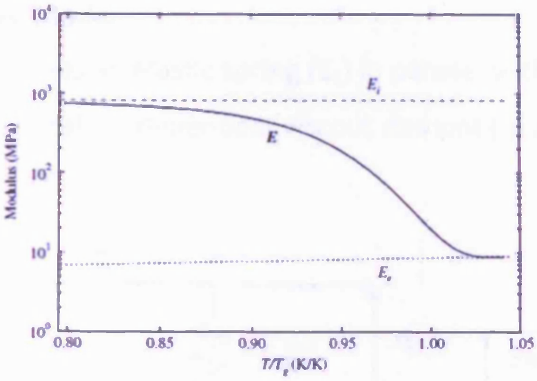

Figure 5.8 - Elastic Moduli with Temperature by Liu et al (Liu et al., 2006)

5.2 1D Polymer Material Model

A constitutive model was developed based on the SLS model of Zener (Zener, 1948) modified with temperature dependent springs and dashpots. Trznadel and Kryszewski (Trznadel & Kryszewski, 1992) states that the "construction of molecular models is extremely difficult" and that their analytical solution is "impossible". Therefore, as Trznadel & Kryszewski suggest and in consideration of the approach taken by Liu et al (Liu et al., 2006), a phenomenological model is more appropriate. The following sections describe a proposed phenomenological representation for PET. The direct use of one of the basic mechanical model such as SLS and four element models cannot replicate the shrinkage behaviour of polymers (Morshedian et al., 2005) and as such a temperature dependence modification was required. Although Morshedian (Morshedian et al., 2005) offers a proposal for the viscosity relationship with temperature and Tobushi (Tobushi & Hashimoto, 1997) proposes that all material parameters will vary with temperature neither were found to be able to simulate the shrinkage behaviour of the PET presented in Chapter 4 and therefore a new hybrid model was required.

In order to introduce this temperature dependence the relationship between Young's modulus and temperature is based on the observations of Tobushi et al (Tobushi et al., 2001) and the experimental data presented in this thesis. The relationship between viscosity and temperature proposed by Morshedian et al (Morshedian et al., 2005) is also drawn upon in order to simulate the viscous behaviour of the polymer. The model aims to simulate the transient thermo-mechanical behaviour of PET in a 1D uniaxial form.

5.2.1 Proposed Constitutive Model

The rheological model comprises an elastic spring (E_1) in parallel with a temperature dependent elastic spring (E_2) and a temperature dependent viscous dashpot (η) as shown in Figure 5.9.

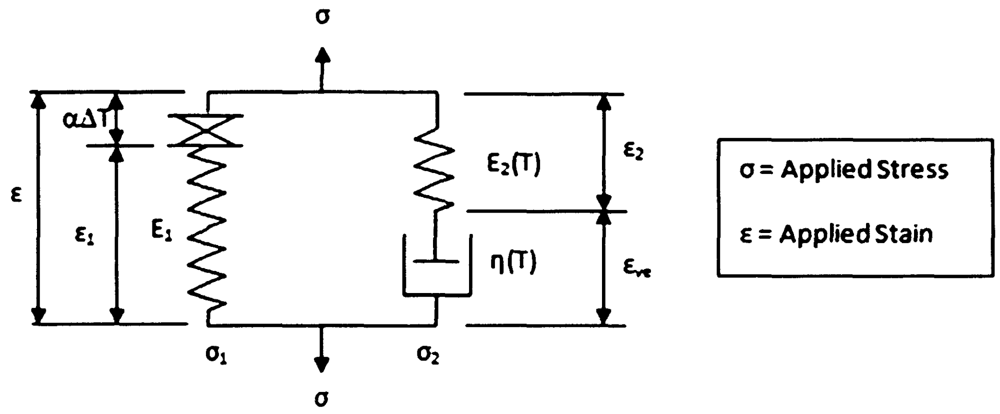

Figure 5.9 - Rheological Representation of Proposed Model

5.2.1.1 *Basic Stress and Strain Conditions*

The total stress (σ) is given by:

$$\sigma = \sigma_1 + \sigma_2 \qquad (5.9)$$

In which the stress component in each arm of the model is as follows:

$$\sigma_1 = E_1 . \varepsilon_1 \qquad (5.10)$$

$$\sigma_2 = E_2(T) . \varepsilon_2 = \eta . \dot{\varepsilon}_{ve} \qquad (5.11)$$

Giving the strain components as follows:

$$\varepsilon = \varepsilon_2 + \varepsilon_{ve} \quad \therefore \quad \varepsilon_{ve} = \varepsilon - \varepsilon_2 \qquad (5.12)$$

$$\dot{\varepsilon} = \dot{\varepsilon}_2 + \dot{\varepsilon}_{ve} \quad \therefore \quad \dot{\varepsilon}_{ve} = \dot{\varepsilon} - \dot{\varepsilon}_2 \qquad (5.13)$$

5.2.1.2 *Derivation of Viscous Elastic Strain Component*

The general SLS equation ignoring temperature dependencies and using equations (5.9)-(5.11) is as follows:

$$\sigma = E_1 \varepsilon + E_2(\varepsilon - \varepsilon_{ve}) \qquad (5.14)$$

From equation (5.11) and the relaxation time ($\tau = \eta / E_2$):

$$\eta.\dot{\varepsilon}_{ve}=\frac{\eta}{\tau}\varepsilon-\frac{\eta}{\tau}\varepsilon_{ve} \tag{5.15}$$

Through rearrangement and collecting terms, the following differential equation is derived:

$$\frac{1}{\tau}\varepsilon=\dot{\varepsilon}_{ve}+\frac{1}{\tau}\varepsilon_{ve} \tag{5.16}$$

Using a standard solution as described in reference (Simo & Hughes, 1998), of equation (5.16) is:

$$\frac{d}{dt}\left(e^{t/\tau}.\varepsilon_{ve}\right)=\frac{1}{\tau}e^{t/\tau}.\varepsilon \tag{5.17}$$

Through rearrangement the following convolution integral is arrived at:

$$\varepsilon_{ve_{(t)}}=\int_{t_0}^{t}\frac{1}{\tau}e^{-(t-s)/\tau}.\varepsilon(s)ds \tag{5.18}$$

To solve the convolution integral in equation (5.18) consider the solution over interval *t* → *t* + *Δt*, and assume that the strain (ε_θ) is the value of strain at t + θΔt, where 0≤θ≤1.

$$\varepsilon_{ve_{(t+\Delta t)}}=\int_{t}^{t+\Delta t}\frac{1}{\tau}e^{-(t+\Delta t-s)/\tau}.\varepsilon_\theta ds+\int_{t_0}^{t}\frac{1}{\tau}e^{-(t+\Delta t-s)/\tau}.\varepsilon(s)ds \tag{5.19}$$

In order to solve equation (5.19) consider each component in turn, with the components being the two right hand side integral terms as shown below alongside their respective solution. The solution to *component 1*, where ε_θ/τ is a constant is as follows:

$$\int_{t}^{t+\Delta t}\frac{1}{\tau}e^{-(t+\Delta t-s)/\tau}.\varepsilon_\theta ds \rightarrow \varepsilon_\theta\left[1-e^{-\Delta t/\tau}\right]$$

The solution to *component 2,* following rearrangement is as follows:

$$\int_{t_0}^{t}\frac{1}{\tau}e^{-(t+\Delta t-s)/\tau}.\varepsilon(s)ds \rightarrow \varepsilon_{ve_{(t)}}e^{-\Delta t/\tau}$$

Combining the above two solutions yields the visco-elastic strain at time t_j in terms of values at time t_{j-1} may be written as follows;

$$\varepsilon_{ve_j}=\varepsilon_{\theta_j}\left(1-e^{-\Delta t/\tau}\right)+\varepsilon_{ve_{j-1}}.e^{-\Delta t/\tau} \tag{5.20}$$

Noting that $\Delta t = t_j - t_{j-1}$ and that θ is taken as 0.5 for the purpose of this model.

5.2.1.3 Introducing Temperature Dependencies

The characteristic forms of the temperature dependency of both η and E_{TOT} are shown in Figure 5.10 and can be derived from experimental data as explained below. Where E_{TOT} is the instantaneous value of $E_1 + E_2$ and the transition zone may be captured with the same form of function, as given below;

$$\eta(T) = \eta_L + (\eta_H - \eta_L)\frac{e^{a\chi(T)}}{e^{a\chi(T)}+b} \qquad \text{If } T > T_L \tag{5.21}$$

$$\eta(T) = \eta_R \qquad \text{If } T \leq T_L \tag{5.22}$$

$$E_{TOT}(T) = E_1 + (E_{TL} - E_1)\frac{e^{c\chi(T)}}{e^{c\chi(T)} + d} \tag{5.23}$$

In which: $\chi(T) = \frac{T-T_g}{T_H-T_L}$

Where T is the current temperature, T_g is the temperature at the centre of the transition region, T_H is the high temperature above which the parameter is constant and T_L is the low temperature at which the parameter is constant prior to transition. The material parameters (a,b,c,d) may be deduced from experiments and are presented in Section 5.2.2. It is noted that the above functions have been simplified from tanh functions.

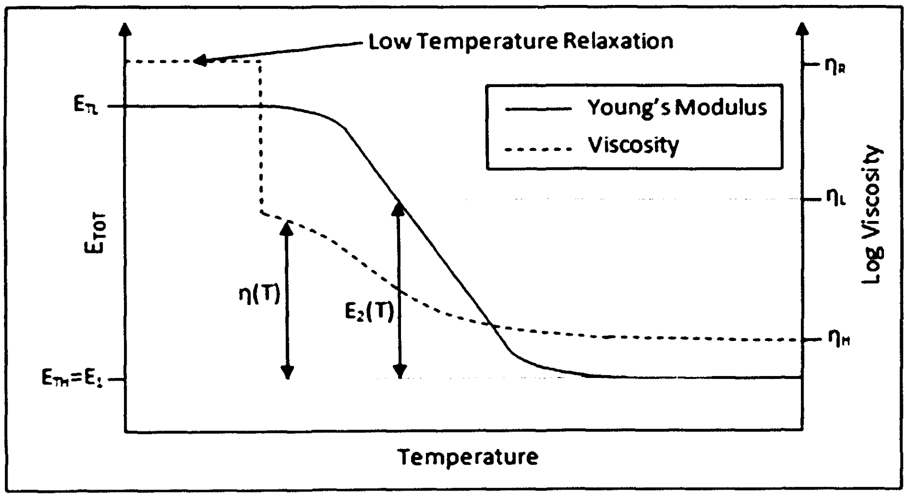

Figure 5.10 - Generalised Representation of η and E_{TOT} versus Temperature

At lower temperatures, the viscosity jumps to a much higher value, η_R (Morshedian et al., 2005) and this governs the long term relaxation, as seen in Figure 5.10 and simulates the locked in stress of the shrinkable polymer (Morshedian et al., 2005).

The measured values of viscosity from the experiments were used to evaluate η_H (the viscosity at the upper temperature limit) and η_L (the viscosity at the low temperature limit) as shown on Figure 5.10. A direct method for calibrating the constants in the viscosity function from experimental data is described in Section 5.2.2. It is assumed that the value of E_1 is equal to E_{TH}, the total short-term Young's modulus at high temperature.

5.2.1.4 Stress Development with Temperature

Assuming a starting temperature of T_0, which takes the value of 293K (20°C) at which point the stress, σ, takes the value zero and the strain, ε, takes the value ε_0. As the specimen is heated the pre-strain is released and hence:

$$\varepsilon_0 = \frac{\sigma_{res}}{E_1} \tag{5.24}$$

In which σ_{res} is the locked in stress, generated during the manufacturing process, which according to Gupta et al (Gupta et al., 1994) is slightly higher than the maximum achievable stress that will be generated upon release. The initial viscous strain at time t=0, ε_{ve0}, is defined as:

$$\varepsilon_{ve0} = \varepsilon_0\big(1 + \alpha(T_0)\big) \tag{5.25}$$

In which $\alpha(T) = E_1/E_2(T)$.

The stress at time increment j may be obtained from equations (5.9), (5.10) and (5.11), and, if thermal expansion is also allowed for in 'arm' 1, this stress is given by:

$$\sigma_j = E_1\big[\varepsilon_j - \alpha_T\big(T_j - T_0\big)\big] + E_2(T).\left(\varepsilon_j - \varepsilon_{ve_j}\right) \tag{5.26}$$

In which α_T is the coefficient of thermal expansion which is known to have a significant effect on the total strain prior to the onset of shrinkage (Trznadel & Kryszewski, 1992).

5.2.2 Calibration of Material Constants

In order to provide a reasonable calibration of material constants, the experimental data needs to be interpreted in the light of the following model assumptions:

i. The apparent Young's modulus is independent of temperature below and above the transition range

ii. The difference between the apparent Young's moduli from the fast and slow loading rate tests is due to temperature dependent viscosity in the transition range

iii. Relaxation from viscosity is insignificant at the fastest loading rate used (i.e. 10N/s)

iv. Short-term relaxation is complete by the end of each step in the 0.1N/s tests

Figure 5.11 presents the data from the Young's modulus versus temperature experiments seen in the previous chapter with error bars for the 0.1N/s and 10N/s loading rates and then shows the associated best fit lines to the original data which comply with the above assumptions. The author considers that the data do reasonably support the assumptions but equally acknowledges that other mechanisms, not accounted for, are in operation. It is also noted that these assumptions are consistent with those of Tobushi et al (Tobushi et al., 2001) and Morshedian et al (Morshedian et al., 2005), and are further supported by the good matches between results from the predictive analyses and experimental data given in Figure 5.14 and Figure 5.15 later in this chapter. These idealised E-value data will be used to calculate the parameters.

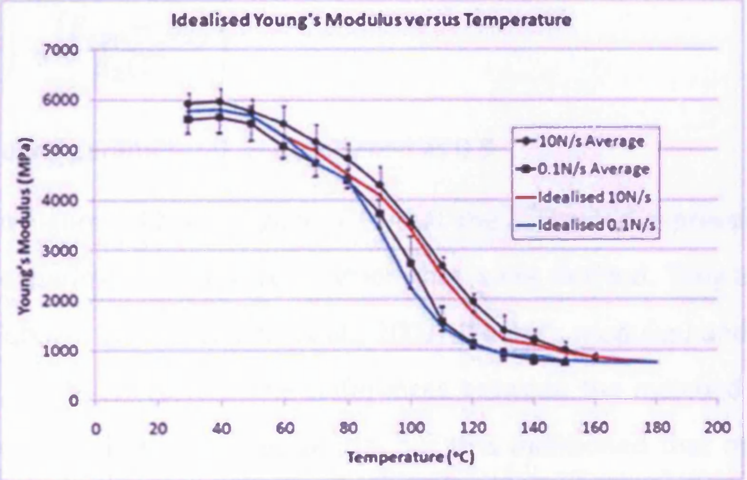

Figure 5.11 - Young's Modulus versus Temperature showing Idealised Values for Viscosity Calculations

The 10N/s E-value tests were used to calculate the material parameters for the E_2 function (Equation (5.23)) as the viscous strain rate is considered negligible at this loading rate. From the experimental data, the value for E_1 is assumed to be equal the value of E_{TH} as shown in Figure 5.10.

In order to determine the value of viscosity for a range of temperatures, an inverse parameter identification exercise was undertaken using the apparent Young's modulus, as defined in equation (5.27) and shown in Figure 5.11. Data from the low loading rate tests were used (i.e. 0.1N/s) since at this rate the viscous response is known to be significant.

$$E_{app} = \frac{\Delta\sigma}{\Delta\varepsilon} \tag{5.27}$$

Equation (5.27) is then used in equation (5.9) and rearranged to determine the change in viscous strain, as follows:

$$\Delta\varepsilon_{ve} = \Delta\varepsilon\left(1 - \frac{E_{app} - E_1}{E_2(T)}\right) \tag{5.28}$$

If it is assumed that full relaxation has taken place prior to the start of a stress excursion (at time t) in an E-value cycle, such that $\varepsilon_t = \varepsilon_{ve_t}$, then the viscosity parameter may be derived from equations (5.18), (5.26) and (5.28) as:

$$\eta = \frac{-\Delta t . E_2}{\ln\left(\left(1 - \frac{1}{\theta_\eta}\right) + \frac{\left(E_{app} - E_1\right)}{E_2(T)}\right)} \tag{5.29}$$

Where the time interval parameter θ_η is here taken as 0.9.

It can be seen from Figure 5.12 and Figure 5.13 that the calibrated expressions for E_{TOT} and η match closely the experimental data from which they were derived. They are also consistent with the work of Tobushi et al (Tobushi et al., 2001) (Young's modulus) and Morshedian et al (Morshedian et al., 2005) (viscosity). The differences between the matched and experimental Young's moduli are considered inconsequential but it is mentioned that other workers have noted a high degree of variation in measured values for Young's modulus (Sperling, 2006).

The sharp drop in the viscosity prior to transition zone is consistent with the model assumptions and is associated with the release of locked in stress (Morshedian et al., 2005). The difference between the derived and experimental viscosities beyond 140°C is partly attributed to the onset of melt and partly to the growth of the crystalline phase at these temperatures, neither of which are addressed in the current model (Morshedian et al., 2005) (Gupta et al., 1994).

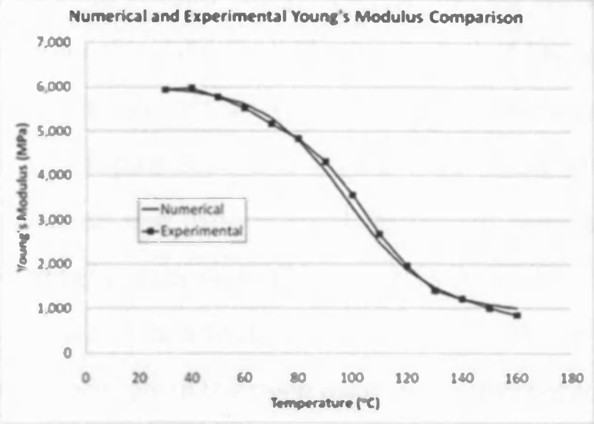

Figure 5.12 - Comparison of Numerical and Experimental Young's Modulus

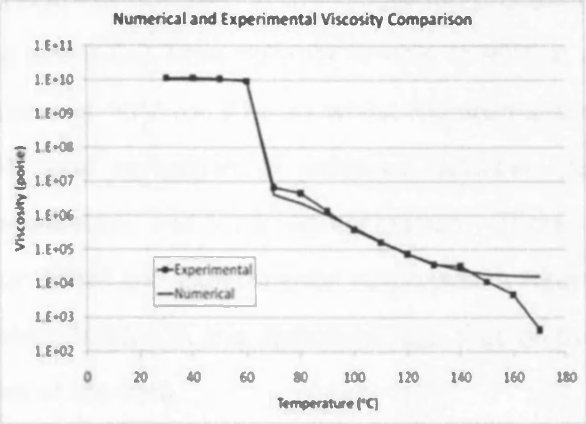

Figure 5.13 - Comparison of Numerical and Experimental Viscosity

5.2.3 Model Assumptions

The above sections have described the individual components of the model. Here, the underlying assumptions are summarised for convenience:

i. The material behaves in a visco-elastic manner
ii. Temperature dependent behaviour can be simulated with a modified SLS model in which the viscous dashpot and linked elastic component are temperature dependent functions.
iii. The temperature dependent elastic component and the viscosity can be reasonably represented with a modified tanh function.
iv. The high temperature response can be used to derive the invariant elastic component
v. Below the glass transition temperature, the viscosity is assumed to be a value associated with long-term relaxation of the polymer at ambient temperature.

The model is considered to be generally suitable for simulating the transient-thermomechanical behaviour of drawn semi-crystalline polymers below melt and its applicability is not restricted to the specific material (PET Shrinktite) considered in this thesis.

5.2.4 Model Validation

A model validation example using the parameters established in the above calibrations and presented in Table 5-1 is now considered. An experiment not used in the calibration process is used for this validation. This consisted of heating a 360x6x2.3mm polymer sample to 90°C at a constant rate and then maintaining the temperature at 90°C for 3 hours whilst monitoring the stress. Figure 5.14 and Figure 5.15 show that good agreement is achieved between the numerical and experimental results for both temperature and time representations. There is however a noticeable difference between the numerical and experimental responses in Figure 5.14, which is attributed to the fact that the temperature in the specimen lags that of the thermocouple in the oven used in the presentation of the data.

Table 5-1 - Numerical Input Values

Name	Symbol	Value	Unit
Ambient Temperature	T_0	30	°C
Coefficient of Thermal Expansion	α_T	$10^{-4.1}$	(-)
Young's Modulus at Low Temperature	E_{TL}	845	MPa
Young's Modulus at High Temperature	E_{TH}	6000	MPa
Transition Start Temperature (Young's Modulus)	T_L	70	°C
Transition End Temperature (Young's Modulus)	T_H	120	°C
Temperature at Centre of Transition (Young's Modulus)	T_g	95	°C
Elastic Modulus Material Parameter	b	3.3	(-)
Elastic Modulus Material Parameter	d	1.2	(-)
Stress at Drawing	σ_{res}	36	MPa
Viscosity at High Temperatures	η_L	1.575×10^4	Poise
Viscosity at Low Temperatures	η_H	7.322×10^4	Poise
Long Term Viscosity	η_R	1×10^{10}	Poise
Transition Start Temperature (Viscosity)	T_L	30	°C
Transition End Temperature (Viscosity)	T_H	110	°C
Temperature at Centre of Transition (Viscosity)	T_g	70	°C
Viscous Material Parameter	c	5	(-)
Viscous Material Parameter	f	0.1	(-)

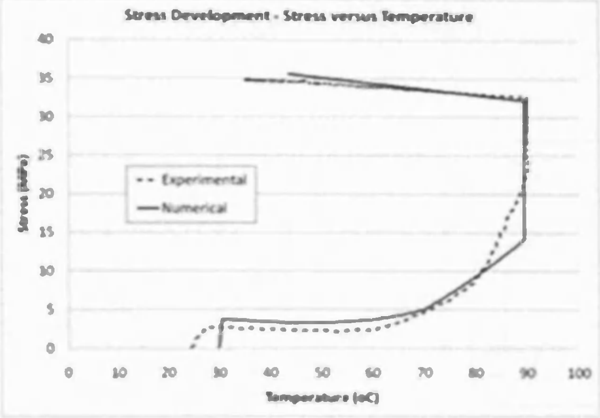

Figure 5.14 - Stress-Temperature Response

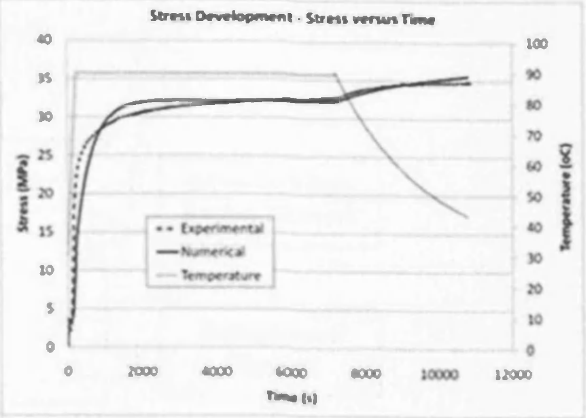

Figure 5.15 - Stress-Time Response

5.3 Extension of the model to three dimensions

The above model is suitable for the LatConX system but some work was undertaken to extend the model to three dimensions. It was found that the components used in the model were compatible with the three dimensional model of Buckley and Jones (Buckley & Jones, 1995). The essential elements of their model, and the manner by which the present functions could incorporated into their model, are described in the following.

A very concise overview of the "Glass-Rubber" model of Buckley is given by Yang et al (Yang et al., 2004) in their work simulating stretch-blow moulding of PET bottles, while a more detailed description is given in the key paper by Buckley and Jones (Buckley & Jones, 1995). The key assumption is that there are two sources for the change in free energy during deformation, each of which can be further decomposed as below and are seen in Figure 5.16:

1. Perturbation of inter-atom potentials giving a bond-stretching stress (σ_b)
    a. Elastic component (i.e. a linear spring)
    b. Viscoplastic component (i.e. an Eyring Dashpot (Halsey et al., 1945))
2. Perturbation of chain conformational entropy giving a conformational stress (σ_c)
    a. Associated with network stretch ratios (i.e. Edwards-Vilgis rubber network (Edwards & Vilgis, 1986))

b. Associated with relaxation of molecular orientation by retraction (i.e. entanglement slippage)

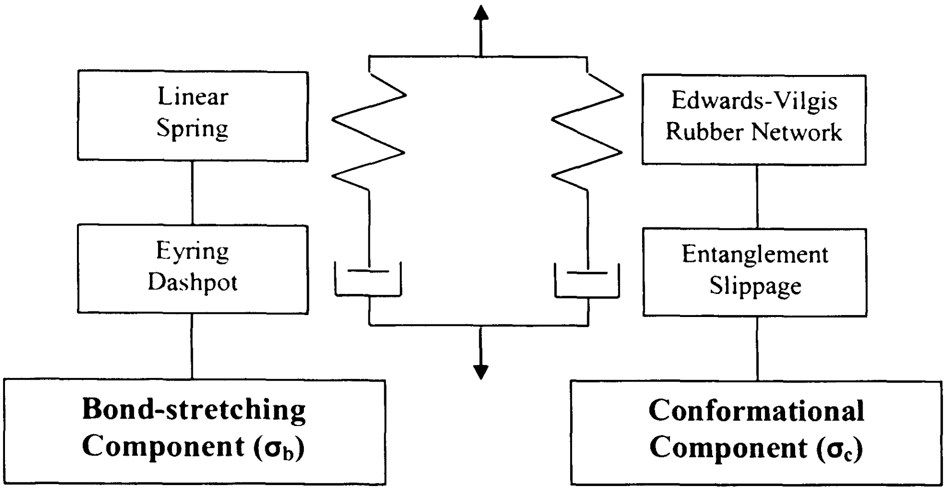

Figure 5.16 - One Dimensional Analogue of "Glass-Rubber" model by Buckley et al

The following assumptions also apply to the model (Buckley & Jones, 1995) (Buckley et al., 1996):

- The relaxation of the bond-stretching stress is that the flow can be represented as the non-Newtonian viscous flow of an isotropic material.
- The flow process can also be described in terms of Eyring kinetics
- A single non-Newtonian flow process accounts for all inelasticity in the polymer response in the time temperature region considered.
- Molecular mobility is fully developed and all molecular conformations are sampled within the time-scale of interest, such that the statistical theory of rubber elasticity applies.

Buckley et al (Buckley et al., 1996) state that the model is most suitable for non-crystalline, non-crosslinked polymers with very high molecular weight at temperatures where the rate of conformational relaxation by entanglement slippage is negligible, thus making the model less desirable when considering conventional film and fibre grade PET. Buckley et al though suggest that work by Ward and co-workers showed that near the transition region these effects have negligible influence on the constitutive behaviour.

In comparing the results of a numerical simulation to experimental data, Buckley et al (Buckley et al., 1996) showed that the material parameters required in the model match well those produced by other authors such as Ward and co-workers. Buckley et al state that where the model deviates from the observed response of PET, it is because of known aspects of behaviour which were ignored in their early version of the model but which has since been included by Adams et al (Adams et al., 2000) and Dooling et al (Dooling et al., 2002).

Adams et al (Adams et al., 2000) highlighted the failure of the "Buckley Model" above 80°C and proposed a modification to capture the effect of strain-stiffening. Their investigations revealed that entanglement slippage was found to arrest spontaneously at a critical level of orientation corresponding to the first appearance of crystallinity. Drawing upon the link between strain-stiffening and stress-induced crystallisation (Zaroulis & Boyce, 1997) the authors introduced this effect via the "viscosity increasing asymptotically at a critical maximum principal network stretch". Dooling et al (Dooling et al., 2002) further modified the model to account for network relaxations caused by entanglement slippage.

It is however apparent that the "Buckley Model" does not have the ability to simulate the stress development with temperature and the subsequent shrinkage behaviour. Some work was undertaken to include the present functions into Buckley's model, essentially by introducing the temperature dependant dashpot and spring as shown in Figure 5.16. However, time did not permit the completion of this work and thus it is only covered briefly in this thesis.

5.4 Conclusions

- The 1D temperature dependant visco-elastic model proposed has been shown to accurately predict the transient shrinkage response of a drawn PET from room temperature to the onset of melt.
- The variation of Young's modulus with temperature follows a modified tanh function as proposed by Tobushi et al (Tobushi et al., 2001) and has been successfully simulated.
- The viscosity also varies with temperature according to a tanh type function following activation from a near solid condition as proposed by Morshedian et al (Morshedian et al., 2005) and has also been simulated with a good accuracy.

- In both cases the glass transition temperature for the PET simulated is approximately 70°C.
- Sufficient work has also been undertaken to show that the temperature dependant functions developed could be incorporated into the 3D model of Buckley and Jones (Buckley & Jones, 1995).

Chapter Six: **LatConX System – Numerical Simulation**

The LatConX system proposed in this thesis has been described in detail in the introduction chapter and "proof of concept" tests have been presented in Chapter 3. Further details are also found in the following journal publications by the author and co-workers (Isaacs et al., 2010) (Jefferson et al., 2010). The present chapter utilises the work presented in the previous two chapters and a journal publication by the author (Dunn et al., 2011). A nonlinear layered beam model of the LatConX system for a case with one major crack is developed and this is then extended for the multi-crack case. Comparisons will be made between the data in Chapter 3 and that generated using the developed model. A review of current work is also given in relation to the simulation of cracks in concrete, in particular using embedded discontinuities as this forms the basis of the detailed crack model presented in section 6.4.

6.1 Numerical Modelling of Concrete Cracking

The success of numerically simulating cracking behaviour and development in concrete plays an important role in the design and assessment of concrete structures. A large number of material models to simulate the cracking behaviour in concrete have been developed and are based on a variety of different theories. Such theories include damage mechanics, fracture mechanics and plasticity theory, although many models combine aspects of these theories to produce hybrid models. Furthermore the development of advanced finite element methods such as the Extended Finite Element Method (XFEM) and embedded crack models have in recent years further broadened the area of crack simulation in concrete. A comprehensive overview of finite element modelling in concrete is given by Jefferson (Jefferson, 2010a) which contains more than 70 references on constitutive modelling techniques for concrete. Jefferson concludes that despite some 40 years of research there is not yet available a reliable method of fully simulating the mechanical behaviour of concrete. This is not to say though that existing models do not have their strengths and many form the basis of FE software packages such as LUSAS which utilises the CRAFT model of Jefferson (Jefferson, 2003) (Jefferson, 2003a) (LUSAS, 2008).

The classical methods of simulating cracking in concrete are based on either the smeared crack approach or the discrete crack approach. Smeared crack models "spread the dissipated energy along a finite width of the localization band", with the width being related to the specific fracture energy. Such models are based on the theory of continuum mechanics, which contrast the discrete crack models which aim to incorporate discontinuous displacement fields to "properly capture the strong discontinuity kinematics of a discreet crack". Discrete crack models are also known as 'cohesive crack models' (Feist & Hofstetter, 2006).

More recently there has been increased interest in the development of approaches which incorporate a strain or displacement discontinuity into standard FE interpolations, as they enable an efficient method of simulating the fracture process zone (FPZ) in concrete, i.e. cracking (Jirasek, 2000). The concept of embedded discontinuities uses additional degrees of freedom in elements which represent the displacement jump across the discontinuity (i.e. crack) (Feist & Hofstetter, 2006). Such models are also known as the "strong discontinuity approach (SDA)" and comprehensive reviews can be found in (Jirasek, 2000), (Oliver et al., 2002) & (Oliver et al., 2003). Jefferson (Jefferson, 2010a) suggests that strong discontinuity approaches will be required in any comprehensive approach at modelling concrete fracture, which highlights the importance of such models.

Due to the fact that embedded crack or strong discontinuity models introduce additional degrees of freedom, the majority utilise the process of static condensation to eliminate the additional degrees of freedom at an element level (Feist & Hofstetter, 2006). However, some models avoid the need for static condensation by determining the additional degrees of freedom at the crack level (Sancho et al., 2007). A further notable approach is that of Armero & Ehrlich (Armero & Ehrlich, 2006) who develops new finite elements that incorporate softening hinges to simulate the strong discontinuities.

6.2 Mortar Constitutive Model

The constitutive equation for the mortar can be seen in Figure 6.1. The compression zone constitutive equation is seen in equation (6.1) where σ is the axial stress (associated with the axial strain,ε) and f_c is the compressive strength of the mortar:

$$\sigma = E.a_c^{-\left(\frac{-\varepsilon}{\varepsilon_c}\right)^{1/\ln(a_c)}}.\varepsilon \qquad (6.1)$$

In which: $a_c = \frac{\varepsilon_c.E}{f_c}$ and a_c & ε_c are positive and ε is negative.

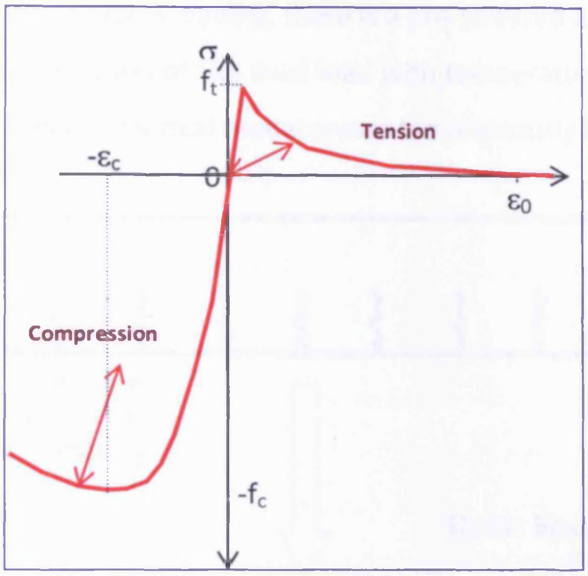

Figure 6.1 - Constitutive Model for Mortar

The constitutive equation for the tension zone in Figure 6.1 is given by equation (6.2), where ω is the damage parameter that depends on the maximum strain parameter, ζ. u_0 is the opening displacement at the end of a stress-opening curve, G_f is the fracture energy and f_t is the tensile strengths of the mortar:

$$\sigma = \left(1 - \omega(\zeta)\right).E.\varepsilon \qquad (6.2)$$

In which: $\omega = 1 - \frac{\varepsilon_t}{\zeta} e^{-c\frac{\varepsilon - \varepsilon_t}{\varepsilon_0 - \varepsilon_t}}$, $\varepsilon_0 = \frac{\mu_0}{w_c}$ and $u_0 \approx \frac{c.G_f}{f_t}$ where c = 5. ω takes the value zero until the tensile strain exceeds ε_t.

6.3 Layered Beam Model of the LatConX System

The LatConX system in its un-notched condition can be simulated with multiple linear elastic engineering beam elements, with axial and bending stiffness's. A non-linear fracture process zone (FPZ), which can be visualised as a hinge, is located at every crack location. A crack is assumed to initiate when the tensile strength in the extreme tension fibre reaches the tensile strength of the material. The system described can be seen in Figure 6.2, which highlights the simplification for a notched specimen as will be used in this analysis. The simplified system comprises two linear elastic beam elements, and a central nonlinear FPZ element, which is assumed to be subject to constant curvature.

In addition, when considering Stage 3 loading, there is a pre-stressed axial element representing the polymer tendon. The generation of the axial load with temperature supplied by the tendon is calculated using the polymer numerical model presented previously in Chapter 5

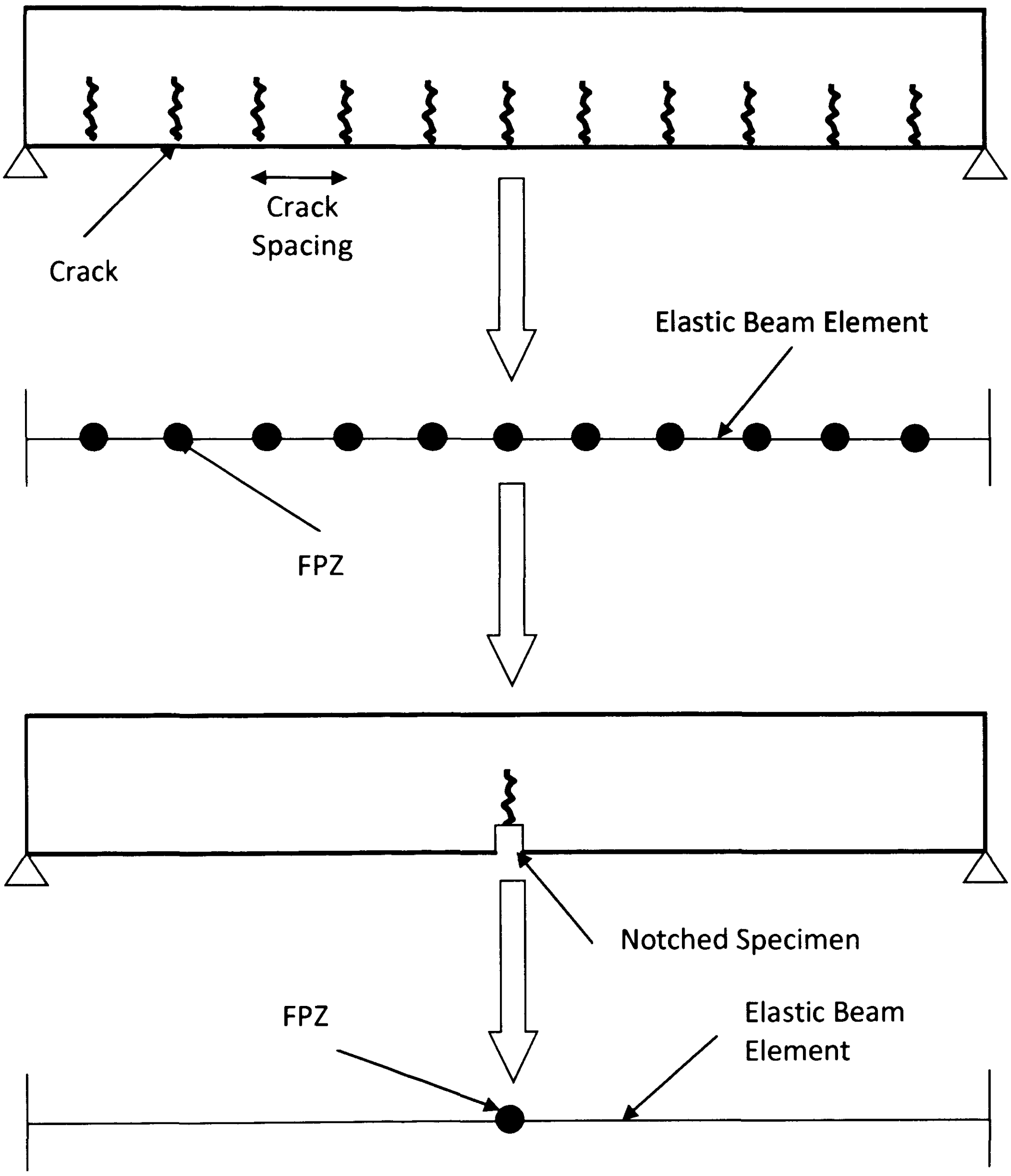

Figure 6.2 - Model Simplification and Identification of FPZ

6.3.1 Model Derivation

The model used for the notched LatConX system can be seen in Figure 6.3.

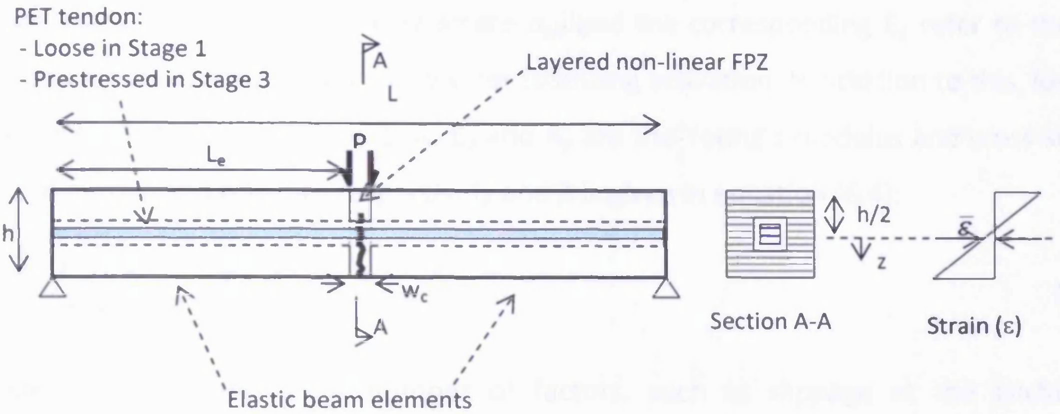

Figure 6.3 - Numerical Simulation of LatConX System

Although a model of the entire beam is illustrated; due to symmetry, only one half of this model was considered in the analysis. A non-linear layered beam model (Zienkiewicz, 1977) will be used to ensure accurate simulation of the LatConX system. Figure 6.4 shows the half beam consideration along with the primary and secondary variables used in the model.

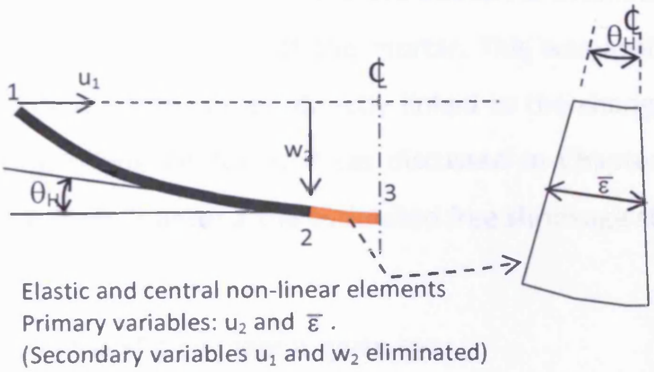

Figure 6.4 - Simplified Representation of Beam

The constitutive model for the mortar can be seen in section 6.1 and was programmed in MathCAD using a Newton procedure to solve the non-linear equations. The essential relationships of the model are given in equations (6.3) to (6.34).

The axial load in the beam (N), which depends on the effective pre-strain (ε_{p0}) that is in the tendon at the start of Stage 3 is given in equation (6.3):

$$N = -\beta\left[\varepsilon_{p0}.L + \bar{\varepsilon}w_c\right] = N_{fx} - \beta\bar{\varepsilon}w_c \tag{6.3}$$

In which the pre-strain (ε_{p0}) is given by $\sigma_{p0}/E_p - \varepsilon_{loss}$ and is computed using the polymer numerical model described previously where σ_{p0} and the corresponding E_p refer to the stress and Young's modulus respectively of polymer following activation. In addition to this, losses are included and are discussed below. E, A, E_p and A_p are the Young's modulus and cross-sectional area of the mortar and polymer respectively and β is given in equation (6.4):

$$\beta = {}^{EA}\!\Big/_{2L_e\left(1 + \frac{EA.L}{2E_pA_pL_e}\right)} \tag{6.4}$$

The losses (ε_{loss}) depend on a number of factors, such as slippage at the anchors and interactions between the time and temperature dependent behaviour of the polymer and mortar. However, any moderate reduction in restraining length (e.g. of less 3%), whilst the polymer is at maximum temperature, is not considered to significantly affect the pre-stress because the free shrinkage strain is so large (i.e. several hundred %). However, reductions in length, once the pre-stress has developed and the polymer has regained its elastic modulus below the transition temperature will affect the pre-stress. An estimate of this was obtained by computing the temperature contraction of the mortar. This was achieved by considering the change in moisture content which can be directly linked to the change in strain due to drying shrinkage via the drying shrinkage constant (as discussed in Chapter 2). For example, using Figure 2.11 and Figure 2.12 in Chapter 2 the estimated free shrinkage strain is 0.001 after 4 days curing.

The strain at any level z in the FPZ element is given by:

$$\varepsilon = \bar{\varepsilon} - \frac{2}{w_c} z\theta_H \tag{6.5}$$

The stress and secant modulus of the mortar (E_s) are functions of the strain (ε) according to the constitutive model outlined in Figure 6.1. The overall relationship between the load/moment and the strain/rotation components is given by:

$$\begin{bmatrix} N_{fx} \\ M \end{bmatrix} = \begin{bmatrix} \sum_{i=1}^{nlay} E_{Si}.b_i.\Delta z_i + \beta.w_c & \frac{-2}{w_c}\sum_{i=1}^{nlay} E_{Si}.b_i.z_i.\Delta z_i \\ \sum_{i=1}^{nlay} E_{Si}.b_i.z_i.\Delta z_i & \frac{-2}{w_c}\sum_{i=1}^{nlay} E_{Si}.b_i.z_i^2.\Delta z_i \end{bmatrix} . \begin{bmatrix} \bar{\varepsilon} \\ \theta_H \end{bmatrix} \qquad (6.6)$$

In which: b_i and Δz_i are the effective width and depth of each layer i and nlay is the total number of layers.

6.3.2 Summary

The simple layered beam model offers a basic method of calculating the effect of a pre-stressing tendon (i.e. shrinkable polymer) on the cracking behaviour of concrete. However the method is limited to central cracks and can only account for a single crack.

6.4 Advanced Multi-Crack Simulation of LatConX System

The model described previously offers a simple model for a central crack, however in order to fully simulate the LatConX system a model is required that can place the crack at any location. What follows is the derivation of a new "Beam-Hinge" element which contains a hinge within it, whilst remaining a two noded element. The hinge, which simulates a crack, can be located at any position within the element although for simplicity the following derivation considers a central crack. Furthermore the element can be placed at any position within the beam. Several verification exercises are presented to confirm the success of the new element.

6.4.1 Beam-Hinge Element Development

The proposed "Beam-Hinge" element can be seen in Figure 6.5:

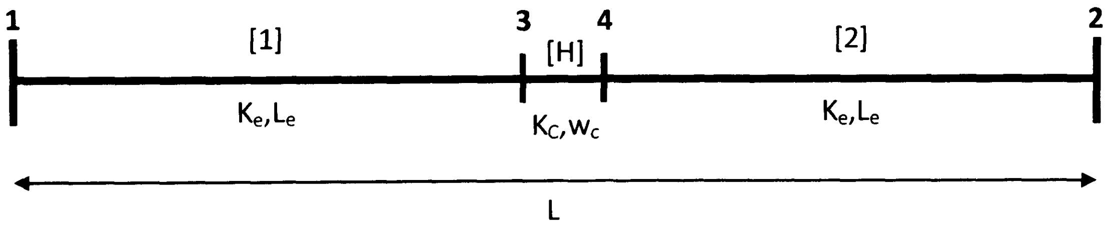

Figure 6.5 - Beam-Hinge Element

The crack is simulated by the central hinge element of length w_c, the fracture process zone (FPZ) width and whose stiffness matrix, K_C, takes the form:

$$K_C = \begin{bmatrix} k_{shr} & 0 & -k_{shr} & 0 \\ 0 & \Omega_c & 0 & -\Omega_c \\ -k_{shr} & 0 & k_{shr} & 0 \\ 0 & -\Omega_c & 0 & \Omega_c \end{bmatrix} \tag{6.7}$$

The crack terms (Ω_c and k_{shr}) will be derived in a subsequent section. Elements 1 and 2 in the "Beam-Hinge" element are Bernoulli-Euler beam elements whose length can be varied to position the crack within the element. However for simplicity they are taken as equal (L_e), hence a central crack. Their stiffness matrix takes the form:

$$K_e = \frac{E.I}{L_e} \begin{bmatrix} {}^{12}/_{L_e^2} & {}^{6}/_{L_e} & -{}^{12}/_{L_e^2} & {}^{6}/_{L_e} \\ {}^{6}/_{L_e} & 4 & -{}^{6}/_{L_e} & 2 \\ -{}^{12}/_{L_e^2} & -{}^{6}/_{L_e} & {}^{12}/_{L_e^2} & -{}^{6}/_{L_e} \\ {}^{6}/_{L_e} & 2 & -{}^{6}/_{L_e} & 4 \end{bmatrix} \tag{6.8}$$

6.4.1.1 Derivation of Beam-Hinge Element

In order to develop a 2 noded element the central nodes (3 and 4) need to be condensed out. This is undertaken using a process of static condensation, which first requires the assembly of the elements in the form shown in Figure 6.5, i.e. the external nodes take the values 1 and 2 and the internal nodes 3 and 4. The assembly yields the following:

$$\begin{bmatrix} F_1 \\ M_1 \\ F_2 \\ M_2 \\ F_3 \\ M_3 \\ F_4 \\ M_4 \end{bmatrix} = \begin{bmatrix} \frac{12EI}{L_e^3} & \frac{6EI}{L_e^2} & 0 & 0 & -\frac{12EI}{L_e^3} & \frac{6EI}{L_e^2} & 0 & 0 \\ \frac{6EI}{L_e^2} & \frac{4EI}{L_e} & 0 & 0 & -\frac{6EI}{L_e^2} & \frac{2EI}{L_e} & 0 & 0 \\ 0 & 0 & \frac{12EI}{L_e^3} & -\frac{6EI}{L_e^2} & 0 & 0 & -\frac{12EI}{L_e^3} & \frac{6EI}{L_e^2} \\ 0 & 0 & -\frac{6EI}{L_e^2} & \frac{4EI}{L_e} & 0 & 0 & -\frac{6EI}{L_e^2} & \frac{2EI}{L_e} \\ -\frac{12EI}{L_e^3} & -\frac{6EI}{L_e^2} & 0 & 0 & \frac{12EI}{L_e^3} + k_{shr} & -\frac{6EI}{L_e^2} & -k_{shr} & 0 \\ \frac{6EI}{L_e^2} & \frac{2EI}{L_e} & 0 & 0 & -\frac{6EI}{L_e^2} & \frac{4EI}{L_e} + \Omega_c & 0 & -\Omega_c \\ 0 & 0 & -\frac{12EI}{L_e^3} & -\frac{6EI}{L_e^2} & -k_{shr} & 0 & \frac{12EI}{L_e^3} + k_{shr} & \frac{6EI}{L_e^2} \\ 0 & 0 & \frac{6EI}{L_e^2} & \frac{2EI}{L_e} & 0 & -\Omega_c & \frac{6EI}{L_e^2} & \frac{4EI}{L_e} + \Omega_c \end{bmatrix} \cdot \begin{bmatrix} u_1 \\ \theta_1 \\ u_2 \\ \theta_2 \\ u_3 \\ \theta_3 \\ u_4 \\ \theta_4 \end{bmatrix} \tag{6.9}$$

The above matrix is then considered in the form;

$$\begin{bmatrix} F_e \\ F_H \end{bmatrix} = \begin{bmatrix} K_e & K_{eH} \\ K_{eH}^T & K_H \end{bmatrix} . \begin{bmatrix} u_e \\ u_H \end{bmatrix} \tag{6.10}$$

In which; $F_e = \begin{bmatrix} F_1 \\ M_1 \\ F_2 \\ M_2 \end{bmatrix}, u_e = \begin{bmatrix} u_1 \\ \theta_1 \\ u_2 \\ \theta_2 \end{bmatrix}, u_H = \begin{bmatrix} u_3 \\ \theta_3 \\ u_4 \\ \theta_4 \end{bmatrix}, F_H = \begin{bmatrix} F_3 \\ M_3 \\ F_4 \\ M_4 \end{bmatrix}$

and; $K_e = \begin{bmatrix} \frac{12EI}{L_e^3} & \frac{6EI}{L_e^2} & 0 & 0 \\ \frac{6EI}{L_e^2} & \frac{4EI}{L_e} & 0 & 0 \\ 0 & 0 & \frac{12EI}{L_e^3} & -\frac{6EI}{L_e^2} \\ 0 & 0 & -\frac{6EI}{L_e^2} & \frac{4EI}{L_e} \end{bmatrix}$ $K_{eH} = \begin{bmatrix} -\frac{12EI}{L_e^3} & \frac{6EI}{L_e^2} & 0 & 0 \\ -\frac{6EI}{L_e^2} & \frac{4EI}{L_e} & 0 & 0 \\ 0 & 0 & -\frac{12EI}{L_e^3} & -\frac{6EI}{L_e^2} \\ 0 & 0 & \frac{6EI}{L_e^2} & \frac{4EI}{L_e} \end{bmatrix}$

$$K_H = \begin{bmatrix} \frac{12EI}{L_e^3} + k_{shr} & -\frac{6EI}{L_e^2} & -k_{shr} & 0 \\ -\frac{6EI}{L_e^2} & \frac{4EI}{L_e} + \Omega_c & 0 & -\Omega_c \\ -k_{shr} & 0 & \frac{12EI}{L_e^3} + k_{shr} & \frac{6EI}{L_e^2} \\ 0 & -\Omega_c & \frac{6EI}{L_e^2} & \frac{4EI}{L_e} + \Omega_c \end{bmatrix}$$

Consider the second line of equations in equation (6.10):

$$K_{eH}^T . u_e + K_H . u_H = F_H \tag{6.11}$$

$$\therefore u_H = (F_H - K_{eH}^T . u_e) K_H^{-1} \tag{6.12}$$

Consider the first line of equations in equation (6.10):

$$K_e . u_e + K_{eH} u_H = F_e \tag{6.13}$$

$$\therefore F_e = K_e . u_e + K_{eH}\left((F_H - K_{eH}^T . u_e) K_H^{-1}\right) \tag{6.14}$$

Equation (6.14) is rearranged into the general form:

$$F_e - F_{red} = K_{cra} . u_e \tag{6.15}$$

In (6.15), K_{cra} is the reduced stiffness matrix, which is referred to as the "Beam-Hinge" matrix and takes the form:

$$K_{cra} = (K_e - K_{eH}.K_H^{-1}.K_{eH}^T) \tag{6.16}$$

In (6.15) F_{red} is the reduced load vector and is required when considering the effect of pre-stress on the system, in all other situations considered in this thesis it will be assumed zero. F_{red} takes the form:

$$F_{red} = K_{eH}.K_H^{-1}.F_H \tag{6.17}$$

In order to verify that the method of condensation and the assembly of the elements are correct, a series of verifications were undertaken using elastic elements.

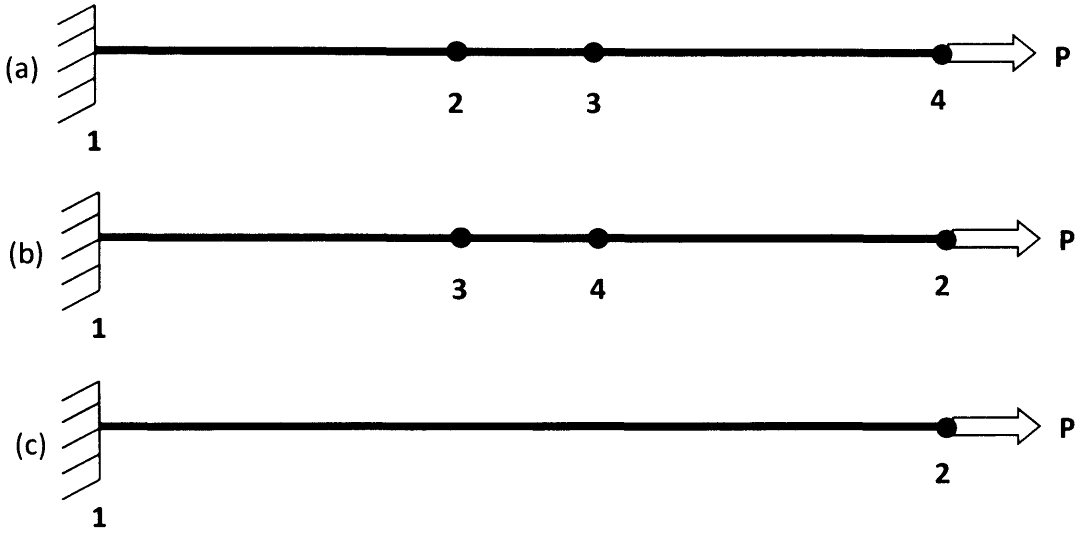

Figure 6.6 - Axial Verification Assembly

Initially a simple elastic bar problem with an applied axial load was simulated with two node configurations, as seen in Figure 6.6 (a) and (b). The results of both were comparable and hence verified that the basic assembly method was correct. The results were then compared to the condensed version seen in Figure 6.6 (c) and again yielded the same results.

The verification was extended to an elastic, simply-supported beam with applied end moments as seen in Figure 6.7. All elements were Bernoulli-Euler beam elements and assembled in two node configurations, seen in Figure 6.7 (a) and (b). The results were compared and yielded the same results, further verifying that the assembly method is correct. Again the condensation method was verified using the condensed beam seen in Figure 6.7 (c) and compared exactly with the previous results.

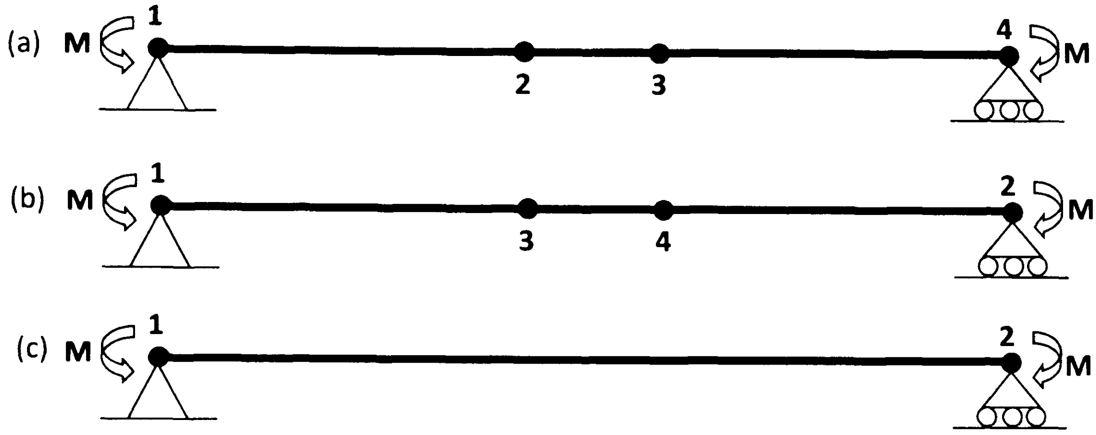

Figure 6.7 - Beam with End Moment Assembly

A completely elastic form of the "Beam-Hinge" element was then located within the elastic beam problem seen in Figure 6.8 and the results compared to the expected analytical solutions for reactions, displacement and rotation. The results compared excellently and thus verified that the elastic "Beam-Hinge" was behaving as expected and that in its elastic form was assembled correctly and also that the process of condensation was undertaken accurately.

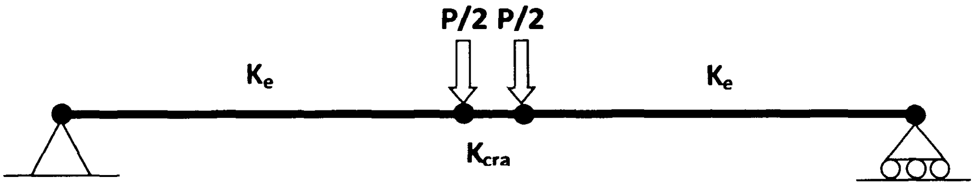

Figure 6.8 - Verification of Elastic "Beam-Hinge"

It has therefore been shown that the concept of a hinge to simulate a crack being condensed out into a modified beam element is valid. The previous verifications have used elastic Bernoulli-Euler beam elements, the following section will derive linear elastic versions of the "crack terms" (Ω_c and k_{shr}) that will be used in the K_H matrix defined previously to form the K_{cra} matrix. This will then be developed further to include pre-stress and non-linear material behaviour.

6.4.2 Development of Crack Terms (Ω_c *and* $\bar{\varepsilon}$)

The following section details the development of the crack terms which are used in the above "Beam-Hinge" element to simulate the hinge. The development is considered in 3 stages. The first considers a linear elastic beam with no crack and no pre-stress to ensure that the method of including the crack terms is correct. The second introduces pre-stress to the linear elastic form and introduces a simple crack. Finally the behaviour is extended to include non-linearity using the constitutive model detailed in Section 6.2 to fully simulate crack development.

6.4.2.1 Linear Elastic Beam-Hinge Element

The hinge construction for the linear elastic beam-hinge element is seen in Figure 6.9, in which w_c is the FPZ width and θ_H is the rotation of the hinge. The layer construction is such that the vertical axis is always centred on the neutral axis and the layer depth is positive down.

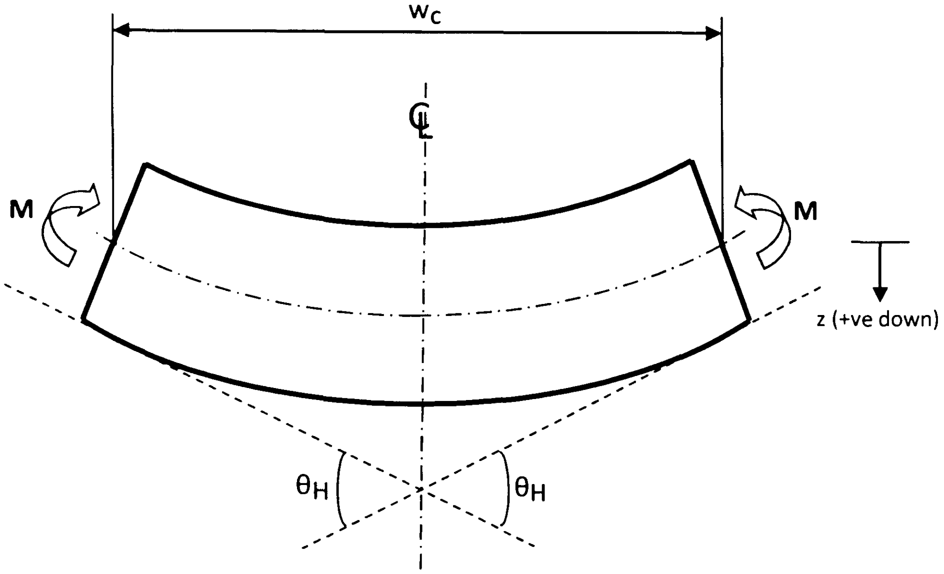

Figure 6.9 - Linear Elastic Beam Element Hinge Construction

The strain in the hinge is given below, in which $\bar{\varepsilon}$ is the strain at the neutral axis and z is the layer depth:

$$\varepsilon = \bar{\varepsilon} - \frac{2.\theta_H.z}{w_c} \tag{6.18}$$

The axial force in the beam is given below in which h is the depth of the beam:

$$N = \int_{-h/2}^{h/2} \sigma.b.dz \tag{6.19}$$

$$\sigma = E.\varepsilon \tag{6.20}$$

Using equation (6.20) and substituting in equation (6.18) for the strain and taking the axial force as equal to zero (for the present no pre-stress case), Equation (6.19) can then be simplified and takes the form:

$$0 = E.b.\bar{\varepsilon}\int_{-h/2}^{h/2} dz - \frac{2.\theta_H.z}{w_c}\int_{-h/2}^{h/2} z.dz \tag{6.21}$$

In equation (6.21); $\int_{-h/2}^{h/2} dz = b$ and $\int_{-h/2}^{h/2} z.dz = 0$ and therefore the strain at the neutral axis, $\bar{\varepsilon} = 0$.

Now consider the moment which takes the form:

$$M = \int_{-h/2}^{h/2} \sigma.b.z.dz \tag{6.22}$$

Again substituting in σ = E.ε, equation (6.18) and noting that $\bar{\varepsilon} = 0$ yields the following:

$$M = \frac{-2.E.\theta_H}{w_c}\int_{-h/2}^{h/2} b.z^2.dz \tag{6.23}$$

In equation (6.23); $\int_{-h/2}^{h/2} b.z^2.dz = I$, where I is the second moment of area. Thus through rearrangement into the form M = $\Omega_c.\theta_H$ the crack term, Ω_c is:

$$\Omega_c = \frac{-2.E.I}{w_c} \tag{6.24}$$

The shear terms of the crack matrix are assumed to take the value:

$$k_{shr} = \frac{E.A}{2.w_c} \tag{6.25}$$

The values of Ω_c and k_{shr} are used in the beam-hinge stiffness matrix (equation (6.16)) to simulate the problem shown in Figure 6.8 and compared to the theoretical solution (Steel Construction Institute, 2003) and the situation when an Euler-Bernoulli element is used. The numerical and analytical results compared excellently and can be seen in Figure 6.10 and Figure 6.11. The simulations were carried out on a beam with similar properties to the beams tested in Chapter 3; these properties can be seen in Table 6-1.

Table 6-1 - Properties for Validation Beam

Property	Symbol (Units)	Value
Load	P (kN)	100
Span	L (mm)	120
Young's Modulus	E (N/mm^2)	25000
Width	b (mm)	25
Depth	h (mm)	25
FPZ width	w_c (mm)	3

The fracture process zone width is taken from the work of Bazant who proposes that the FPZ width, w_c = 3*Aggregate Size (Bazant & Oh, 1983). The aggregate used in the LatConX beams tested in Chapter 3 was passed through a 1mm sieve and therefore w_c = 3mm. In addition the ratio of FPZ width to elastic element length (L_e in Figure 6.5) is taken as 5.

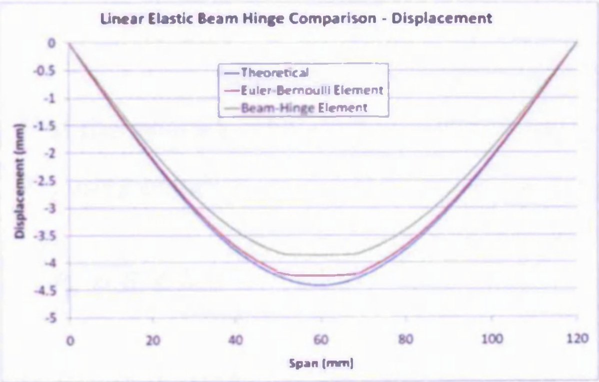

Figure 6.10 - Linear Elastic Beam Hinge Comparison (Displacement)

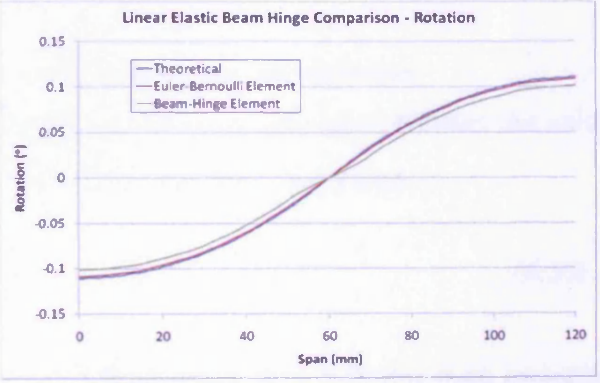

Figure 6.11 - Linear Elastic Beam Hinge Comparison (Rotation)

6.4.2.2 Linear Elastic Beam-Hinge Element with Pre-stress and Simple Crack

The element derived in the previous section is modified to include a pre-stressing tendon passing through the centre of the beam with a load of P_p and a notch. The axial load is determined using the polymer shrinkage model derived in the previous chapter and detailed in Section 6.3.1 above. The notch is defined in size by dn, which is defined as a proportion α of the depth of the beam. α takes the value of zero when no notch is present. As the crack develops it reduces the size of the section and thus the geometric properties; I_n the second moment of area and A_n the area. Furthermore, as the crack develops the eccentricity of the pre-stress tendon effectively increases which will result in a modified $\bar{\varepsilon}$, although the equation for strain still takes the form of equation (6.18).

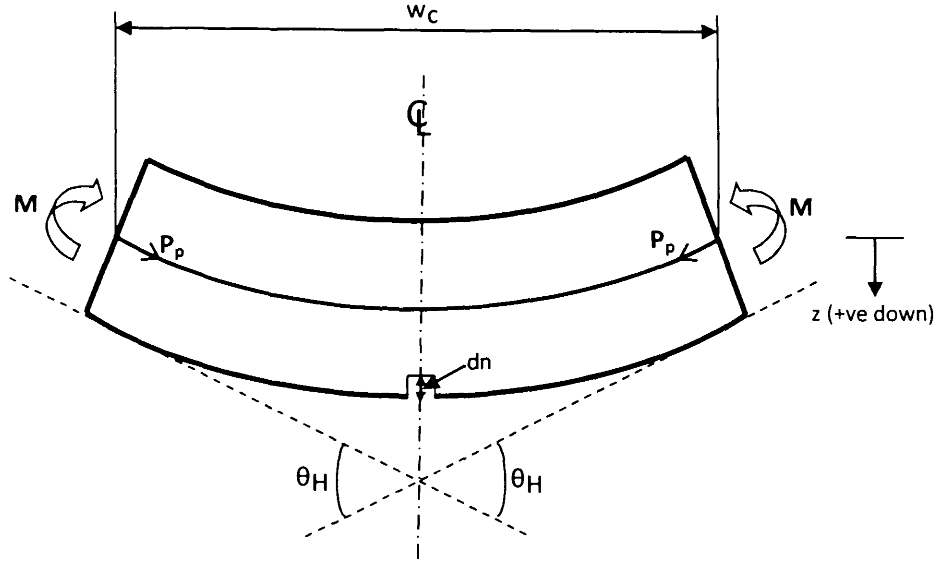

Figure 6.12 - Linear Elastic Beam Element with Pre-stress Hinge Construction

First the axial equilibrium is considered using equation (6.19). In this situation N takes the value P_p, using equation (6.20) and substituting in equation (6.18) for the strain yields:

$$P_p = E.\bar{\varepsilon}.b\int_{dn-h/2}^{h/2} dz - \frac{2.\theta_H.E.b}{w_c}\int_{dn-h/2}^{h/2} z.dz \tag{6.26}$$

Noting that; $\int_{dn-h/2}^{h/2} z.dz = 0$, $\int_{dn-h/2}^{h/2} dz = h - dn$ and the area, A_n = b.(h-dn) then equation (6.26) is rearranged such that the strain at the neutral axis is:

$$\bar{\varepsilon} = \frac{P_p}{E.A_n} \tag{6.27}$$

The moment equilibrium is now considered using equation (6.22) and substituting in equation (6.20), equation (6.18) and equation (6.26), such that through rearrangement it can be expressed in the form:

$$M - P_p.\beta = \Omega_c.\theta_H \tag{6.28}$$

Where: $\beta = \int_{-h/2}^{h/2} \frac{E.b.z.dz}{\int_{dn-h/2}^{h/2} E.b.dz}$ and;

$$\Omega_c = \int_{dn-h/2}^{h/2} \frac{\frac{2}{w_c}\int_{dn-h/2}^{h/2} E.b.z.dz}{\int_{dn-h/2}^{h/2} E.b.dz} E.b.z.dz - \int_{dn-h/2}^{h/2} \frac{2.E.b.z^2}{w_c}.dz$$

Noting that; $\int_{dn-h/2}^{h/2} z.dz = 0$ and $\int_{dn-h/2}^{h/2} b.z^2 dz = I_n$ the crack term, Ω_c can be evaluated as:

$$\Omega_c = \frac{-2.E.I_n}{w_c} \tag{6.29}$$

Equation (6.29) compares to the non-crack version and the shear term, k_{shr} is taken as defined in equation (6.25).

The above procedure modifies the moment within the hinge component and therefore this modification must also be made to the load vector, F_H, by applying $M_3 = -M_4 = \beta.P_p$. This in turn activates the reduced load vector F_{red} given in equation (6.17). Noting that the matrices K_{eH} and K_H are given in equation (6.10) yields:

$$F_{red} = \begin{bmatrix} -\frac{12EI}{L_e^3} & \frac{6EI}{L_e^2} & 0 & 0 \\ -\frac{6EI}{L_e^2} & \frac{4EI}{L_e} & 0 & 0 \\ 0 & 0 & -\frac{12EI}{L_e^3} & -\frac{6EI}{L_e^2} \\ 0 & 0 & \frac{6EI}{L_e^2} & \frac{4EI}{L_e} \end{bmatrix} \cdot \begin{bmatrix} \frac{12EI}{L_e^3} + k_{shr} & -\frac{6EI}{L_e^2} & -k_{shr} & 0 \\ -\frac{6EI}{L_e^2} & \frac{4EI}{L_e} + \Omega & 0 & -\Omega \\ -k_{shr} & 0 & \frac{12EI}{L_e^3} + k_{shr} & \frac{6EI}{L_e^2} \\ 0 & -\Omega & \frac{6EI}{L_e^2} & \frac{4EI}{L_e} + \Omega \end{bmatrix}^{-1} \cdot \begin{bmatrix} 0 \\ \beta.P_p \\ 0 \\ -\beta.P_p \end{bmatrix} \tag{6.30}$$

Equation (6.30) reduces to:

$$F_{red} = \begin{bmatrix} 0 \\ -\frac{\beta.P_p.E.I}{E.I + 2.L_{cH}.\Omega_c} \\ 0 \\ \frac{\beta.P_p.E.I}{E.I + 2.L_{cH}.\Omega_c} \end{bmatrix} \tag{6.31}$$

A simple case using the properties given previously in Table 6-1, was chosen for evaluation. This used a pre-stress value (P_p) of 625N and a crack ratio (α) of 0.25. The results showed as expected that the value of β was identical to the eccentricity (e) of the local neutral axis of the cracked section from the global neutral axis of the whole beam. Furthermore a simple problem was set up with the same geometric/material properties but the condensation procedure was removed and instead a point moment was applied either side of the FPZ. The point moment took the value $P_p.e$. The results of both the condensed and simple simulations were identical and thereby the procedure was verified.

6.4.2.3 Extension to Non-Linear Material Behaviour

In order to extend the material behaviour to include non-linearity, the constitutive model described in section 6.1 of this chapter is implemented. On implementing this constitutive model, the effective Young's modulus will vary in each layer as the crack develops and therefore the crack term Ω_c and the term β must account for this varying Young's modulus in the integration as follows in which nlay is the total number of layers:

$$\beta = \int_{i=1}^{nlay} \frac{E_i.b_i.z_i.dz}{\int_{i=1}^{nlay} E_i.b_i.dz} \tag{6.32}$$

$$\Omega_c = \int_{i=1}^{nlay} \frac{\frac{2}{w_c}\int_{i=1}^{nlay} E_i.b_i.z_i.dz}{\int_{i=1}^{nlay} E_i.b_i.dz} E_i.b_i.z_i.dz - \int_{i=1}^{nlay} \frac{2.E_i.b_i.z_i^2.}{w_c} dz \tag{6.33}$$

6.4.3 Summary and Future Work

The previous section has detailed the development of an element which includes a built in crack formed using a hinge construction. The crack can be located at any location within the element. Furthermore, the beam-hinge element can be located at any position within a structural simulation.

The element can be further developed by allowing loads to be applied at the nodes which are condensed out; such a development will require further modification of the reduced load vector.

6.5 Simulation of LatConX System

6.5.1 Simulation Data

The data to be simulated was given in Chapter 3 of this thesis. The mean properties measured in these tests are seen in Table 6-2, with pre-strain values and material properties for the polymer taken from the model and results presented previously in Chapters 4 and 5.

The Crack Mouth Opening Displacement (CMOD), which in the experiments in Chapter 3 was measured with the DIC equipment at a level approximately h/14 from the underside of the beam, is given by:

$$CMOD = \bar{\varepsilon} w_c - \left(\frac{h}{2} - \frac{h}{14}\right)\theta_H \tag{6.34}$$

The load is then obtained from the moment using statics, i.e:

$$P = M\frac{2}{L_e} \tag{6.35}$$

Table 6-2 - Measured Material Parameters used for Analysis

	E kN/mm^2	A_p mm^2	w_c mm	f_c N/mm^2	$f_{t\,(Stage\,1)}$ N/mm^2	$f_{t\,(Stage\,3)}$ N/mm^2	G_f N/mm
Mean	24.8	20.7	5	19.5	2.0	0.09	0.025
CoV (%)	1.6	-	-	8.3	7.3	10.6	11.7

Note: f_c is taken as $0.85 \cdot f_{cu}$, where f_{cu} was the strength obtained from 40mm cubes

6.5.2 Simulation Results

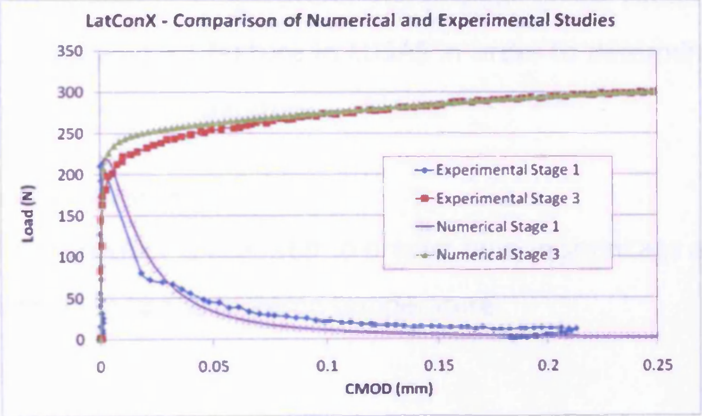

Figure 6.13 - Numerical and Experimental Comparison

Results from the analysis are compared with the experimental data presented previously in Chapter 3 and is shown in Figure 6.13. The graph shows good agreement between the numerical and experimental data. The model assumes that complete stiffness is regained when the crack is closed by polymer activation whereas in reality there will be some reduction in stiffness upon closure (Reinhardt, 1984) due to misalignment of the crack surfaces at micro and sub micro scales. The stiffness regains approximately 85% of its original value and is the probable cause for differences between the observed and predicted behaviour for the Stage 3 tests. The Stage 1 fracture softening curve is considered to be within the bounds of experimental variation and is therefore adjudged to be acceptable.

6.5.3 Summary

The numerical analysis used to consider the experiments produces results in good agreement with the test data. This demonstrates that the method of analysis is appropriate for the cracking behaviour of the LatConX system and the subsequent effect of pre-stressing. The results also show that the results obtained in Chapter 3 and thus the physical behaviour of the system is as designed. The results also validate the success of the polymer numerical model proposed and evaluated in Chapter 5.

6.6 Simple Thermal Analysis of the LatConX System

A simple thermal analysis of the LatConX system and polymer was carried out. The analysis of the polymer was carried out using a MathCAD sheet developed by the author to determine the time taken to reach the required temperature. The analysis of the LatConX beam was carried out using the thermal field analysis feature in LUSAS in order to determine the time taken for the cavity to reach the required temperature.

6.6.1 Thermal Analysis of Polymer

A thermal analysis of the polymer is required to predict tendon shrinkage and the time taken to fully heat the entire specimen to the required temperature.

6.6.1.1 Theory

There are three methods of heat transfer, namely; conduction, convection and radiation. For the following thermal investigations, radiation will be ignored, however conduction and convection are considered. Conduction refers to the ability of heat to be transferred through the contact of two surfaces whereas convection accounts for the action of heat transfer caused by fluid motion, for example the forced convection of an environment chamber and will act as a boundary condition. The theory of heat transfer states:

"The amount of thermal and mechanical energy that enters a control volume, plus the amount of thermal energy that is generated within the control volume, minus the amount of thermal and mechanical energy that leaves the control volume must equal the increase in the amount of energy stored in the control volume." (Incropera & DeWitt, 1996)

The above statement can be represented numerically as follows:

$$\dot{E}_{in} + \dot{E}_g - \dot{E}_{out} = \dot{E}_{st} \tag{6.36}$$

The energy conservation equation seen in equation (6.36) consists of three key components; the energy generated within the body ($\dot{E}_g$), the conduction in and out of the body ($\dot{E}_{in}$ & $\dot{E}_{out}$) and the energy stored in the body ($\dot{E}_{st}$). The heat generation ($\dot{E}_g$) is given by:

$$\dot{E}_g = Q.dx.dy.b \tag{6.37}$$

The heat stored in the body is given by:

$$\dot{E}_{st} = \rho.c.\frac{\partial T}{\partial t}.dx.dy.b \tag{6.38}$$

In which; ρ is the density, c is the specific heat capacity, $\frac{\partial T}{\partial t}$ is the rate of change of temperature and (dx.dy.b) is the volume. The conduction rates constituting the energy inflow and outflow are:

$$\dot{E}_{in} - \dot{E}_{out} = q_x.dy.b + q_y.dx.b - \left(q_x + \frac{\partial q_x}{\partial x}dx\right)dy.b - \left(q_y + \frac{\partial q_y}{\partial y}dy\right)dx.b \tag{6.39}$$

Equations (6.37), (6.38) and (6.39) are substituted into equation (6.36) and simplified to give:

$$\frac{\partial q_x}{\partial x} + \frac{\partial q_y}{\partial y} - Q + \rho.c.\frac{\partial T}{\partial t} = 0 \tag{6.40}$$

The heat conductivity law, which states that when a temperature gradient exists within a body, heat energy will flow from the region of high temperature to the region of low temperature is described by Fourier's Law and given in equation (6.41) in which, k is the thermal conductivity:

$$q = -k.\frac{\partial T}{\partial x} \tag{6.41}$$

Equation (6.41) can then be substituted into equation (6.40), yielding:

$$k\frac{\partial^2 q_x}{\partial x^2} + k\frac{\partial^2 q_y}{\partial y^2} + Q - \rho.c.\frac{\partial T}{\partial t} = 0 \tag{6.42}$$

For steady state conditions, where no heat is stored within the body, equation (6.42) can be simplified as:

$$k\frac{\partial^2 q_x}{\partial x^2} + k\frac{\partial^2 q_y}{\partial y^2} + Q = 0 \tag{6.43}$$

The above steady state differential equation (6.43) is solved using the Galerkin weighted residual approach and generalized by replacing the general weighted function with a shape function N and restricting the domain to the element (Ω_e). Thus the discretised solution of equation (6.44) is:

$$\underline{K}.\underline{T} = \underline{F} \tag{6.44}$$

where $\underline{K} = \sum_{elements} \underline{K_e}$ and $\underline{F} = \sum_{elements} \underline{f_e}$ and

$$\underline{K_e} = \int_1^{\Omega_e} k\left(\frac{\partial N_i}{\partial x}\frac{\partial N_j}{\partial x} + \frac{\partial N_i}{\partial y}\frac{\partial N_j}{\partial y}\right) dx\, dy \tag{6.45}$$

$$\underline{f_e} = \int_1^{\Omega_e} Q N_e \, dx\, dy - \int_1^{\Gamma_e} N_e \bar{q}\, d\Gamma \tag{6.46}$$

The boundary conditions are represented in equation (6.46) by Γ_e and in the case of heat flow theory in an environment chamber, the boundary condition accounts for the convective heat flow. Assuming an air temperature of T_e, the convective heat flow is given by equation (6.47) where h_c is the convection heat transfer coefficient:

$$q_c = h_c(T - T_e) \tag{6.47}$$

Equation (6.44) is now modified to account for the boundary conditions such that equations (6.45) and (6.46) now become (6.48) and (6.49) respectively:

$$\underline{K_e} = \int_1^{\Omega_e} k\left(\frac{\partial N_i}{\partial x}\frac{\partial N_j}{\partial x} + \frac{\partial N_i}{\partial y}\frac{\partial N_j}{\partial y}\right) dx\, dy + h_c\int_1^{\Gamma} N_i N_j\, d\Gamma \tag{6.48}$$

$$\underline{f_e} = \int_1^{\Omega_e} QN\,dx\,dy + \int_1^{\Gamma_e} N\,q\,d\Gamma_q + h_c \int_1^{\Gamma_e} NT_e\,d\Gamma_e \tag{6.49}$$

In equation (6.49) each integral can be identified as representing a form of boundary as follows; $\int_1^{\Omega_e} QN\,dx\,dy$ represents the body generated heat, $\int_1^{\Gamma_e} N\,q\,d\Gamma_q$ represents heat flux and $h_c \int_1^{\Gamma_e} NT_e\,d\Gamma_e$ represents the environmental influence of the heat on the edges of the body.

In order to deal with the transient behaviour the governing equation (6.42) is considered and C_e can be defined as:

$$C_e = \rho.c. \int_1^{\Omega_e} N_i N_j d\Omega_e \tag{6.50}$$

The discretised form of the governing equation can be expressed as:

$$\underline{C}.\underline{T} + \underline{K}.\underline{T} = \underline{F} \tag{6.51}$$

In which; $\underline{C} = \sum_{elements} C_e$. The governing differential equation can then be solved using a Crank-Nicholson scheme.

6.6.1.2 Material Properties

In order to undertake the thermal analysis of the polymer the material properties in Table 6-3 were used:

Table 6-3 - Thermal Properties for Polymer

	Density (kg/m^3)	Specific Heat Capacity (J/kg.K)	Thermal Conductivity (W/m.K)	Convection Heat Transfer Coefficient ($W/m^2.K$)	Environmental Temperature (K)	Ambient Temperature (K)
Value	1250	1200	0.025	20	363	298

6.6.1.3 Results

Using the theory given in Section 6.6.1.1 and the material properties given in Section 6.6.1.2, the results shown in Figure 6.14 are achieved for the central temperature with time for different specimen thicknesses. Figure 6.14 also presents the temperatures recorded on the thermocouple in the environment chamber which are used for the analysis in Chapter 5 and highlights the temperature lag in heating the polymer.

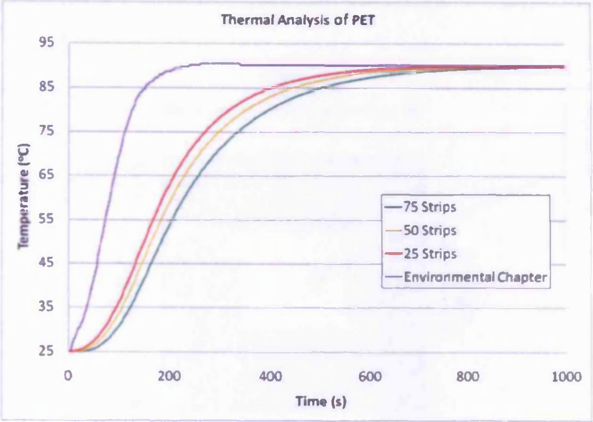

Figure 6.14 - Thermal Analysis of PET

6.6.1.4 Summary

The thermal analysis highlights that there is a lag in the temperature at the centre of the specimen in comparison to the temperature of the environmental chamber, however after 930 seconds (15.5 minutes) the temperatures are the same. Furthermore it is clear that thicker specimens take slightly longer to heat up which clearly highlights that there will be temperature gradients through the specimen and that external tendon fibres will begin to shrink before the internal fibres.

6.6.2 Thermal Analysis of the LatConX Beam

A thermal analysis of the LatConX beam is required to understand the time taken for the temperature in the cavity to reach the required temperature.

6.6.2.1 Modeling Methodology

A simple 2D transient thermal analysis was carried out using LUSAS of the cross-section illustrated in Figure 6.15. The transient field analysis feature in LUSAS was used (LUSAS, 2008). The environmental temperatures prescribed were 90°C on the outer edge of the specimen and 20°C in the cavity. The thermal conductivity of mortar at 4 days was taken to be 3.45 W.m^{-1}.°C^{-1} (Rousan & Roy, 1983). The convective heat transfer coefficient within the convection oven was taken as 10 W.m^{-2}.K^{-1} (Carson et al., 2006). The specific heat capacity of mortar is assumed to be 750 J.kg^{-1}.°C^{-1} (Poděbradská et al., 2007)

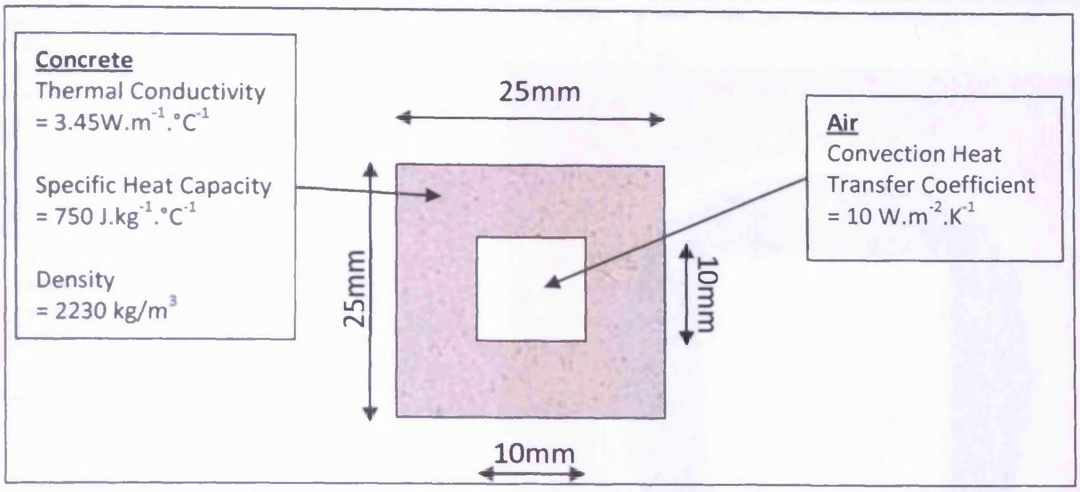

Figure 6.15 - 2D LatConX Beam Modelling Details

A full 3D analysis was considered to be over-complicating the problem due to the length of the specimen and although it is accepted that the anchor plates will allow heat penetration at the ends, the effects from this will be localised and would not significantly affect the temperature at the centre of the beam.

6.6.2.2 Results and Discussions

An initial steady state thermal analysis was undertaken to determine the maximum temperature that the cavity would reach and this can be seen in Figure 6.16, which shows a temperature of 88.8°C. It is therefore reasonable to assume that the polymer will reach a temperature of approximately 90°C as per the prior analysis, as the thermal analysis undertaken ignores the effect of heat transfer via the end plates.

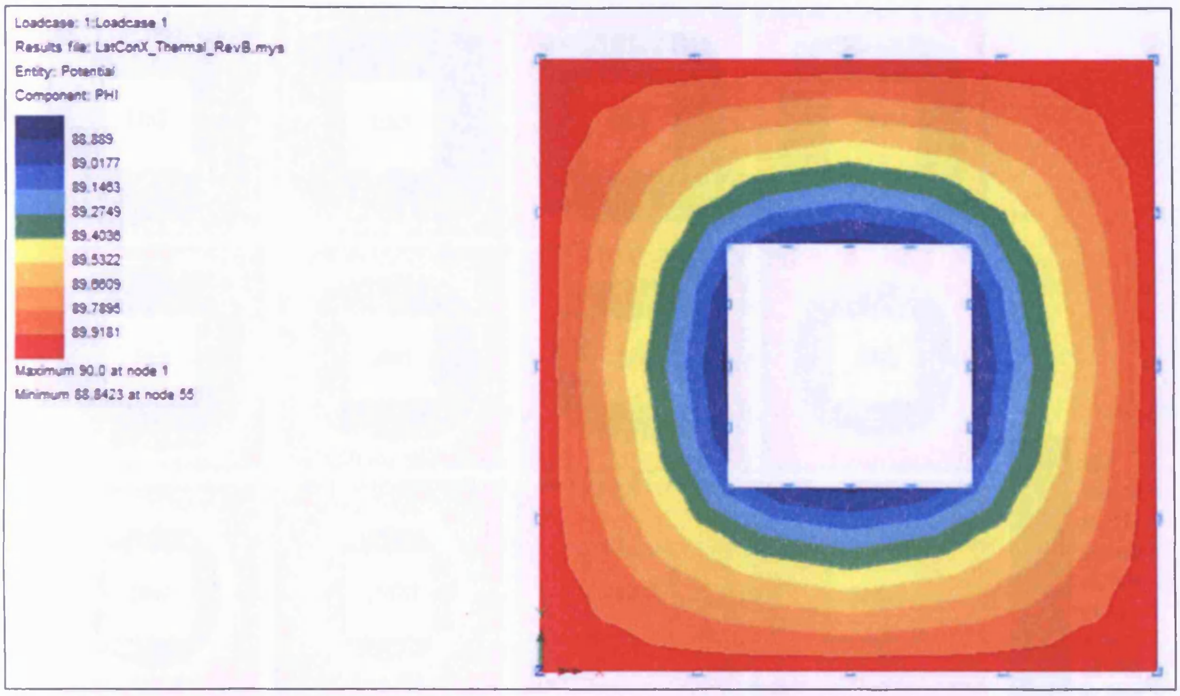

Figure 6.16 - Steady State Thermal Analysis of LatConX Beam

The steady state conditions can be seen in Figure 6.17 to take approximately 100s to occur. It can therefore be assumed that the time required for the cavity to reach the required temperature is negligible in comparison to the 10 hour soak time experienced in the experiments presented in Chapter 3. Figure 6.18 shows the development of the temperature during the initial 100s of the simulation.

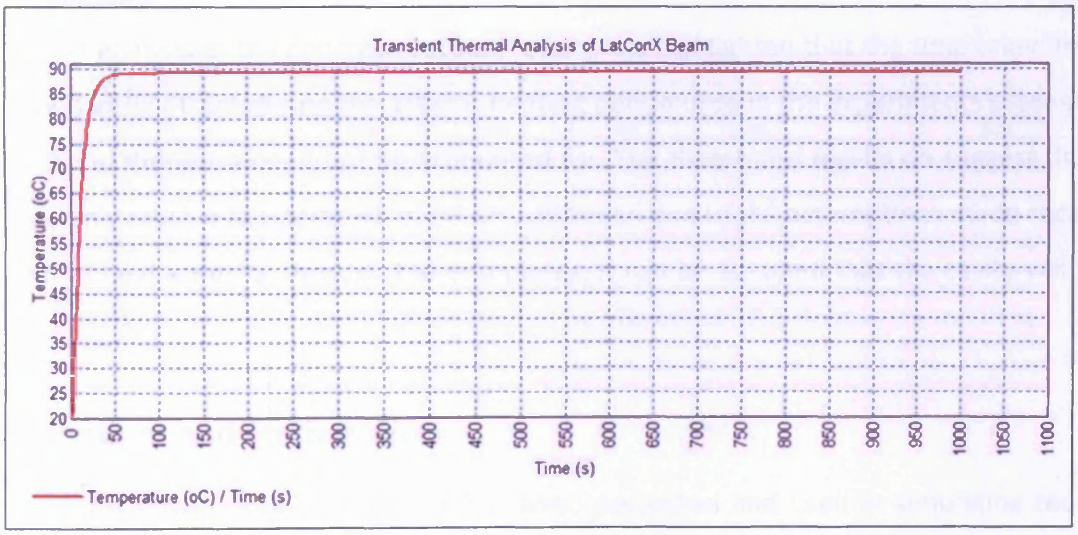

Figure 6.17 - Transient Thermal Analysis of LatConX Beam

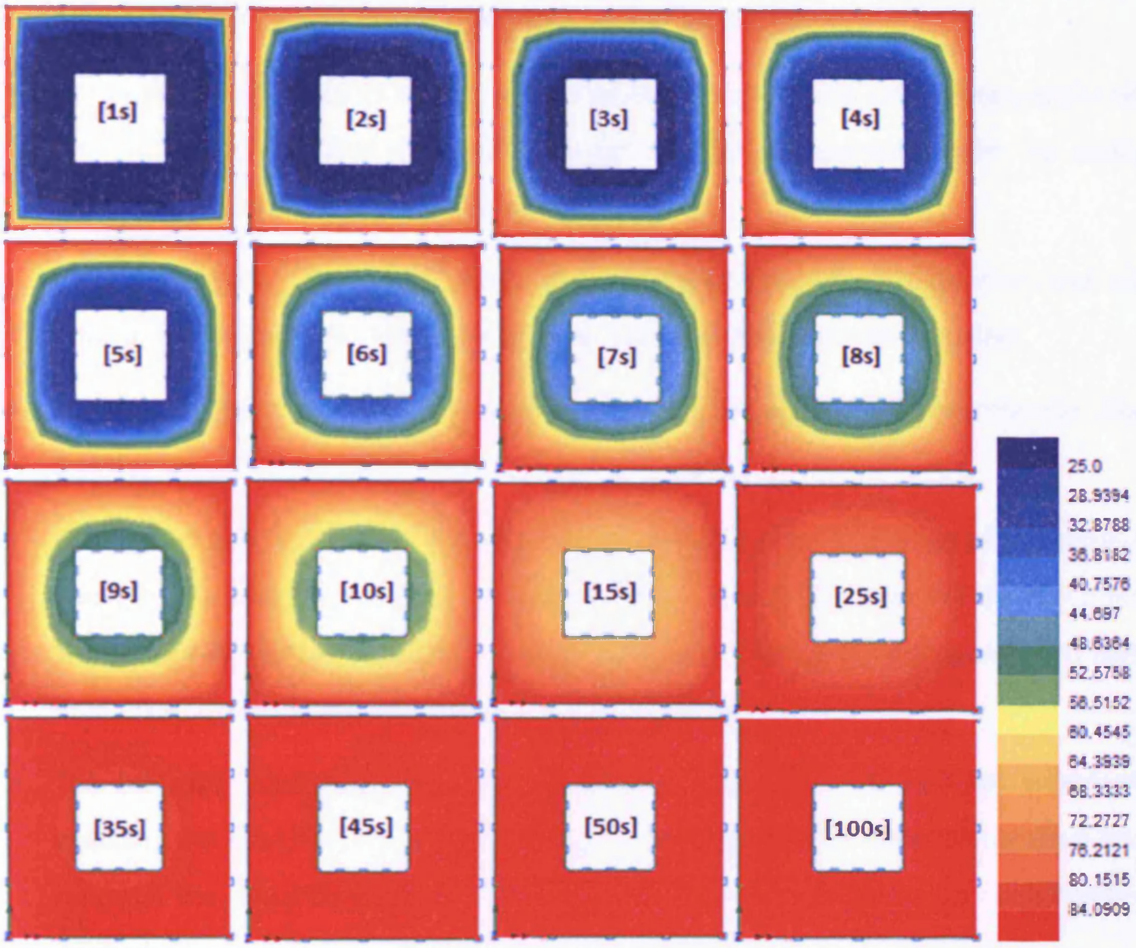

Figure 6.18 - Transient Thermal Analysis of LatConX Beam (Contour Plot)

6.6.2.3 Summary

The thermal analysis of the concrete LatConX beam has highlighted that the time taken to heat the cavity is insignificant during the 10hour heating period used in the experiments presented in Chapter 3 and therefore need not be accounted for. The theoretical results do suggest that the cavity will only reach a temperature of 88.8°C, although due to the assumptions made regarding the effect of heat entering through the end plates; it can be assumed that the cavity will reach 90°C.

6.7 Conclusions and Further Work

- A constitutive model for mortar has been presented and used in simulating the non-linear behaviour of the LatConX system.

- A simple single central crack model was successfully developed.
- The approach was further developed for multiple cracks using a hinge element in which the crack hinge variables are condensed out to yield a 2 noded element. The ability to simulate pre-stressing was also included.
- Various validations were undertaken at each stage of the element development and to ensure that each of the building-blocks for the overall element were correct.
- The element was then used to simulate accurately the experiments described in Chapter 3 of this thesis.
- Finally, two sets of thermal analysis were undertaken; the first to understand the time taken for the polymer to reach the required 90°C, which was found to be 15.5 minutes. The second simulated the LatConX mortar beam and highlighted the assumption that the time taken for the cavity reaches 90°C was insignificant.
- The LatConX simulation could be extended further and the element enhanced by including the effect of creep and shrinkage in both the polymer and mortar specimens. A proposal for modelling creep behaviour using Eurocode formulae is presented in Appendix A.

Chapter Seven: **Conclusions and Future Outlook**

This chapter presents the general conclusions that have been drawn from work reported in this thesis and comments on the potential for further work in this research area. For specific conclusions and future work suggestions the author refers the reader to conclusions drawn at the end of each section.

The research objectives, as outlined in the introduction to this thesis, were to:

a) Develop an optimum system for confining cementitious materials
b) Utilise shrinkable polymers and develop a relevant numerical model
c) Evaluate the response of the combined polymer-cementitious composite system

In respect to each of the three objectives, the following research has been undertaken, which has led to the following conclusions being made:

a) A novel system has been developed called LatConX which has the ability to close cracks and the potential for full confinement in cementitious materials. An experimental programme has been designed, developed and completed to prove that the concept works. The main conclusions drawn are:

    i. Autogenous crack healing is enhanced by using the LatConX system by means of the crack closure mechanism. Levels of 80% strength recovery and complete visual sealing were achieved.

    ii. The choice of the activation and curing regimes is critical in the effectiveness of the LatConX system. Dry activation with water curing and steam activation with steam curing were found to be the most successful regimes.

    iii. Post peak ductility was observed during secondary loading after the polymer tendons had been activated showing clear potential for the polymers to act as pre-stressing tendons.

b) A series of preliminary studies were undertaken to investigate potential polymers to act as tendons in the LatConX system. Following the determination of a suitable polymer, more detailed investigations were carried out to determine the transient-thermal properties of the polymer. A parametric study was then undertaken to fully understand the thermal-shrinkage behaviour of the chosen polymer. Existing numerical models were investigated and found to be inadequate for simulating the shrinkage behaviour observed in the experiments. A new transient thermo-mechanical model, capable of simulating the experiments undertaken, was therefore developed which drew upon aspects of previous models.

   i. Polyethylene terephthalate (PET) was found to be the most suitable polymer for the LatConX system and was found to generate a shrinkage-stress of 32.5MPa which exceeded the 20MPa required. The stress was also generated at a temperature of 90°C which was low enough not to cause damage to the cementitious matrix.

   ii. An experimental procedure was developed that minimised slip of the tendons at the grips of the tensile testing machine by the use of a mechanical lock system. A manufacturing method was also developed to enable use of the PET in the LatConX system, which bonded individual tendons at their ends to allow free shrinkage along their length.

   iii. Detailed studies showed that the measured shrinkage behaviour was independent of the specimen geometry (i.e. length and cross-section), for the testing procedure developed, provided that a soak time of 15.5 minutes was used. Furthermore it was found that the time taken to heat the cavity of the LatConX beams to the desired temperature was insignificant in comparison with the time taken for shrinkage-stress development.

   iv. The effective Young's modulus was found to follow a tanh type transition (of temperature) through the glass transition region of 60°C-120°C. The apparent

    Young's modulus was also found to vary with heating rate which suggested that viscosity also varies with temperature.

    v. The numerical model was found to accurately simulate the variation of effective Young's modulus and viscosity with temperature.

    vi. The numerical model developed was found to simulate the shrinkage development with both time and temperature with good accuracy.

c) A "beam-hinge" element has been developed to simulate the nonlinear behaviour of a beam formed from the LatConX system. A 1D plastic-damage constitutive model has been used for the concrete and this has been combined with the polymer numerical model to simulate the LatConX experiments presented in this thesis.

    i. The "beam-hinge" model has been found to accurately simulate a variety of test situations and has the ability to model multiple cracks at any point within the structure without the introduction of extra degrees of freedom.

    ii. The combined concrete-polymer model has been used to accurately simulate the behaviour of the LatConX system. This both validates the model and confirms that the system behaves as expected.

As discussed in the literature review of this thesis, the concept of "self-healing" cementitious materials is a novel and interesting step toward a more sustainable concrete. The adverse environmental impact of the manufacture of cementitious materials is considered to be a major problem and the LatConX system, presented in this thesis, offers a valuable addition to the growing area of self-healing materials. Further development is still required of the LatConX system before it is a viable alternative to traditional methods.

At present only 80% strength recovery has been achieved and the future success of the system will require detailed studies to further enhance autogenous healing. This will involve investigation of curing conditions, activation times and mix design.

Furthermore the area of polymer science has a major part to play in developing materials that are capable of generating higher levels of shrinkage-stress. An increased level of shrinkage-stress will enable the system to be used as an alternative to traditional pre-stressing, with polymers replacing the steel tendons. The literature review has also highlighted the possibility of alternative activation methods using electrical, magnetic or chemical processes. Such alternatives, most notably electricity would be better suited to a construction site where large heating operations would be uneconomic and dangerous. Unlike steel pre-stressing, the polymers could have staged activation, such that a certain level of pre-stress is introduced at different stages. This would enable healing of different types of cracking, such as early age thermal cracking or cracking due to live loading, to be healed at different times.

With increased levels of pre-stressing, comes a further potential development; full triaxial confinement, which will produce a much more ductile cementitious material as seen in Figure 7.1. Such a material which would be free from cracks would be of great benefit to the nuclear industry and applicable to water retaining structures.

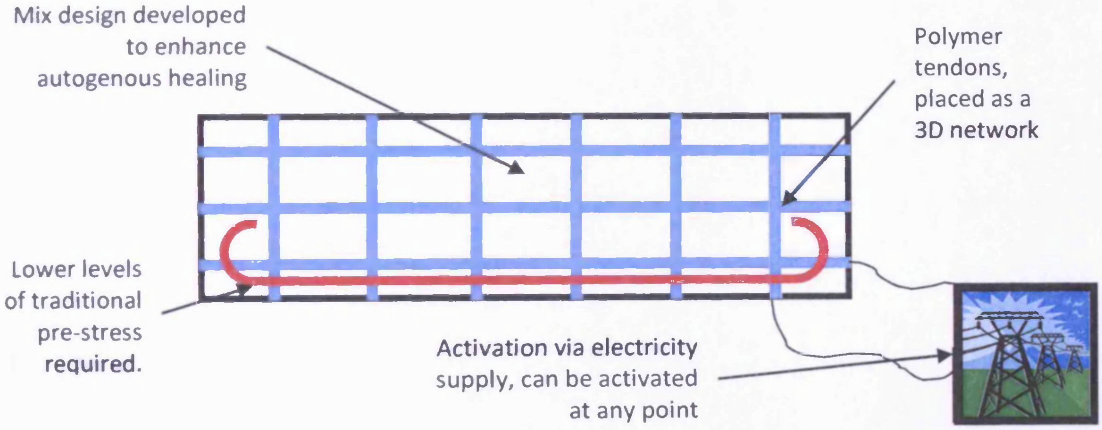

Figure 7.1 - Full Triaxially Confined version of LatConX

As the system progresses and moves towards larger scale and more complicated structures a full 3D model will be required. It has been shown in this thesis that the potential for extension to 3D of the polymer model is possible and suggestions have been made in this regard. Both the polymer and concrete models will also require development to include time dependant behaviour such as creep and shrinkage.

Finally, the biggest obstacle that must be overcome is that of acceptance by clients and engineers. Any system that utilises such technology as LatConX is ultimately going to have a greater initial cost, but a reduced life cost due to reduced maintenance and longer lifespan. At present, especially in hard economic times, clients are looking for the most economical construction solutions and are perhaps neglecting the concept of whole-life costing. Clients must therefore recognise the idea of life cost evaluation before the area of self-healing materials will be widely adopted and developed.

Bibliography

Abbasnia, R., Kanzadi, M., Shekarchi Zadeh, M. & Ahmadi, J., 2009. Prediction of Free Shrinkage Strain Related to Internal Moisture Loss. *International Journal of Civil Engineering*, 7(2), pp.92-98.

Abdel-Bary, E.M., 2003. *Handbook of Plastic Films*. Shrewsbury, UK: Rapra Technology Limited.

Abrahamson, E.R., Lake, M.S., Munshi, N.A. & Gall, K., 2003. Shape Memory Mechanics of an Elastic Memory Composite Resin. *Journal of Intelligent Material Systems and Structures*, 14, pp.623-32.

ACI Committee 548, 2009. ACI 548.1R-09 *Guide for the Use of Polymers in Concrete*. ACI.

Adams, A.M., Buckley, C.P. & Jones, D.P., 2000. Biaxial hot drawing of poly(ethylene terephthalate): measurements and modelling of strain-stiffening. *Polymer*, 41, pp.771-86.

Ahn, T.H. & Kishi, T., 2009. Crack Healing Behaviour of Cementitious Composite Materials incorporating Geo-Materials. Chicago, 2009. 2nd International Conference on Self-healing Materials.

Akhmedov, F.A., Aikhodzhaev, B.I. & Talipov, G.S., 1968. Effect of crystallization on the mechanical properties of cellulose triacetate and acetosorbates. *Mechanics of Composite Materials*, 4(4-6), pp.626-29.

Al-Gadhib, A.H., Rahman, M.K. & Baluch, M.H., 2008. *Prediction of shrinkage and creep stresses in concrete repair systems*. King Fahd University of Petroleum & Minerals.

Altoubat, S.A. & Lange, D.A., 2001. The Pickett Effect at Early Age and Experiment Separating its Mechanisms in Tension. *Materials and Structures*, 35, pp.211-18.

American Chemistry Council, 2009. *The Safety of Polyethylene Terephthalate (PET)*. [Online] Available at: http://www.plasticsinfo.org/s_plasticsinfo/sec_generic.asp?CID=657&DID=2605 [Accessed 10 November 2009].

Andrews, R.D., 1955. Retraction of Oriented Polystyrene Monofilaments. *Journal of Applied Physics*, 26(9), p.1061.

Anslyn, E.V. & Dougherty, D.A., 2005. *Modern Physical Organic Chemistry*. 1st ed. Sausalito, California: University Science Books.

Argon, A.S., 1973. A theory for the low-temperature plastic deformation of glassy polymers. *Philosophical Magazine*, 28(4), pp.839-65.

Armero, F. & Ehrlich, D., 2006. Numerical modeling of softening hinges in thin Euler-Bernoulli beams. *Computers & Structures*, 84(10-11), pp.641-56.

Asad, M. et al., 1995. Moisture Diffusion and Shrinkage in Concrete Repair Systems., 1995. The 4th Saudi Engineering Conference - Volume II.

Asad, M., Baluch, M.H. & Al-Gadhib, A.H., 1997. Drying shrinkage stresses in concrete patch repair systems. *Magazine of Concrete Research*, 49(181), pp.283-93.

Azom, 2003. *Polyethylene Terephthalate Polyester (PET, PETP) – Properties and Applications.* [Online] Available at: http://www.azom.com/details.asp?ArticleID=2047 [Accessed 9 November 2009].

Baschek, G. & Hartwig, G., 1998. Parameters influencing the thermal expansion of polymers and fibre composites. *Cryogenics*, 38(1), pp.99-103.

Bazant, Z.P., 2001. Prediction of concrete creep and shrinkage: past, present and future. *Nuclear Engineering and Design*, 203(1), pp.27-38.

Bazant, Z.P. & Chern, J.C., 1985. Concrete Creep at Variable Humidity: Constitutive Law and Mechanism. *Materials and Structures*, 18(103), pp.1-20.

Bazant, Z.P., Cusatis, G. & Cedolin, L., 2004. Temperature Effect on Concrete Creep Modeled by Microprestress-Solidification Theory. *Journal of Engineering Mechanics*, 130(6), pp.691-99.

Bazant, Z.P. & Najar, 1971. Drying of Concrete as a Nonlinear Diffusion Problem. *Cement and Concrete Research*, 1(5), pp.461-73.

Bazant, Z.P. & Oh, B.H., 1983. Crack band theory for fracture of concrete. *Materials and Structures*, 16(93), pp.155-77.

BBC Radio 4, 2010. *Materials World.* [Online] Available at: http://www.bbc.co.uk/programmes/b006qyyb [Accessed 2010 September 2].

Behl, M. & Lendlein, A., 2007. Shape-Memory Polymers. *Materials Today*, 10(4), pp.20-28.

Benboudjema, F., Meftah, F. & Torrenti, J.M., 2005. Interaction between drying, shrinkage, creep and cracking phenomena in concrete. *Engineering Structures*, 27(2), pp.239-50.

Benyoucef, S., Tounsi, A., Benrahou, K.H. & Adda Bedia, E.A., 2007. Time-dependent behavior of RC beams strengthened with externally bonded FRP plates: interfacial stresses analysis. *Mechanics of Time-Dependant Materials*, 11(3-4), pp.231-48.

Bhattacharyya, A. & Tobushi, H., 2000. Analysis of Isothermal Mechanical Response of SMP Rheological Model. *Polymer Engineering and Science*, 40(12), p.2498.

Bhushan, B., 2000. *Mechanics and reliability of flexible magnetic media - 2nd Edition.* New York: Springer-Verlag.

Bisschop, J., 2002. *Drying Shrinkage microcracking in cement-based materials.* PhD Thesis. MG Delft: DELFT University Press.

Bornert, M. et al., 2009. Assesment of digital image correlation measurement errors: methodology and results. *Experimental Mechanics*, 49(3), pp.353-70.

Bower, D.I., 2002. *An Introduction to Polymer Physics.* Cambridge: Cambridge University Press.

Boyce, M.C., Socrate, S. & Llana, P.G., 2000. Constitutive model for the finite deformation stress-strain behaviour of PET above the glass transition. *Polymer*, 41(6), pp.2183-201.

Brandrup, J., ed., 1996. *Recycling and recovery of plastics.* Munich, Germany: Carl Hanser Verlag.

BSI, 2004. *Eurocode 2: Design of concrete structures - Part 1-1: General rules and rules for buildings. EN1992-1-1.* European Committee for Standardisation.

BSI, 2006. EN 14889-2:2006 *Fibres for concrete - Part 2: Polymer fibres - Definitions, specifications and conformity.* British Standard Institution.

Buckley, C.P. & Jones, D.C., 1995. Glass-Rubber constitutive model for amourphous polymers near the glass transition. *Polymer*, 36(17), pp.3301-12.

Buckley, C.P., Jones, D.C. & Jones, D.P., 1996. Hot-drawing of PET under biaxial stress: application of a three-dimensional glass rubber constitutive model. *Polymer*, 37(12), pp.2403-14.

Cambridge, 2004. *The Glass Transition in Polymers.* [Online] Available at: http://www.doitpoms.ac.uk/tlplib/glass-transition/printall.php [Accessed 02 April 2008].

Campbell, D.H. & Folk, R.L., 1991. Ancient Egyptian Pyramids--Concrete or Rock. *Concrete International*, 13(8), pp.30-39.

Capaccio, G. & Ward, I.M., 1982. Shrinkage, shrinkage force and the structure of ultra high modulus polyethylenes. *Colloid and Polymer Science*, 260(1), pp.46-55.

Carson, J.K., Willix, J. & North, M.F., 2006. Measurements of heat transfer coefficients within convection ovens. *Journal of Food Engineering*, 72(3), pp.293-301.

Chandran, P. & Jabarin, S.A., 1993a. Biaxial orientation of poly (ethylene terephthalate). Part II: The strain–hardening parameter. *Advances in Polymer Technology*, 12(2), pp.133-51.

Chandran, P. & Jabarin, S.A., 1993. Biaxial orientation of poly(ethylene terephthalate). Part I: Nature of the stress—strain curves. *Advances in Polymer Technology*, 12(2), pp.119-32.

Chen, X. et al., 2002. A Thermally Re-mendable Cross-Linked Polymeric Material. *Science*, 295(5560), pp.1698-702.

Cheremisinoff, N.P., 1989. *Handbook of Polymer Science and Technology - Volume 2: Performance Properties of Plastics and Elastomers.* New York: Marcel Dekker Inc.

Clear, C.A., 1985. *Effects of autogenous healing upon the leakage of water through cracks in concrete - Technical Report.* Cement and Concrete Association 31p.

Construction Civil, 2010. *Concrete Shrinkage.* [Online] Available at: http://www.theconstructioncivil.com/2010/02/concrete-shrinkage.html [Accessed 5 July 2010].

Conti, S., Lenz, M. & Rumpf, M., 2007. Macroscopic behaviour of magnetic shape-memory polycrystals and polymer composites. *Materials Science and Engineering A*, 481-482, pp.351-55.

Copuroglu, O., Sisomphon, K. & Komatsu, S., 2009. Selh Healing of cement Paste By Calcium Aluminate Based Agents. Chicago, 2009. 2nd International Conference on Self-healing Materials.

Currie, R.J. & Crammond, N.J., 1994. Assessment of Existing High Alumina Cement Construction in the UK. *Proceedings of the ICE - Structures and Buildings*, 104(1), pp.83-92.

Daniels, C.A., 1989. *Polymers - Structure and Properties.* Pennsylvania, USA: Technomic Publishing Company Inc.

Davidovits, J., 2010. *Geopolymer Cement for Mitigation of Global Warming.* [Online] Available at: http://www.geopolymer.org/applications/global-warming [Accessed 19 February 2010].

Department of Trade and Industry, 2001. *Foresight: Constructing The Future*. London: Crown Copyright.

Department of Trade and Industry, 2006. *Construction statistics annual report 2006*. London: TSO.

Dismore, P.F. & Statton, W.O., 1966. Chain folding in oriented 66-nylon fibers. *Journal of Polymer Science, Part C*, 13(1), pp.133-48.

Dooling, P.J., Buckley, C.P., Rostami, S. & Zahlan, N., 2002. Hot-drawing of PMMA and the simulation using a glass-rubber constitutive model. *Polymer*, 43(8), pp.2451-65.

Doolittle, A.K., 1951. Studies in Newtonian Flow. II. The Dependence of the Viscosity of Liquids on Free-Space. *Journal of Applied Physics*, 22(12), pp.1471-75.

Drozdov, A.D. & Christiansen, J.d., 2003. Modelling the viscoplastic response of polyethylene in uniaxial loading-unloading tests. *Mechanics Research Communications*, 30(5), pp.431-42.

Dry, C.M., 1994. Matrix cracking repair and filling using active and passive modes for smart timed release of chemicals from fibers into cement matrices. *Smart Materials and Structures*, 3(2), pp.118-23.

Dunn, S.C., Jefferson, A.D., Lark, R.L. & Isaacs, B., 2011.. Investigation into the shrinkage behaviour of Polyethylene Terephthalate (PET) for a new cementitious–shrinkable polymer material system. *Applied Polymer Science*, 120(5), pp.2516-26.

Dusunceli, N. & Colak, O.U., 2008. Modelling effects of degree of crystallinity on mechanical behaviour of semicrystalline polymers. *International Journal of Plasticity*, 24(7), pp.1224-42.

Duxson, P., Provis, J.L., Lukey, G.C. & van Deventer, J.S.J., 2007. The role of inorganic polymer technology in the development of 'green concrete'. *Cement and Concrete Research*, 37(12), pp.1590-97.

Edvardsen, C., 1999. Water Permeability and Autogenous Healing of Cracks in Concrete. *American Concrete Institute: Materials Journal*, 96(4), pp.448-54.

Edwards, S.F. & Vilgis, T.H., 1986. The effect of entanglements in rubber elasticity. *Polymer*, 27(4), pp.483-92.

El-Tawil, S. & Ortega-Rosales, J., 2004. Prestressing concrete using shape memory alloy tendons. *ACI Structural Journal*, Nov-Dec, p.846–851.

Energy Efficiency News, 2008. *Energy efficient cement could radically cut emissions*. [Online] Available at: http://www.energyefficiencynews.com/i/1665/ [Accessed 20 December 2009].

Fanourakis, G.C. & Ballim, Y., 2003. Predicting Creep deformation of Concrete: A Comparison of Results from Different Investigations. Santorini, Greece, 2003. 11th FIG Symposium on Deformation Measurements.

Feist, C. & Hofstetter, G., 2006. An embedded strong discontinuity model for cracking of plain concrete. *Computer Methods in Applied Mechanics and Engineering*, 195(52), pp.7115-58.

Food Production Daily, 2002. *Mitsubishi Polyester film announces PET shrink film lines.* [Online] Available at: http://www.foodproductiondaily.com/Packaging/Mitsubishi-Polyester-film-announces-PET-shrink-film-lines [Accessed 9 November 2009].

Foresight Smart Materials Taskforce, 2004. *Smart Materials for the 21st Century.* London: The Institute of Materials, Minerals and Mining.

Fowler, D.W., 1989. Future Trends in Polymer Concrete. In Mendis, P. & McClaskey, C. *Polymers in Concrete: Advances and Applications.* Detroit, Michigan: American Concrete Institute.

Fox, T.G. & Flory, P.J., 1950. Second-Order Transition Temperatures and Related Properties of Polystyrene. I. Influence of Molecular Weight. *Journal of Applied Physics*, 21(6), pp.581-91.

Freed, Y. & Aboudi, J., 2008. Micromechanical investigation of plasticity-damage coupling of concrete reinforced by shape memory alloy fibers. *Smart Materials and Structures*, 17(1).

Freyermuth, C.L., 2001. Life-cycle cost analysis for large segmental bridges. *Concrete International*, 23(2), pp.89-95.

Furness, J., 2001. *Thermoplastics - An Introduction.* [Online] Available at: http://www.azom.com/details.asp?ArticleID=83 [Accessed 02 April 2008].

Gartner, E., 2004. Industrially interesting approaches to "low-CO2" cements. *Cement and Concrete Research*, 34(9), pp.1489-98.

Ghosh, S.K., 2009. *Self-healing Materials: Fundamentals, Design Strategies, and Applications.* 1st ed. Weinheim: Wiley-VCH.

Global Association of Manufacturers of Polyester Film, 2009. *Polyester Film Manufacturing and Technology.* [Online] Available at: http://www.ampef.com/technology.html [Accessed 9 November 2009].

Granger, L., 1996. *Comprtement differe du beton dans les enceintes de centrales nucleaires: analyse et modelisation.* PhD Thesis [In French]. Marne-La-Vallee, France: Ecole Nationale des Ponts et Chausses.

Guiu, F. & Pratt, P.L., 1964. Stress Relaxation and the Plastic Deformation of Solids. *Physica Status Solidi (b)*, 6(1), pp.111-20.

Gupta, V.B., Radhakrishnan, J. & Sett, S.K., 1994. Effect of processing history on shrinkage stress in axially oriented poly(ethylene terephthalate) fibres and films. *Polymer*, 35(12), pp.2560-67.

Halsey, G., White, H.J. & Eyring, H., 1945. Mechanical Properties of Textiles, I. *Textiles Research Journal*, 15(9), p.295.

Haward, R.N. & Thackray, G., 1968. The use of a mathematical model to describe isothermal stress-strain curves in glassy thermoplastics. *Proceedings of the Royal Society of London, Series A, Mathematical and Physical Sciences*, 302(1471), pp.453-72.

Haworth, B., Dong, Z.W. & Davidson, P., 1993. Characterisation of Shrinkage in Oriented PET Films and Containers by Thermomechanical Analysis (TMA). *Polymer International*, 32(3), pp.325-35.

Hayashi, S., Tasaka, Y., Hayashi, N. & Akita, Y., 2004. *Development of Smart Polymer Materials and its Various Applications.* Mitsubishi Heavy Industries Ltd - Technical Review Vol. 41 No.1.

Hearn, N., 1998. Self-sealing, autogenous healing and continued hydration: What is the difference? *Materials and Structures*, 31(212), pp.563-567.

Hendriks, C.A. et al., 1998. *Emission Reduction of Greenhouse Gases from the Cement Industry.* IEA Greenhouse Gas R&D Programme.

Hendrik, G. & van Oss, G., 2005. Open-file report 2005-1152 *Background Facts and Issues Concerning Cement and Cement Data.* US Dept. of the Interior & US Geological Survey.

Hing, L.E., 2007. *Application of Polymer in Concrete Construction.* Kuala Lumpur: Faculty of Civil Engineering, Universiti Teknologi Malaysia.

Idiart, A.E., 2009. *Coupled analysis of degradation processes in concrete specimens at the meso-scale.* PhD Thesis. Barcelona: Universitat Politecnica De Catalunya, Department of Geotechnical Engineering and Geosciences.

Incropera, F.P. & DeWitt, D.P., 1996. *Fundamentals of Heat and Mass Transfer.* 4th ed. New York, USA: John Wiley & Sons Inc.

International Life Sciences Institute, 2000. *Packaging Materials - 1. Polyethylene Terephthalate (PET) for Food Packaging Applications.* Brussels, Belgium: ILSI Europe.

Isaacs, B., 2010. *Self-Healing Cementitous Materials.* PhD Thesis. Cardiff: Cardiff School of Engineering Cardiff University.

Isaacs, B. et al., 2010. Autogenous Healing in an SMP Cementitiuos Material System. *Cement and Concrete Composites*, Submitted.

Janke, L., Czaderski, C., Motavalli, M. & Ruth, J., 2005. Applications of Shape Memory Alloys in Civil Engineering Structures - Overview, limits and new ideas. *Materials and Structures*, 38(279), pp.578-92.

Jefferson, A.D., 2003a. Craft - a plastic-damage-contact model for concrete II. Model implementation with implicit return mapping algorithm and consistent tangent matrix. *International Journal of Solids and Structures*, 40(22), pp.6001-22.

Jefferson, A.D., 2003. Craft - a plastic-damage-contact model for concrete. I. Model theory and thermodynamic considerations. *International Journal of Solids and Structures*, 40(22), pp.5973-99.

Jefferson, A.D., 2010a. Finite Element Material Models for Concrete - A Review. In *CST2010: The Tenth International Conference on Computational Structures Technology.* Valencia, 2010a.

Jefferson, A.D. et al., 2010. A new system for crack closure and post-tensioning of cementitious materials using shrinkable polymers. *Cement and Concrete Research*, 40(5), pp.795-801.

Jirasek, M., 2000. Comparative study on finite elements with embedded discontinuities. *Computer methods in applied mechanics and engineering*, 188(1), pp.307-30.

Jog, J.P., 1995. Crystallization of Polyethyleneterephthalate. *Polymer Reviews*, 35(3), pp.531-53.

Johnson, R. et al., 2004. *Experimental evaluation os seismic performance of SMA bridge retainers.* Reno, Nevada: Centre for Civil Engineering Earthquake Research, Department of Civil Engineering University of Nevada.

Jonkers, H.M. & Schlangen, E., 2009. Towards a sustainable bacterially -mediated self healing concrete. Chicago, 2009. 2nd International Conference on Self Healing Materials.

Jo, B.W., Park, S.K. & Park, J.C., 2008. Mechanical properties of polymer concrete made with recycled PET and recycled concrete aggregates. *Construction and Building Materials*, 22(12), p.2281–2291.

Joseph, C., 2008. *Experimental and numerical study of the fracture and self-healing of cementitious materials.* PhD Thesis. Cardiff: Cardiff School of Engineering Cardiff University.

Kambe, H. & Kato, T., 1973. *Applied Polymer Symposium*, 20, p.365.

Kardon, J.B., 1997. Polymer-Modified Concrete: Review. *Journal of Materials in Civil Engineering*, 9(2), pp.85-92.

Kennett, S., 2009. *Green Cement; An Industry Revolution.* [Online] Available at: http://www.building.co.uk/story.asp?storycode=3133227 [Accessed 19 February 2010].

Kenplas Industry Limited, 2010. *What is PET (Polyethylene Terephthalate)?* [Online] Available at: http://www.kenplas.com/project/pet/ [Accessed 9 August 2010].

Khonakdar, H.A. et al., 2003. Thermal and Shrinkage Behaviour of Stretched Peroxide-crosslinked High-density Polyethylene. *European Polymer Journal*, 39(8), pp.1729-34.

Klompen, E.T.J., 2005. *Mechanical properties of solid polymers.* PhD Thesis. Eindhoven: Technische Universiteit Eindhoven.

Lendlein, A., Jiang, H., Junger, O. & Langer, R., 2005. Light-induced shape-memory polymers. *Nature*, 434, pp.879-82.

Lendlein, A. & Kelch, S., 2002. Shape-Memory Polymers. *Angewandte Chemie International Edition*, 41(12), pp.2034-57.

Li, V.C., 2008. Engineered Cementitious Composites (ECC) – Material, Structural, and Durability Performance. In Nawy, E. *Concrete Construction Engineering Handbook.* CRC Press.

Li, V.C. et al., 2004. Development of Green Engineered Cementitious Composites for Sustainable Infrastructure Systems. In Wang, K. *Proceedings of the International Workshop on Sustainable Development and Concrete Technology.* Beijing, China: Iowa State University. pp.181-92.

Limess, 2010. *Limess.* [Online] Available at: http://www.limess.com/ [Accessed 1 March 2009].

Liu, Y. et al., 2006. Thermodynamics of Shape Memory Polymers: Uniaxial experiments and constitutive modelling. *International Journal of Plasticity*, 22(2), pp.279-313.

Liu, C., Qin, H. & Mather, P.T., 2007. Review of Progress in Shape-memory Polymers. *Journal of Materials Chemistry*, 17(16), pp.1543-58.

Li, Y., White, D.J. & Lee Peyton, R., 1998. Composite Material from Fly ash and Post-consumer PET. *Resources, Conservation and Recyling*, 24(2), pp.87-93.

Li, V.C., Yun Mook, L. & Yin-Wen, C., 1998. Feasibility study of a passive smart self-healing cementitious composite. *Composites Part B: Engineering*, 29(6), pp.819-27.

Long, S.D. & Ward, I.M., 1991. Shrinkage force studies of oriented polyethylene terephthalate. *Journal of Applied Polymer Science*, 42(7), pp.1921-29.

Lothenbach, B. et al., 2007. Effect of Temperature on Pore Solution, Microstructure and Hydration Products of Portland Cement Pastes. *Journal of Cement and Concrete Research*, 37(4), pp.483-91.

Lura, P., Van Breugel, K. & Marauyama, I., 2001. Effect of curing btemperature and type of cement on early-age shrinkage of high-performance concrete. *Journal of Cement and Concrete Research*, 31(12), pp.1867-72.

LUSAS, 2008. *Theory Manual - LUSAS Version 14.3*. Surrey, UK: LUSAS.

Maji, A.K. & Negret, I., 1998. Smart prestressing with shape-memory alloy. *Journal of Engineering Mechanics*, 124(10), pp.1121-28.

Makradi, A., Ahzi, S., Gregory, R.V. & Edie, D.D., 2005. A two-phase self-consistent model for the deformation and phase transformation behaviour of polymers above the glass transition temperature: application to PET. *International Journal of Plasticity*, 21(4), pp.741-58.

Mark, J.E. et al., 1993. *Physical Properties of Polymers*. 2nd ed. Washington DC: American Chemical Society.

Marusin, S.L., 1996. Ancient Concrete Structures. *Concrete International*, 18(1), pp.56-58.

Matthews, R.G., Ajji, A., Dumoulin, M.M. & Prud'homme, R.E., 2000. The effects of stress relaxation on the structure and orientation of tensile drawn PET. *Polymer*, 41(19), pp.7139-45.

McCrum, N.G. & Buckley, C.P., 1997. *Principles of Polymer Engineering*. Oxford: Oxford University Press.

McLeod, R.S., 2005. Ordinary Portland Cement. *Building For a Future Magazine*.

Mihashi, H., Kaneko, Y., Nishiwaki, T. & Otsuka, K., 2000. Fundamental study on development of intelligent concrete characterized by self-healing capability for strength. *Transactions of the Japan Concrete Institute*, 22, pp.441-50.

Mitsubishi Heavy Industries, 2002. Shape Memory Polymers. *Smart Materials Bulletin*, August, p.4.

Mody, R., Lofgren, E.A. & Jabarin, S.A., 2001. Shrinkage Behaviour of Oriented Poly(ethylene terephthalate). *Journal of Plastic Film and Sheeting*, 17(2), pp.152-63.

Morshedian, J., Khonakdar, H.A. & Rasouli, S., 2005. Modeling of Shape Memory Induction and Recovery in Heat Shrinkable Polymers. *Macromolecular Theory and Simulations*, 14(7), pp.428-34.

Moser, K., Bergamini, A., Christen, R. & Czaderski, C., 2005. Feasibility of concrete prestressed by shape memory alloy short fibres. *Materials and Structures*, 38(279), pp.593-600.

Neville, A.M., 1995. *Properties of Concrete*. 4th ed. Essex: Longman.

Oliver, J., Huespe, A.E., Pulido, M.D.G. & Chaves, E., 2002. From continuum mechanics to fracture mechanics: the strong discontinuity approach. *Engineering Fracture Mechanics*, 69(2), pp.113-36.

Oliver, J., Huespe, A.E. & Samaniego, E., 2003. A study on finite elements for capturing strong discontinuities. *International Journal for Numerical Methods in Engineering*, 56(14), pp.2135-61.

Otsuka, K. & Kakeshita, T., 2002. Science and Technology of Shape Memory Alloys. New Developments. *MRS Bulletin*, 27(2), pp.91-100.

Pakula, T. & Trznadel, M., 1985. Thermally stimulated shrinkage forces in oriented polymers. I: Temperature dependence. *Polymer*, 26(7), pp.1011-18.

Pearce, F., 1997. The Concrete Jungle Overheats. *New Scientist*.

Peterlin, A., 1971. *Polymer Science Symposium*, 32, pp.297-317.

Pickett, G., 1946. Shrinkage Stresses in Concrete. *Journal of the American Concrete Institute*, 17(3), pp.165-95.

Plastics Federation of South Africa, 2009. *Polyethylene Terephthalate (PET)*. Plastics Federation of South Africa.

Podĕbradská, J., Pavlik, J., Toman, J. & Cerny, R., 2007. *Specific Heat Capacity of Cementitious Composites in High Temperature Range*. Katowice: Construction Engineering Division Polish Academy of Sciences.

Portland Cement Association, 2010. *Bendable Concrete*. [Online] Available at: http://www.cement.org/tech/cct_con_design_bendable.asp [Accessed 29 March 2010].

Prevorsek, D.C., Tirpak, G.A., Harget, P.J. & Reimschuessel, A.C., 1974. Effects of thermal contraction on structure and properties of PET fibers. *Journal of Macromolecular Science, Part B: Physics*, 9(4), pp.733-59.

Qian, S. et al., 2009. Self-Healing Cementitious Composites under Bending Loads. Chicago, 2009. 2nd International Conference on Self-healing Materials.

Ramm, W. & Biscoping, M., 1998. Autogenous healing and reinforcement corrosion of water-penetrated separation cracks in reinforced concrete. *Nuclear Engineering and Design*, 179(2), pp.191-200.

Rebeiz, K.S., 1995. Time-temperature Properties of Polymer Concrete Using Recycled PET. *Cement and Concrete Composites*, 17(2), pp.119-24.

Rebeiz, K.S., Fowler, D.W. & Paul, D.R., 1991. Recycling Plastics in Polymer Concrete Systems for Engineering Applications. *Polymer-Plastics Technology and Engineering*, 30(8), pp.809-25.

Reinhardt, H.W., 1984. Fracture mechanics of an elastic softening material like concrete. *Heron*, 29(2), pp.1-42.

Reinhardt, H. & Jooss, M., 2003. Permeability and self-healing of cracked concrete as a function of temperature and crack width. *Cement and Concrete Research*, 33(7), pp.981-85.

Ribnick, A., 1969. The thermal shrinkage of an-oriented Polyester Yarn as a function of Time, Temperature and Stress. *Textiles Research Journal*, 39, p.428.

Richardson, M.G., 2002. *Fundamentals of Durable Reinforced Concrete.* London: Spon Press.

RILEM, 2009. *STAR - Self Healing Materials (DRAFT).* RILEM.

Rousan, A.A. & Roy, D.M., 1983. A Thermal Comparator Method for Measuring Thermal Conductivity of Cementitious Materials. *Industrial and Engineering Chemistry, Product Research and Development*, 22(2), p.349–351.

Saiidi, M.S., Sadrossadat-Zadeh, M., Ayoub, C. & Itani, A., 2007. Pilot Study of Behaviour of Concrete Beams Reinforced with Shape Memory Alloys. *Journal of Materials in Civil Engineering*, 19(6), pp.454-61.

Sakata, K., 1983. A Study on Moisture Diffusion in Drying and Drying Shrinkage of Concrete. *Cement and Concrete Research*, 13(2), pp.216-24.

Sancho, J.M. et al., 2007. An embedded crack model for finite element analysis of concrete fracture. *Engineering Fracture Mechanics*, 74(1-2), pp.75-86.

Sato, A., Yamaji, Y. & Mori, T., 1986. Physical Properties controlling shape memory effect in Fe-Mn-Si alloys. *Acta Metallurgica*, 34(2), pp.287-94.

Schmets, A.J.M., 2003. Self-healing: an emerging property for new materials. *Leonardo Times.*

Sharma, S.K. & Mishra, A., 1987. The effect of stretching conditions on properties of amorphous polyethylene terephthalate film. *Journal of Applied Polymer Science*, 34(6), pp.2231-47.

Sharp, S.R. & Clemena, G.G., 2004. *State of the art survey of advanced materials and theirpotential application in highway infrastructure.* Charlottesville: Virginia Transportation Research Council. pp1-41.

Sherby, O.D. & Dorn, J.B., 1958. Anelastic creep of polymethyl methacrylate. *Journal of the Mechanics and Physics of Solids* , 6(2), p.145.

Shih, W.K., 1994. Shrinkage Modeling of Polyester Shrink Film. *Polymer Engineering and Science*, 34(14), pp.1121-28.

Shyam Plastic Machinery, 2009. *PET Moulding - Mould Your Shape.* [Online] Available at: http://www.petmachine.in/index.htm [Accessed 9 November 2009].

Simo, J.C. & Hughes, T.J.R., 1998. *Computational Inelasticity.* New York, NY, USA: Springer-Verlag.

Smith, F.S. & Steward, R.D., 1974. The crystallization of oriented poly(ethylene terephthalate). *Polymer*, 15(5), pp.283-86.

Sperling, L.H., 2006. *Introduction to Physical Polymer Science.* 4th ed. New Jersey: John Wiley & Sons.

Steel Construction Institute, 2003. *Steel Designers Manual.* 6th ed. Oxford, UK: Blackwell Science Ltd.

Suwito, A., Ababneh, A., Xi, Y. & Willam, K., 2006. The coupling effect of drying shrinkage and moisture diffusion in concrete. *Computers and Concrete*, 3(2/3), pp.103-22.

Sweeney, J., Shirataki, H., Unwin, A.P. & Ward, I.M., 1999. Application of a Necking Criterion to PET Fibers in Tension. *Journal of Applied Polymer Science*, 74(14), pp.3331-41.

Sweeney, J., Shirayaki, H., Unwin, A.P. & Ward, I.M., 1999. Application of a Necking Criterion to PET Fibers in Tension. *Journal of Applied Polymer Science*, 74, pp.3331-41.

Sweeney, J. & Ward, I.M., 1990. A unified model of stress relaxation and creep applied to oriented polyethylene. *Journal of Materials Science*, 25(1), pp.697-705.

Sweeney, J. & Ward, I.M., 1995. Rate dependent and network phenomena in multiaxial drawing of poly(vinyl chloride). 36(2), pp.299-308.

Takagi, T., 1996. Recent Research on Intelligent Materials. *Journal of Intelligent Material Systems and Structures*, 7(3), pp.346-52.

Tanabe, Y. & Kanetsuna, H., 1979. Mechanism for thermal shrinkage of oriented polystyrene monofilaments. *Polymer*, 20(9), pp.1121-28.

Tarmac, 2007. *CEMROK/AM Product Information*. Data Sheet. Derbyshire: Tarmac Industries.

Taylor, M., Tam, C. & Gielen, D., 2005. *Energy Efficiency and CO2 Emissions from the Global Cement Industry*. Energy Technology Policy Division.

ter Heide, N. & Schlangen, E., 2007. Self Healing of Early Age Cracks in Concrete. Noordwijk aan Zee, 2007. 1st International Conference on Self-healing Materials.

ter Heide, N., Schlangen, E. & van Breugel, K., 2005. Experimental Study of Crack Healing of Early Age Cracks. In *Knud Hoejgaard Conference on Advanced Cement-Based Materials*. Technical University of Denmark, 2005.

Tobushi, H. & Hashimoto, T., 1997. Thermomechanical Constitutive Modeling in Shape Memory Polymer of Polyurethane Series. *Journal of Intelligent Material Systems and Structures*, 8(8), pp.711-18.

Tobushi, H., Okumura, K., Hayashi, S. & Ito, N., 2001. Thermomechanical constitutive model of shape memory polymer. *Mechanics of Materials*, 33(10), pp.545-54.

Trau, M., Saville, D.A. & Aksay, I.A., 1997. Assembly of Colloidal Crystals at Electrode Interfaces. *Langmuir 1997, 13, 6375-6381*, 13(24), pp.6375-81.

Trznadel, M., 1986. Thermally stimulated shrinkage forces in oriented polymers: Induction time. *Polymer*, 27(6), pp.871-76.

Trznadel, M. & Kryszewski, M., 1992. Thermal Shrinkage of Oriented Polymers. *Polymer Reviews*, 32(3/4), pp.259-300.

Trznadel, M., Pakula, T. & Kryszewski, M., 1985. Thermally stimulated shrinkage forces in oriented polymers: 2. Time dependance. *Polymer*, 26(7), pp.1019-24.

United Nations, 2009. Framework Convention on Climate Change. Copenhagen, 2009.

University College Cardiff Consultants Limited, 2007. *Pre-stressing or confinement of materials using polymers.* GB0715123.

van Breugel, K., 2007. Is there a market for selh-healing cement-based materials?. Noordwijk aan Zee, 2007. 1st International Conference on Self-healing Materials.

van Breugel, K., 2009. Self healing concepts in Civil Engineering for sustainable solutions: Potential and constraints. Chicago, 2009. 2nd International Conference on Self-healing Materials.

van der Zwaag, S., 2007. *Self Healing Materials: An alternative Approach to 20 Centuries of Materials Science.* 1st ed. AA Dordrecht: Springer.

van der Zwaag, S. et al., 2009. Self-healing behaviour in man-made engineering materials: bioinspired but taking into account their intrinsic character. *Philosophical Transactions of the Royal Society A*, 367, pp.1689-704.

van Oss, H.G., 2005. Open File Report 2005-1152 *Background Facts and Issues Concerning Cement and Concrete Data.* US Department of the Interior and US Geological Survey.

van Tittelboom, K. & De Belie, N., 2009. Autogeneous Healing of Cracks in Cementitious Materials with Varying Mix Compositions. Chicago, 2009. 2nd International Conference on Self Healing Materials.

van Tittelboom, K. & De Belie, N., 2009. Self-Healing Concrete by the Internal Release of Adhesive from Hollow Glass Fibres Embedded in the Matrix. Chicago, 2009. 2nd International Conference on Self-healing Materials.

Volk, B., 2005. *Characterization of Shape Memory Polymers.* Langley: NASA Langley Research Centre.

Ward, I.M. & Sweeney, J., 2004. *An Introduction to the Mechanical Properties of Solid Polymers.* 2nd ed. Chichester, West Sussex/England: John Wiley & Sons Ltd.

Weager, B., 2008. *Shape Memory Chords in a Cementitious Composite: Development of Polymer and Composite Chords.* NetComposites.

White, S.R. et al., 2001. Autonomic healing of polymer composites. *Nature*, 409(6822), pp.794-797.

Wilding, M.A. & Ward, I.M., 1981. Creep and recovery of ultra high modulus polyethylene. *Polymer*, 22(7), pp.870-76.

Williams, M.L., Landel, R.F. & Ferry, J.D., 1955. The Temperature Dependence of Relaxation Mechanisms in Amorphous Polymers and Other Glass-forming Liquids. *Journal of American Chemistry Society*, 77(14), pp.3701-07.

Worrell, E., Price, L., Hendricks, C. & Ozawa Meida, L., 2001. Carbon Dioxide Emisions from the Global Cement Industry. *Annual Review of Energy and Environment*, 26, pp.117-143.

Wu, J.J. & Buckley, C.P., 2004. Plastic Deformation of Glassy Polystyrene: A Unified Model of Yield and the Role of Chain Length. *Journal of Polymer Science: Part B: Polymer Physics*, 42(11), pp.2027-40.

Yang, Z.J., Harkin-Jones, E.M.A., Armstrong, C.G. & Menary, G.H., 2004. Finite element modelling of stretch-blow moulding of PET bottles using Buckley model: plant tests and effects of process conditions and material parameters. *Proceedings of Institution of Mechanical Engineers*, 218(Part E: Journal of Process Mechanical Engineering), pp.237-50.

Yang, Y., Lepech, M.D., Yang, E. & Li, V.C., 2009. Autogenous healing of engineered cementitious composites under wet–dry cycles. *Cement and Concrete Research*, 39(5), pp.382-90.

Zaroulis, J.S. & Boyce, M.C., 1997. Temperature, strain rate, and strain state dependence of the evolution in mechanical behaviour and structure of poly(ethylene terephthalate) with finite strain deformation. *Polymer*, 38(6), pp.1303-15.

Zener, C., 1948. *Elasticity and Anelasticity of Metals*. Chicago: Chicago University Press.

Zienkiewicz, O.C., 1977. *The Finite Element Method*. London: McGraw-Hill.

APPENDIX A: CREEP DETERMINATION IN EUROCODES

Creep as defined by Eurocode 2 depends on "the ambient humidity, the dimensions of the element and the composition of the concrete" in addition to the age of concrete when first loaded and the duration of that load. The creep deformation, $\varepsilon_{cc}(\infty, t_0)$ at a time t = ∞ for a constant compressive stress σ_c applied at concrete age of t_0 is:

$$\varepsilon_{cc}(\infty, t_0) = \varphi(\infty, t_0).(\sigma_c/E_c) \qquad \text{(A.1)}$$

E_c is taken as $1.05E_{cm}$, if compressive stress does not exceed 45% of the compressive strength of the concrete then E_c can be found from Figure A1 below, taken from Eurocode 2.

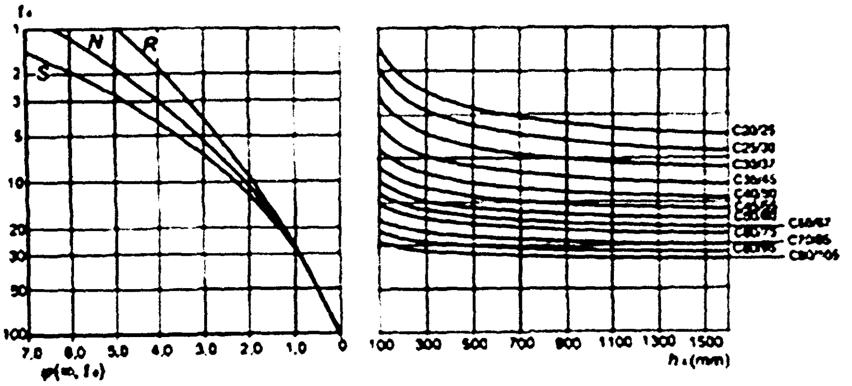

a) inside conditions - RH = 50%

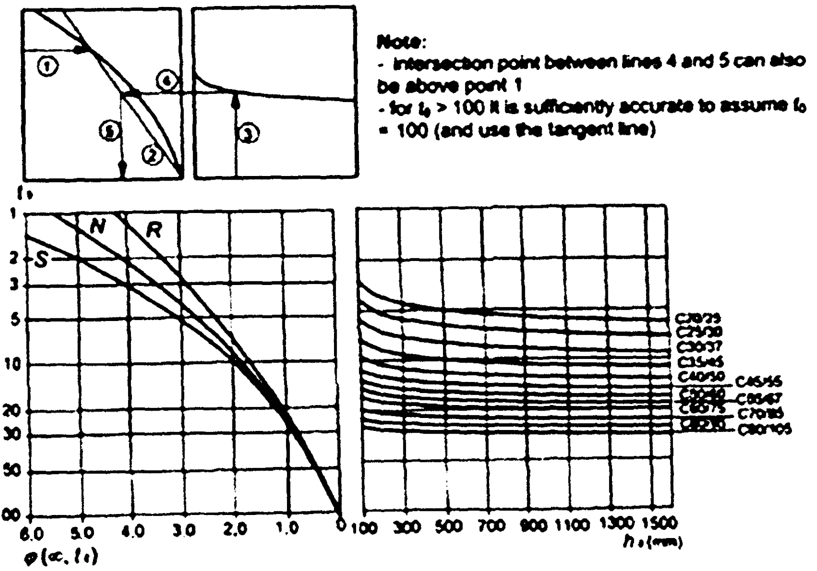

Note:
- intersection point between lines 4 and 5 can also be above point 1
- for t_0 > 100 it is sufficiently accurate to assume t_0 = 100 (and use the tangent line)

b) outside conditions - RH = 80%

Figure 3.1: Method for determining the creep coefficient $\varphi(\infty, t_0)$ for concrete under normal environmental conditions

Figure A1 - Eurocode 2 Section 1.1 (Figure 3.1)

The creep coefficient, $\varphi(\infty, t_0)$ is given by:

$$\varphi(\infty, t_0) = \varphi_o . \beta_c(t, t_0) \tag{A.2}$$

The notional creep coefficient, φ_o is estimated as:

$$\varphi_o = \varphi_{RH} . \beta(f_{cm}) . \beta(t_0) \tag{A.3}$$

φ_{RH} is a factor allowing for the effect of relative humidity on notional creep coefficient and is given by:

$$\varphi_{RH} = 1 + \frac{1 - RH/100}{0.1 . \sqrt[3]{h_0}} \qquad \text{for } f_{cm} \leq 35\text{MPa} \tag{A.4}$$

$$\varphi_{RH} = \left[1 + \frac{1 - RH/100}{0.1 . \sqrt[3]{h_0}} . \alpha_1\right] . \alpha_2 \quad \text{for } f_{cm} \leq 35\text{MP} \tag{A.5}$$

RH is the relative humidity of the ambient environment in % and h_0 is the notional size of the member in mm and given below, in which A_c is the cross-sectional area and u is the perimeter of the member in contact with the atmosphere:

$$h_0 = \frac{2A_c}{u} \tag{A.6}$$

Furthermore in order to allow for the effect of concrete strength on the notional creep coefficient the factor $\beta(f_{cm})$ is taken as:

$$\beta(f_{cm}) = \frac{16.8}{\sqrt{f_{cm}}} \tag{A.7}$$

In which the mean compressive strength in concrete at 28 days, f_{cm} is given in MPa. In order to account for the effect of concrete age at loading on the notional creep coefficient a factor, $\beta(t_0)$ is given as:

$$\beta(t_0) = \frac{1}{(0.1 + t_0^{0.2})} \tag{A.8}$$

Finally, $\beta_c(t, t_0)$ is introduced to describe the development of creep with time after loading and may be estimated using the following equation:

$$\beta_c(t, t_0) = \left[\frac{(t - t_0)}{(\beta_H + t - t_0)}\right]^{0.3} \qquad \text{(A.9)}$$

In which t is the age of concrete in days at the moment considered, t_0 is the age of concrete at loading in days and $t\text{-}t_0$ is the non-adjusted duration of loading in days. A further coefficient, β_H is introduced which depends on the RH (in %) and the notional member size (h_0 in mm) and is given by:

$$\beta_H = 1.5[1 + (0.012\,\text{RH})^{18}]h_0 + 250 \leq 1500 \qquad \text{for } f_{cm} \leq 35 \qquad \text{(A.10)}$$

$$\beta_H = 1.5[1 + (0.012\,\text{RH})^{18}]h_0 + 250\,\alpha_3 \leq 1500\,\alpha_3 \qquad \text{for } f_{cm} \leq 35 \qquad \text{(A.11)}$$

The coefficients $\alpha_{1/2/3}$ are introduced to consider the influence of concrete strength and are given by:

$$\alpha_1 = \left[\frac{35}{f_{cm}}\right]^{0.7} \qquad \text{(A.12)}$$

$$\alpha_2 = \left[\frac{35}{f_{cm}}\right]^{0.2} \qquad \text{(A.13)}$$

$$\alpha_3 = \left[\frac{35}{f_{cm}}\right]^{0.5} \qquad \text{(A.14)}$$

APPENDIX B: REQUIRED COMPRESSIVE STRESS FOR LATCONX SYSTEM

Using simple statics:

$$\sigma_c = \frac{P_p}{A} + \frac{M.y}{I} \tag{B.1}$$

In which; σ_c is the extreme fibre stress, P_p is the polymer pre-load, A is the cross-section area of the beam (A = b.h) and I is the second moment of area of the beam ($I = bh^3/12$) and:

$$P_p = \sigma_p.A_p \tag{B.2}$$

$$M = \sigma_p.A_p.e \tag{B.3}$$

$$y = \frac{h}{2} \tag{B.4}$$

Noting that e is the eccentricity and σ_p is the pre-stress due to the polymer. Equation (B.1) therefore expands to:

$$\sigma_c = \frac{\sigma_p.A_p}{b.h} + \frac{\sigma_p.A_p.e.\left(\frac{h}{2}\right)}{\left(\frac{b.h^3}{12}\right)} \tag{B.4}$$

Let $\rho = \frac{A_p}{b.h}$

$$\sigma_c = \sigma_p.\rho + \frac{6.\sigma_p.A_p.e}{b.h^2} \tag{B.5}$$

$$\sigma_c = \sigma_p.\rho + \frac{6.\sigma_p.\rho.e}{h} \tag{B.6}$$

Let $\eta = \frac{e}{h}$

$$\sigma_c = \sigma_p.\rho + 6.\sigma_p.\rho.\eta \tag{B.7}$$

$$\sigma_c = \sigma_p.\rho.(1 + 6.\eta) \tag{B.8}$$

Therefore, if the polymer tendons have an area equal to 2% of the cross-sectional area of the gross cementitious beam area (i.e. $\rho=0.02$) and are placed at an eccentricity of h/4 (i.e. $\eta=0.25$) then a polymer shrinkage-stress of 20N/mm^2 will be required to generate an extreme fibre stress of 1N/mm^2 which is twice that specified in the literature (ter Heide et al., 2005).